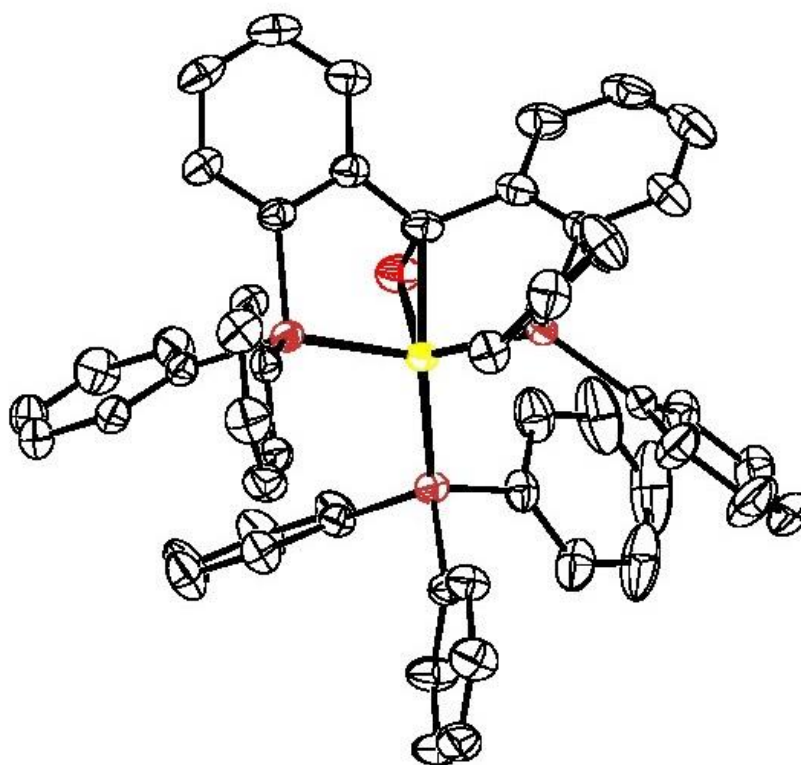


Nickel complexes of a diphosphine-ketone ligand: oxidation-state dependant coordination

B.W.H. Saes

Supervision: Dr. Marc-Etienne Moret, Prof. Dr. R. J. M. Klein Gebbink



30th of October 2014
Organic Chemistry & Catalysis
Debye Institute for Nanomaterials Science
Utrecht University



Abstract

Conversion of carbon dioxide to useable commodity chemicals or fuels in an efficient and inexpensive way potentially forms a partial solution to the energy problem. However, it is still a challenge in chemistry. The catalytic polar bond hydrogenation of the gas has been found to be catalysed by second- and third-row transition metal complexes^[1,2]. Advances towards the use of first-row transition metals instead are being made. Recently, the hydrogenation of CO₂ has been reported catalysed by an organometallic cobalt complex^[3]. The process would be more attractive using the more abundant and less costly first-row transition metal based complexes. One of the possibly useful metals for this role is nickel.

In this research, the synthesis of bis(2-diphenylphosphinophenyl)methanone (DPK) and complexations between DPK and nickel salts were attempted with as goal the synthesis of various nickel based complexes. The chelating ketone-diphosphine ligand system in this complex is an electron-donating system, yet it is also able to accept electrons via back donation. The combination of these electronic effects is meant to aid in facilitating the heterolytic hydrogenation of polar bonds. Eventually, synthesis of this DPK ligand was successful as well as the complexations to various nickel salts to yield four different isolatable complex systems, ranging from Ni(0) to Ni(II) complexes.

Analysis of the formed compounds and complexes was performed by use of Nuclear Magnetic Resonance (NMR), Fourier Transform - Infra Red spectroscopy (FT-IR), Ultraviolet - visible spectroscopy (UV-Vis), Cyclic Voltammetry (CV), Electron Paramagnetic Resonance (EPR), Electron Spray Ionization - Mass Spectrometry (ESI-MS), X-Ray Diffraction (XRD) and Elemental analysis (EA). In addition, Density Functional Theory (DFT) calculations were used to support hypotheses on the formation of desired compounds and complexes and effects of modification of functionalities therein.

Title page image: XRD crystal structure of the Ni(0) complex with a benzophenone-based tridentate diphosphine-ketone (DPK) ligand and triphenylphosphine (PPh₃) (complex **8**).



Contents

Abstract	3
1. Background.....	8
1.1. Hydrogenation of carbon dioxide.....	8
1.2. Organometallic catalysed hydrogenations.....	9
1.3. Polar bond hydrogenation.....	9
1.4. Catalyst design.....	11
1.4.1. Possible nickel-based polar bond hydrogenation catalysts	11
1.4.2. Considerations derived from literature.....	12
1.4.2.1. Hydride addition versus H ₂ σ -complex generation	12
1.4.2.2. Facilitation of the carbon dioxide insertion	13
1.4.2.3. η^2 -CO coordination and two electron process facilitation.....	13
2. Aim of the project.....	15
3. Results and Discussion	16
3.1. The diphosphine-ketone ligand.....	16
3.1.1. Diphosphine-ketone synthesis	16
3.1.2. Diphosphine-ketone analysis	17
3.1.2.1. Ligand ¹ H-NMR analysis.....	17
3.1.2.2. Ligand ESI-MS analysis.....	19
3.1.2.3. Ligand EPR analysis.....	20
3.2. Complexation reactions.....	22
3.2.1. Ni(0) complex synthesis.....	22
3.2.2. Ni(0) complex analysis.....	23
3.2.2.1. [Ni(0) ₂ (DPK) ₃] NMR analysis	23
3.2.2.2. [Ni(0) ₂ (DPK) ₃] FT-IR analysis	26
3.2.2.3. [Ni(0) ₂ (DPK) ₃] synthesis and NMR analysis.....	27
3.2.2.4. [Ni(0)(DPK)(PPh ₃)] XRD & IR analysis.....	29
3.2.2. Ni(I) and Ni(II) synthesis	30
3.2.3. Ni(I) analysis	31
3.2.3.1. [Ni(I)Cl(DPK)] NMR analysis.....	31
3.2.3.2. [Ni(I)Cl(DPK)] IR analysis.....	33
3.2.3.3. [Ni(I)Cl(DPK)] EPR analysis.....	33
3.2.3.4. [Ni(I)Cl(DPK)] CV analysis.....	35
3.2.4. Ni(II) analysis	36



3.2.4.1. [Ni(II)Cl ₂ (DPK)] ¹ H-NMR analysis.....	36
3.2.4.2. [Ni(II)Cl ₂ (DPK)] Evans Method	37
3.2.4.3. [Ni(II)Cl ₂ (DPK)] IR analysis.....	37
3.2.4.4. [Ni(II)Cl ₂ (DPK)] CV analysis	38
3.2.4.5. [Ni(II)Cl ₂ (DPK)] Elemental analysis	38
3.2.5. Comparison between the various nickel-based complexes	39
3.2.5.1. Crystal structure comparison	39
3.2.5.2. UV-Vis comparison	44
4. Conclusions.....	45
5. Future Outlook	46
6. Experimental	48
6.1. General working procedures	48
6.2. Analysis methods.....	48
6.3. DFT.....	49
6.4 Syntheses procedures	49
7. Acknowledgements	53
8. References	54
9. Addendum	57



List of abbreviations

General

VE	Valence Electron(s)
ppm	parts per million
kg	kilogram
mg	milligram
(M)Hz	(mega)hertz
J	coupling constant
s	singlet/second
d	doublet
t	triplet
dd	doublet of doublets
dt	doublet of triplets
m	multiplet
B3LYP	Becke, three-parameter, Lee-Yang-Parr
HOMO	Highest Occupied Molecular Orbital
LUMO	Lowest Unoccupied Molecular Orbital
SOMO	Singly Occupied Molecular Orbital

Analysis methods

¹ H-NMR	Proton Nuclear Magnetic Resonance
¹³ C-NMR	Carbon Nuclear Magnetic Resonance
³¹ P-NMR	Phosphorus Nuclear Magnetic Resonance
VT-NMR	Variable Temperature Nuclear Magnetic Resonance
ESI-MS	Electron Spray Ionization - Mass Spectrometry
FT-IR	Fourier Transform - Infra Red
XRD	X-Ray Diffraction
EA	Elemental Analysis
EPR	Electron Paramagnetic Resonance
CV	Cyclic Voltammetry
GC-MS	Gas Chromatography - Mass Spectrometry
DFT	Density Functional Theory

Chemicals

DPK	diphosphine ketone ligand (5); bis(2-diphenylphosphinophenyl)methanone
CO ₂	carbon dioxide
H ₂	hydrogen gas
(CD ₃)CO	deuterated acetone
CDCl ₃	deuterated chloroform
C ₆ D ₆	deuterated benzene
C ₇ H ₈ (/C ₇ D ₈)	toluene (deuterated)
COD	1,5-cyclooctadiene
DME	dimethoxy ethane
dppp	1,3-bis(diphenylphosphino)propane
dppe	1,2-bis(diphenylphosphino)ethane
THF	tetrahydrofuran
Et ₂ O	diethylether
DMF	N,N-dimethylformamide
DCM	dichloromethane
Et ₃ N	triethylamine
<i>i</i> -PrEt ₂ N	N-isopropyl-diethylamine
(CF ₃ SO ₂) ₂ O	trifluoromethanesulfonic anhydride
HPPH ₂	diphenylphosphine
PPh ₃	triphenylphosphine
Ph	phenyl(group)
Ar	aryl(group)



1. Background

1.1. Hydrogenation of carbon dioxide

In our current global energy balance, fossil fuels are popular. About 90 per cent of our energy demand is generated through the combustion of different fossil fuels such as natural gas, oil and coal^[4]. The combustion of those fuels comes at a high price, however: for each kilogram (kg) of carbon present in the fuel, 3.5 kg of carbon dioxide (CO₂) is released. These vast amounts of gases being generated tremendously increase the concentration of CO₂ in the atmosphere. Being a major greenhouse gas, this increase of CO₂ concentration will induce a climate change through global warming. So why do fossil fuels retain such popularity? Their convenience is multifarious: aside being relatively inexpensive, widely available and only mildly dangerous to users who handle them with care, they are easily adaptable to applications, easily transported and without equal in use for transportation itself. Used for transport, they are portable in a convenient way and contain tremendous amounts of stored chemical energy. On top of that, their easy accessibility throughout the world has cooperated in generating an interest in the optimization of the effective use of fossil fuels: combustion of these fuels has been studied for several centuries, ranging from the fundamental ideas^[5] such as those originally proposed by Carnot, Stirling and other founding pioneers to the constant development of application guided research.

An efficient and cheap catalytic conversion method from CO₂ to useful products would not only provide a 'green' process for the chemical synthesis of fuel, but would also assume an important role in tackling the major problem of the combustion of fossil fuels: the vast issue of global CO₂ emissions. By following a sequence of hydrogenation and dehydration steps summarized in Figure 1, a range of products can be obtained which are either useful as commodity chemicals, as sustainable fuels or both^[1].

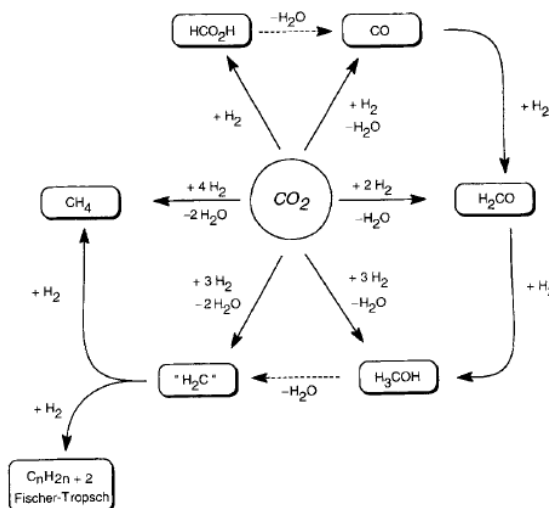


Figure 1: Reduction of CO₂ as a source for industrially important products^[1].

Ultimately, the overall process could lead to an advantageous combination of the capture of carbon dioxide and the production of sustainable fuels and commodity chemicals. Moreover, there is yet another advantage of this process with regard to alternative sustainable evolutions, as conveniently expressed by Z. Jiang et al^[4]:

'Its real attraction is that this approach offers the prospect of decarbonizing transport without the paradigm shift in infrastructure required by electrification of the vehicle fleet or by conversion to a hydrogen economy.'

1.2. Organometallic catalysed hydrogenations

The homogeneously catalysed hydrogenation of unsaturated substrates, among them CO₂, has been established to be viable at low pressures under homogeneous catalysis. Examples of hydrogenation include work performed on the Noyori asymmetric hydrogenation^[6,7] with Ru(II)-BINAP complexes, work with Ru(II)-pincer complexes^[1,8] and other works using catalysts which make use of rhodium^[9] or palladium^[10]. These catalytic hydrogenation reactions are highly efficient. The hydrogenation reactions are in principle always atom-economical and proceed under mild temperatures and pressures possibly in the absence of solvent with no waste generation. Attributing these characteristics, they are classified as so-called 'green' reactions. However, these reactions require the use of costly and scarcely available metals. Partly due to the high costs of these catalyst materials, the direct hydrogenation of CO₂ to methanol under mild conditions has not yet been developed as a practical homogeneous catalytic process^[2].

As an alternative to those high cost rare metals, cheaper metals can be modified to have resembling properties. During recent years, a multitude of catalytic processes have been developed based on abundant and cheap first-row transition metals, such as nickel, often with the goal to replace earlier developed, costlier catalysts. Examples include the work done on amination of aryl and heteroaryl chlorides and bromides catalysed by a BINAP-ligated single-component Ni(0) complex by Hartwig et al^[11,12], oxygen-atom insertion from nitrous oxide into nickel(II) alkyls by Figg et al^[13] and Hillhouse et al^[14-16], the insertion of carbon monoxide and ethylene into to nickel(II) alkyls Hillhouse et al^[17] and the activation of water and ammonia by phosphorus-carbene-phosphorus nickel(II) pincer complexes by Piers et al^[18].

Work towards syntheses of first-row transition metal based complexes suitable for polar bond hydrogenation is in progress. One of the promising functionalities for such complexes is the inclusion of a η^2 nickel-bound polar unsaturation such as a ketone, imine or alkene. The reason why these functionalities are promising, are discussed later. Examples of nickel complexes with such a functionality exist^[19-22]. In some works, homogeneous nickel-catalysed hydrogenation is included. The hydrogenation of ketones still requires high temperatures (150°C) and long reaction times (± 80 hours) using 4 bar of H₂ pressure^[23]. Hydrogenation of imines occurs under milder conditions (100°C, 15 bar H₂) and only hydrogenates specific substrates^[20]. Hydrogenation and isomerization of 1-octene has been shown to occur catalysed by Ni(II) complexes with bidentate diarylphosphane ligands^[24]. Activation of molecular hydrogen (H₂) and its reversible addition across a nickel-borane unit has been observed by J.C. Peters et al^[25]. CO₂ hydrogenation has been shown to occur catalysed by the [Co(dmpe)₂] complex under mild conditions (21°C, 1 bar 50:50 H₂/CO₂)^[1].

1.3. Polar bond hydrogenation

The polarity of the carbon-oxygen bond in the gaseous CO₂ substrate molecule has an immense effect on the chemistry of the reaction. In general, the chemical properties of the hydrogen atoms which are added to the substrate should match the polarity of the bond to be hydrogenated. Whilst for hydrogenation of apolar bonds, the hydrogen atoms which are added should be chemically near-equivalent, the hydrogen atoms should be chemically different for hydrogenation of polar bonds. Therefore, for an efficient catalysis to happen, the hydrogen atoms should be chemically non-equivalent after activation by the catalyst. Examples of the non-equivalent activation of hydrogen include the work done by Noyori^[5,6] and Milstein^[26,27], and the work done by Huff^[28] who proceeded on the work of Milstein.

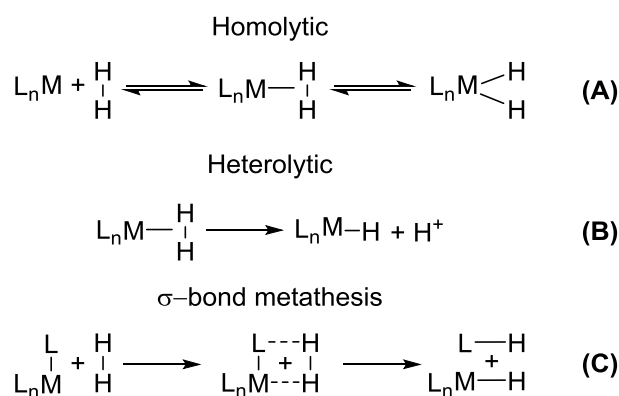


Figure 2: H-H σ -bond activation types.

The requirement of chemically different activated hydrogen atoms also affects the hydrogen bond activation reaction type by the metal centred catalyst. Different H-H σ -bond activation types have been established^[29,30], as can be seen in Figure 2.

In the homolytic pathway ((**A**) in Figure 2), the two hydrogen atoms are both oxidatively added to the metal centre, yielding two chemically near-equivalent hydrogen atoms bound to the metal centre. The chemical properties of the two hydrogen atoms can still vary through influences of other ligands bound to the metal and their respective coordination with regards to the metal-bonded hydrogen atoms (for example, through the trans-effect in square-planar, trigonal bipyramidal or octahedral complexes). Important to note in this reaction type is the fact that the oxidation state of the metal centre is increased by two during the addition.

Through the heterolytic hydrogen activation ((**B**) in Figure 2), the hydrogen is split up into a hydride, which binds to the metal, and a proton, which is adsorbed by a present base. In this reaction type it is important to note that the oxidation state of the metal does not change during the reaction. This type of reaction generally happens under the cooperative functions of an electron-deficient transition-metal and an electron-rich Lewis base^[29]. The hydride is accepted by the metal centre whilst the proton is trapped by a Lewis base nearby, which might be incorporated in the metal complex as a ligand. Heterolytic cleavage is generally more facile than homolytic cleavage because the formal oxidation state and coordination number of the metal centre do not change during the reaction. Non-innocent auxiliary ligand rearrangement may influence the geometry of the complex during the reaction, causing a slight distortion around the metal centre throughout the process. The intramolecular heterolytic cleavage where the generated hydride and proton both coordinate to the ligand-non-innocent organometallic complex through a reaction incorporating one single transition state can be regarded to be a metathesis. If the metathesis only rearranges bonds with σ -character throughout the reaction, the reaction is called a σ -bond metathesis ((**C**) in Figure 2). This type of hydrogen activation is probably the most promising for use in homogeneous catalytic polar bond hydrogenation. The reason that this is the most promising activation type during this reaction, is twofold. Firstly, both hydrogen atoms will be kept in close proximity to each other in the hydrogenated catalyst complex once coordinated to the metal. Secondly, they will be different in terms of chemical properties.

1.4. Catalyst design

1.4.1. Possible nickel-based polar bond hydrogenation catalysts

A general structure for a possible nickel-based diphosphine-ketone (DPK) catalyst is proposed in Figure 3. The catalyst design is based on considerations as proposed in various sources of literature and the functionalities of this complex structure will be discussed in this chapter.

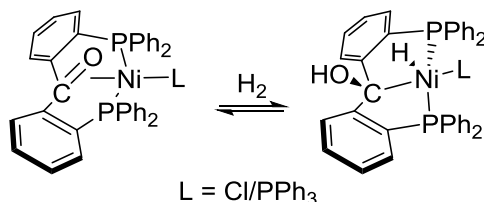


Figure 3: General structure for possible DPK ligated 18/17 VE Ni(0)/Ni(I)/Ni(II) based polar bond hydrogenation catalysts and their hydrogenation reactions.

In this structure, the two phosphine groups coordinated to the nickel provide the first-row transition metal centre with additional electron-richness. Chelation of the phosphine residues combined with the constrained rotation of the molecule is to orient the ligand to the metal in such a way that the carbonyl entity will be pushed towards the metal, resulting in stable nickel(0/I/II) complexes. In this system the complex conformation is locked throughout the reaction through multiple chelation by the ligand.

A key feature of the ligand will be the cooperative character deriving from the carbonyl moiety. Upon hydrogenation of the nickel metal centre by molecular hydrogen, the Lewis basic to-the-metal coordinated carbonyl functionality can rehybridize to coordinate its electrons from the carbonyl-nickel bond to the hydrogen, polarizing the hydrogen-hydrogen bond in the to-the-metal η^2 - σ -coordinated hydrogen molecule. Ultimately, the carbonyl oxygen can abstract a proton from the η^2 - σ -coordinated hydrogen molecule and partake in the stabilization of the hydrogen coordination to the complex.

Comparable nickel complexes have been synthesized by Tsou et al^[19] incorporating a diphosphine and separate η^2 -bound benzophenone ligand, by Kuang et al^[31] which incorporates an oxydibenzene-derived structure instead of a benzophenone-derived structure, by Flores-Gaspar et al^[23] where the nickel is η^2 -bound to the C=O of a di-2-pyridyl ketone and by Arévalo et al^[22] who also use the oxydibenzene ligand (amongst others) and show that this complex can bind to alkenes with a η^2 hapticity. Overall in these works, the nickel shows a preference for $\eta^2(\pi)$ -bonding rather than $\eta^1(\sigma)$ -bonding to either the carbon or the oxygen of the carbonyl moiety. A general preference for the η^2 -coordination is known for various metal-carbonyl complexes^[32]. In some of the by Huang discussed complexes, the η^2 -coordination is shown to activate the carbonyl for further reactions, such as reactions with electro- or nucleophiles, insertion reactions or thermal reactions.

The orbital diagram corresponding to a general 18 VE tetrahedral Ni(0) complex is shown in Figure 4.

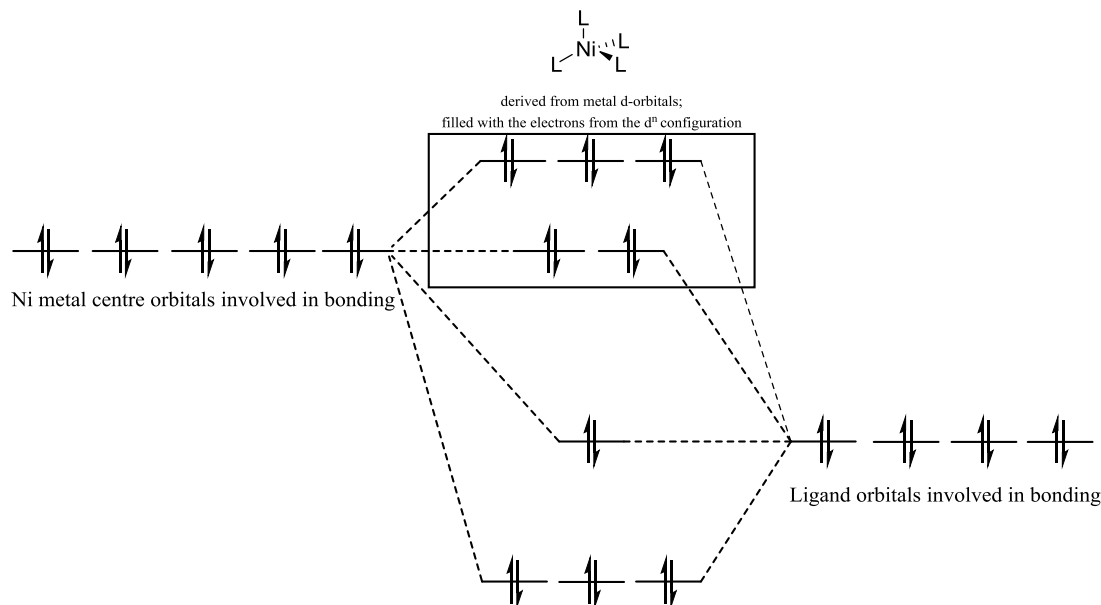


Figure 4: Orbital splitting diagram for a general tetrahedral 18 valence electron (VE) nickel(0) complex.

The use of nickel as a first-row transition metal is currently less prevalent than the use of other first-row transition metals such as iron or cobalt. However, nickel has certain advantages. Ni(0)- and square planar Ni(II)-complexes are diamagnetic because of the even filling of the organometallic molecular orbitals, causing no uncoupled electrons to be present in those complexes. This simplifies analysis by Nuclear Magnetic Resonance (NMR). Use of nickel in organometallic chemistry also has another practical advantage: nickel precursors with weakly coordinating ligands are widely available for different oxidation states of nickel. For example, as a source of Ni(0), bis(1,5-cyclooctadiene)nickel(0) ($[\text{Ni}(\text{COD})_2]$) can be used whilst the nickel(II) chloride ethylene glycol dimethyl ether complex ($[\text{NiCl}_2(\text{DME})]$) is a convenient precursor in nickel(II) chloride complex syntheses.

1.4.2. Considerations derived from literature

In order to be able to catalytically hydrogenate polar bond substrates in the heterolytic way as described in chapter 1, section 3, it is crucial for the catalyst design to make use of previous work done on relating subjects. In literature, several chemical considerations have been reported.

1.4.2.1. Hydride addition versus H_2 σ -complex generation

Two different metal-hydrogen adducts can be formed by addition of molecular hydrogen (H_2) to a metal centre in an organometallic complex^[29,30,33]. The two possible products obtained after hydrogen addition to the metal-centred complex are depicted in Figure 5. Following the mechanism of the heterolytic cleavage of H_2 , out of these two different conformers, stabilization of the H_2 σ -complex is desired. This geometry is favoured as from this state, the system can be further converted to the product after heterolytic cleavage of the hydrogen.



Figure 5: Structural representation of the metal-hydride and σ -bound hydrogen complexes.

Factors that play a crucial role in stabilizing H₂ σ -complex generation over generation of a metal-hydride complex are^[30]:

- presence of electron-withdrawing auxiliary ligands
- cationic character of the metal centre in the complex
- use of less electron-rich metal centres
- high orbital hybridization, for example, d⁶ metals in an octahedral coordination

Opposed to this, the use of ligand-metal systems which are in full contrast to the above-mentioned factors promotes formation of the metal-hydride complex. The generation of a metal hydride complex can also be achieved through use of highly electron-donating ligands coordinated to the metal centre. The reason for this is that when back donation becomes strong enough, the H-H bond can be broken to form a dihydride because of overpopulation of the antibonding σ^* -orbital^[34]. The choice of 3d-nickel metal centre rather than 4d-Pd or 5d-Pt also has an effect on this preference for either of the hydrogen adducts. As the basicity of the metal centres increases going from first-row transition metals down to second-row and third-row transition metals^[34], electron donation occurs more easily and the system favours formation of the metal-hydride complex. In the proposed catalyst structure, the empty phosphorus σ^* orbitals and C=O π^* orbitals serve as acceptors from the nickel. By accepting the nickel electrons from back donation the nickel centre becomes more electron-poor. A preference for a H₂ σ -complex over the metal-hydride complex is to be generated by the use of those electron withdrawing ligands. Depending on the oxidation state of the nickel, the system might still favour hydride complex generation for the most reduced [Ni(0)]-complexes.

1.4.2.2. Facilitation of the carbon dioxide insertion

Conversely, the addition of hydrogen to the catalyst is not the only process for which the system should be suited. Followed by the coordination of the hydrogen, substrate molecules such as CO₂ should insert into the metal-hydride bond to be able to sequentially form the hydrogenated end product. For Ru(II) pincer complexes, it is stated that strong donor ligands facilitate the insertion of CO₂ into the ruthenium-hydride bond^[35]. This is in sharp contrast to the statement that electron-withdrawing ligands should be preferred^[30] as they aid in giving preference for the formation of a H₂ σ -complex rather than the metal-hydride complex. A compromise between both extremes should be made for catalytic polar bond hydrogenation to occur.

1.4.2.3. η^2 -CO coordination and two electron process facilitation

One of the challenges in using first-row transition metals rather than noble metals, is their tendency to undergo one-electron redox processes rather than two-electron redox processes^[33]. Regarding this challenge, P.J. Chirik and K. Wieghardt^[36] state:

'To mimic noble metals, one-electron redox changes must be suppressed and two-electron redox events facilitated.'

One way to circumvent this problem is to turn the two-electron redox process into a one-electron redox process through the use of a redox non-innocent ligand. The metal-supporting organic framework should be able to participate in the redox reaction occurring upon coordination of hydrogen to the catalyst. Suitable for such a chemical reaction is a η^2 -coordinated carbonyl where reduction of this unsaturated carbon-oxygen functionality yields the corresponding alcohol.

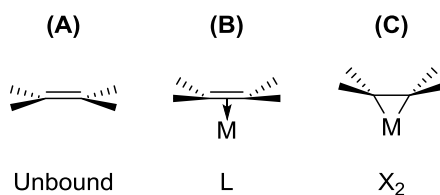


Figure 6: Representation of the unbound unsaturated ligand (A), the formal L-type Dewar-Chatt-Duncanson π -bound ligand (B) and the formal X₂-type metalacycle extreme (C).

Coordination of a ketone ligand to a NiL₃ centre in a η^2 -coordination yields an 18-VE complex. The formal oxidation state of the nickel in this proposed complex is an object open for discussion. In theory, the mutual bonding between the metal and the carbonyl moiety involves donation of the C=O π electrons to an empty d_σ orbital on the metal which is accompanied by back donation from a metal d_π orbital into the ligand lowest unoccupied molecular orbital (LUMO), which is in this case the C=O π^* orbital^[33]. Caused by a combination of these two interactions, the C=O bond is lengthened on coordination to the metal. In addition, the substituents present on the to-the-metal coordinated atoms bend away as a combined result of rehybridization of the ligand atoms and steric interactions between the metal centre and substituents ((B) in Figure 6). A strongly π -basic metal can push this elongation thus far, that the bond is almost reduced to a single bond. In the most extreme cases, for example for various platinum based organometallic complexes^[37], the bond is in fact reduced to a single bond and the coordination process is best described as an oxidative addition to the metal centre creating a three-coordinate metalacycle. An additional effect of this extreme is the full rehybridization of the to-the-metal bound carbons from a sp^2 hybridization to a sp^3 hybridization ((C) in Figure 6).

If this metalacycle extreme is applicable to the proposed Ni(0)L₃(η^2 -CO) complex, the complex should rather be regarded to be a Ni(II)L₃X₂ complex. To distinguish between the two plausible oxidations is complex: both conformations have a full filling of the bonding metal-carbonyl orbital and it is a matter of formalism to regard the orbital occupying electrons as belonging to the carbonyl residue or to the metal.

The hydrogenation of the catalyst structure as proposed in Figure 3 can be regarded in two ways based on the two resonance structures of the η^2 carbonyl-nickel complexes. These two reaction pathways are shown in Figure 7.

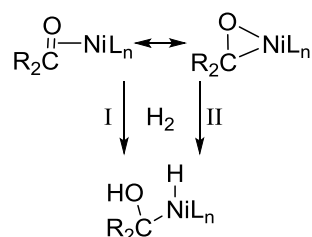


Figure 7: Proposed hydrogenation reactions I and II for the two resonance structures for the DPK-nickel complexes.

In both pathways, the redox non-innocent carbonyl accepts the proton generated in the heterolytic H-H σ -bond activation. Whether the addition of hydrogen to the complex is an oxidative addition which changes the oxidation state of the metal by two (pathway I) or a σ -metathesis with the nickel-oxygen bond in a Ni(II)-complex which rearranges its electrons to accept the incoming hydrogen (pathway II), the result is the same: a Ni(II) complex where the carbonyl functionality has been reduced to an alcohol and the now saturated, sp^3 -hybridized carbon is bound to the metal. In both pathways, the metal-supporting organic framework is able to participate in the redox reaction occurring upon coordination of hydrogen to the catalyst.

2. Aim of the project

The overall aim of the project is to design a novel benzophenone-derived diphosphine-ketone chelating ligand ligated nickel-based homogeneous catalyst for use in polar bond hydrogenation reactions, under which specifically in the hydrogenation of CO₂.

The first subgoal is to synthesize a ligand suitable for the synthesis of nickel based complexes as depicted in Figure 3. This benzophenone derived ligand molecule is depicted in Figure 8. Synthesized ligand products will be analysed using ¹H-NMR, ¹³C-NMR, ³¹P-NMR, FT-IR spectroscopy and EPR.

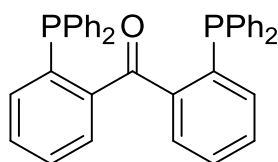


Figure 8: The bis(2-diphenylphosphinophenyl)methanone ligand (DPK) molecule.

The second sub goal is to complexate this diphosphino-ketone (DPK) ligand molecule to a variation of nickel sources to form a scope of chelating phosphorus-bridged carbonyl-ligated Ni(0)-, Ni(I)- and Ni(II)-complexes and full analysis of such complexes by ¹H-NMR, ¹³C-NMR, ³¹P-NMR, FT-IR, EA, UV-Vis, EPR, CV and XRD.

After the synthesis of such a scope of complexes, the analyses can be used to determine the binding mode of the carbonyl moiety of the DPK ligand to the different nickel metal centres. First of all, it should be determined if the carbon-oxygen moiety is in any way coordinated to the metal centres in differently oxidized nickel(0)-, nickel(I)- and nickel(II)-complexes.

In case of η²-coordination to the nickel centres, it should be determined if the L-type Dewar-Chatt-Duncanson model or X₂-type metalacycle extreme is more applicable.

If it proves to be successful to synthesize the proposed potential polar bond hydrogenation catalysts, their susceptibility towards hydrogen coordination and activation and activity in homogeneous hydrogenation can be tested. The consecutive catalysis experiments can be monitored by NMR techniques and GC-MS measurements.

3. Results and Discussion

3.1. The diphosphine-ketone ligand

3.1.1. Diphosphine-ketone synthesis

Initial attempts at the synthesis of the bis(2-diphenylphosphinophenyl)methanone chelating ligand (DPK, **5**) were based on work done by K. Ding et al^[38]. Their procedure is summarized in Figure 9. ¹H-NMR was used to follow the progression of the reactions. The pathway includes constant modification of functionalities in the molecules which are distinctive in NMR analysis. On account of this, NMR proved to be a convenient analysis method. For syntheses of the intermediates, the yields in which they were isolated as pure compounds have been included in Figure 9.

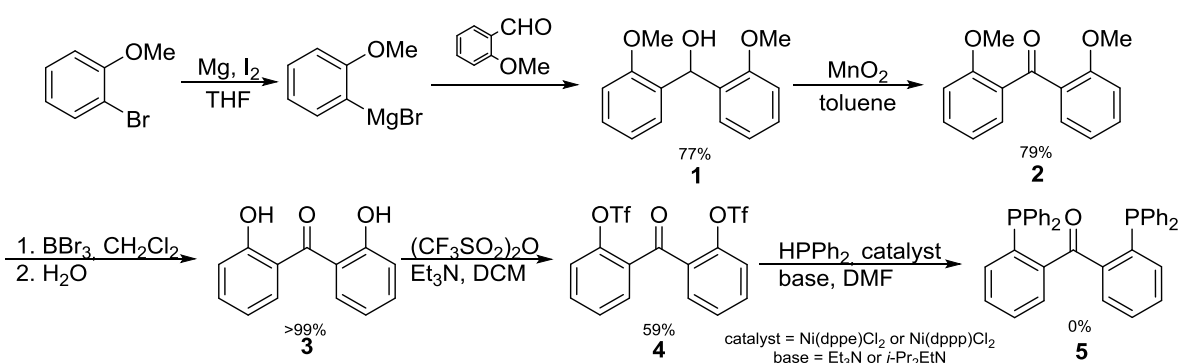


Figure 9: Reaction pathway for the synthesis of the bis(2-diphenylphosphinophenyl)methanone ligand.

The first step in the synthesis is the generation of a Grignard reagent at room temperature using an excess of magnesium and a small amount of I₂ to activate the magnesium. After the generation of this intermediate, the aryl group of the reagent is able to perform a nucleophilic attack on the carbonyl functionality on the 2-methoxybenzaldehyde. The mixture of aldehyde and Grignard reagent was heated to reflux temperature in THF (66 °C) to speed up the reaction. The synthesized intermediate (**1**) was then oxidized using MnO₂ in toluene at an elevated reflux temperature of 110°C. Isolation of the pure compound **2** from the black solid MnO₂ and derivate salts proceeded easily. The next step was the deprotection of the methoxy functionalities using BBr₃ at -78°C (product **3**). This intermediate step was needed in order to enable subsequent conversion of the methoxy groups into triflate (CF₃SO₂O-/TfO-) groups, which are good leaving groups. This was done using trifluoromethanesulfonic anhydride ((CF₃SO₂)₂O) in the step thereafter under mild basic conditions at room temperature (rt). In order to afford this desired product (**4**), it is important to work under inert (N₂) conditions. Otherwise, (CF₃SO₂)₂O reacts with moisture in the atmosphere, generating the corresponding acid, harshly limiting the reactivity of the molecule and thereby the progression of the reaction. The final step in the synthesis of the ligand would be the cross-coupling between HPPH₂ and the TfO-substituted intermediate (**4**) catalysed by [1,3-bis(diphenylphosphino)ethane]dichloronickel(II) ([NiCl₂(dppe)]) or [1,3-bis(diphenylphosphino)propane]dichloronickel(II) ([NiCl₂(dppp)])*. This reaction would, according to the literature, occur in presence of mild base at a temperature of 100°C. Various attempts were made, varying the amount as well as type of catalyst and base. Also, temperature and reaction time were varied for the reaction. All attempts were unfruitful except for one of the experiments for which ³¹P-NMR showed a minor singlet peak around -7.3 ppm, the reported shift^[38] for the end product of the procedure (**5**). This singlet peak indicated plausible generation of the desired product, though isolation of the final product **5** was unsuccessful.

*This cross-coupling reaction was discussed^[38] to proceed under catalysis by NiCl₂(dppe). The experimental section of the paper however specifies that NiCl₂(dppp) was used instead. The corresponding author of the paper was contacted and it was claimed that the NiCl₂(dppp) complex was the correct catalyst. No successful synthesis was perceived using this catalyst however.



As after several attempts the final product could not be isolated using the procedure as described in the literature, an alternative two-step synthesis route was devised. Synthesis of the DPK product (**5**) was eventually successful in an overall reaction yield of 48%. This reaction pathway can be found in Figure 10.

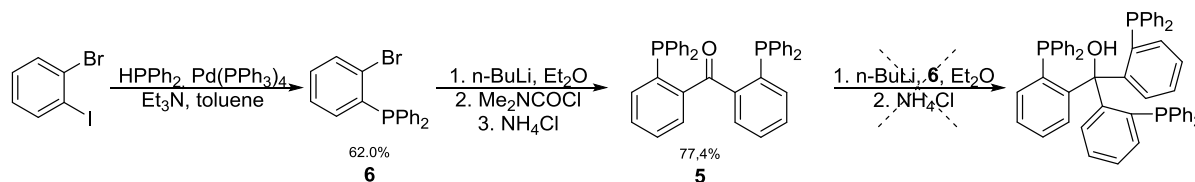


Figure 10: Alternative reaction pathway for the synthesis of the DPK ligand.

Once again, $^1\text{H-NMR}$ techniques proved to be useful in following the reaction progress. For both reactions, pure product was isolated. This synthesis pathway is based on different sources of literature^[39-41]. The first step in this reaction pathway was performed under inert atmosphere (N_2) to prevent oxidation of the diphenylphosphine, tetrakis(triphenylphosphine)palladium(0) catalyst and o-bromophenyldiphenyl-phosphine product. The second step was carried out at low temperature to prevent a second, consecutive addition of the o-bromotriphenylphosphine (**6**) to the desired end product **5** to generate the tris(2-diphenylphosphinophenyl)methanol as shown on the right in Figure 10.

3.1.2. Diphosphine-ketone analysis

Ligand **5** was analysed by $^1\text{H-NMR}$, $^{13}\text{C-NMR}$, $^{31}\text{P-NMR}$, FT-IR, UV-Vis, ESI-MS and EPR. An X-ray diffraction measurement on this compound in its yellow crystalline form had already been done by K. Ding et al^[38]. As combination of the experimental results of the various analysis methods gave clear confirmation that the synthesized material was the DPK, it was decided that an X-ray geometry determination was redundant. For all of the used analysis methods, spectra have been included in the addendum section.

3.1.2.1. Ligand $^1\text{H-NMR}$ analysis

In $^1\text{H-NMR}$, the protons of the ligand only resonate in the aromatic region. This is also what is to be theoretically expected, as all of the protons available on the molecule are bound to phenyl rings. However, minor differences between the chemical environments around the protons attached to the phenyl rings cause them to resonate at slightly different frequencies. The $^1\text{H-NMR}$ spectrum as obtained for the ligand could be fully assigned because of this. A zoom of this spectrum is shown in Figure 11.

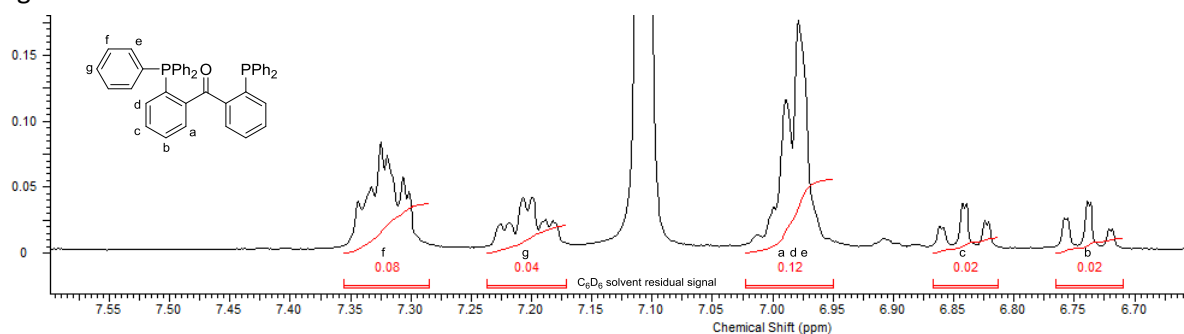


Figure 11: Zoom of the aromatic region of the $^1\text{H-NMR}$ spectrum of DPK in C_6D_6 . Relative values for the areas integrated under the peaks have been included in red.

Unfortunately, it is not convenient to use the phenyl region of this ^1H -NMR spectrum to determine whether the desired product has been formed in a reaction: in the different syntheses performed during this work, a number of compounds with resemblance to this ligand molecule have been synthesized. Besides substrate and product molecules in such a synthesis, minor side products are often formed whose chemical composition is derived from the substrate or which resembles the product. The substrate and all those (side) products resonate in the region from 7-8 ppm in ^1H -NMR. As this gives rise to a lot of overlap in the aromatic regions of these spectra, it is not useful in monitoring the reaction progress.

For phosphorus containing diamagnetic compounds, ^{31}P -NMR provides a quick and easy way to follow the reaction progress. As can be seen in Figure 12, the signal originating from the phosphorus in the ligand (**5**) is a sharp singlet in ^{31}P -NMR. Any generated diamagnetic phosphorus containing (side) products can be easily detected in ^{31}P -NMR.

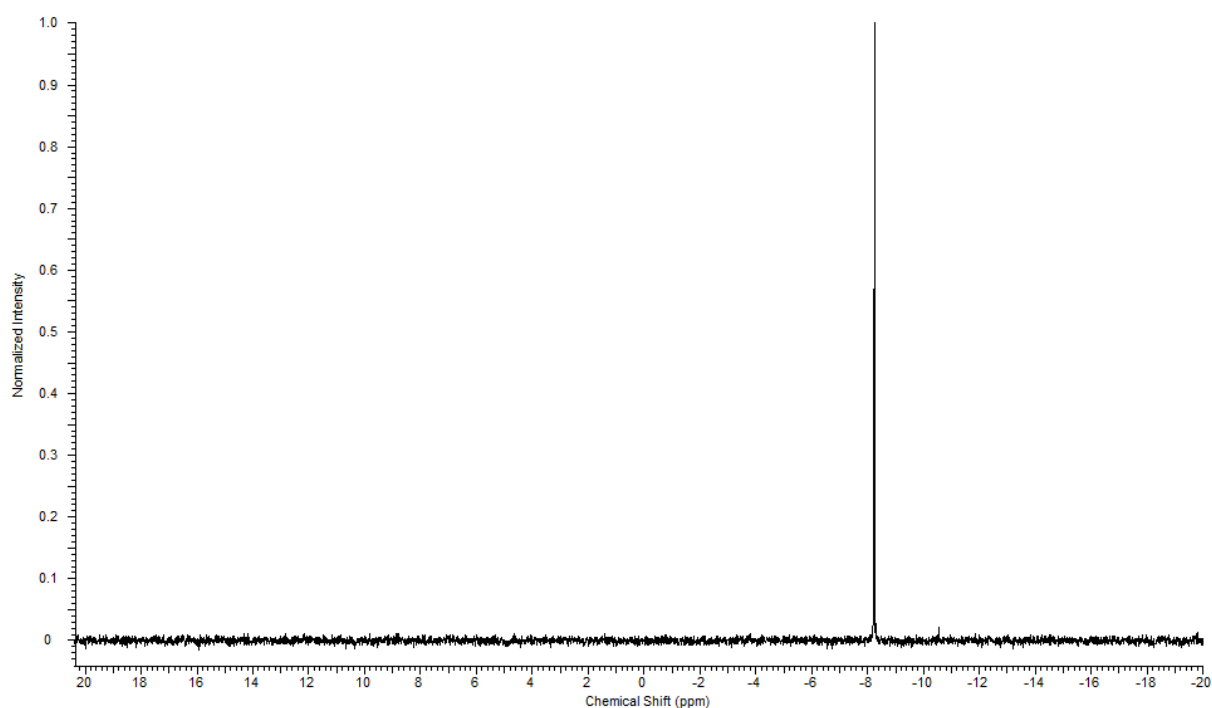


Figure 12: ^{31}P -NMR spectrum of DPK ligand **5**. As can be seen, a sharp singlet is obtained around -8.2 ppm.

3.1.2.2. Ligand ESI-MS analysis

In order to be able to perform Electron Spray Ionization – Mass Spectrometry (ESI-MS) analysis, the DPK ligand **5** was complexed with Ag^+ from AgNO_3 in water/acetonitrile to form $[\text{Ag}_x(\text{DPK})_y]$ complexes. Signals for these silver-ligand complexes were observed at 675–680 m/z and at 1243–1248 m/z . Both signals had an isotope pattern corresponding to a carbon-rich monosilver complex. The signal patterns could be described with the empirical chemical formulas $\text{C}_{37}\text{H}_{30}\text{AgO}_2\text{P}_2$ and $\text{C}_{74}\text{H}_{60}\text{AgO}_4\text{P}_4$ respectively. These empirical formulas can be assigned to the composition of the clusters that caused those signals. As compound **5** contains exactly 37 carbon atoms, it is plain to conclude that the cluster causing the first signal contains one ligand molecule, whilst the cluster that caused the second signal contains two ligand molecules. Water, which is also included in the clusters, completes the chemical formulas. The isotope patterns as calculated using the aforementioned chemical compositions are consistent with the isotope pattern as obtained from the measurements as can be seen in Figure 13. A summary on the analysis of these clusters is given in table 1. Apart from providing a confirmation on the success in the synthesis of **5**, this also indicates that **5** forms clusters with $\text{Ag}(\text{I})$ either in a 1 : 1 or 2 : 1 ratio.

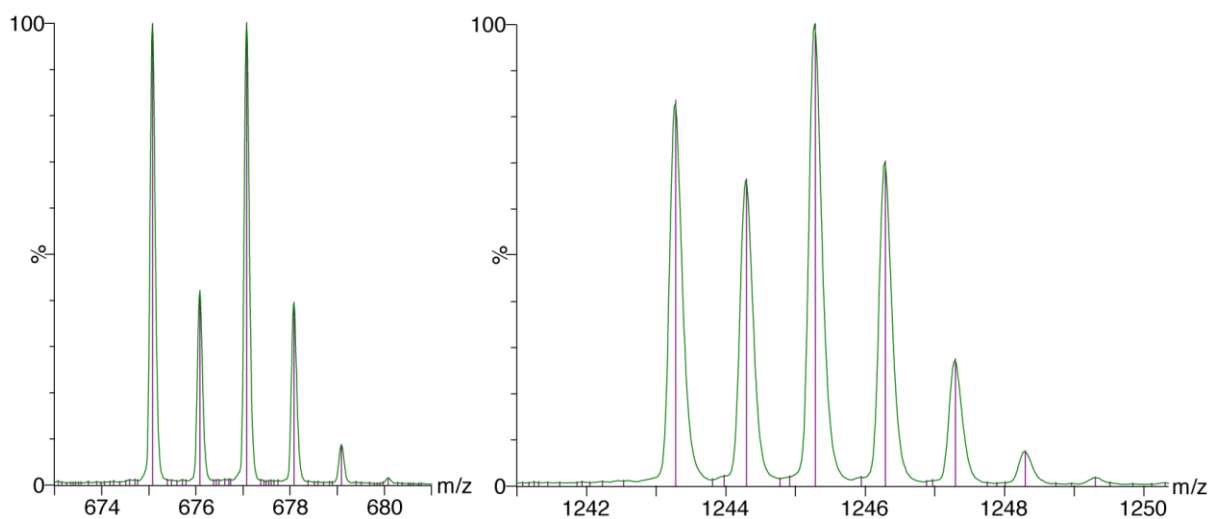


Figure 13: Ligand-derived signals obtained from ESI-MS. The obtained signal is indicated by a green solid line, the calculated values are indicated by red lines.

	<i>Signal 1</i>	<i>Signal 2</i>
<i>m/z range</i>	675-680 m/z	1243-1248 m/z
<i>chemical formula</i>	$\text{C}_{37}\text{H}_{30}\text{AgO}_2\text{P}_2$	$\text{C}_{74}\text{H}_{60}\text{AgO}_4\text{P}_4$
<i>composition</i>	<ul style="list-style-type: none"> · one silver centre (Ag) · one ligand molecule ($\text{C}_{37}\text{H}_{28}\text{OP}_2$) · one water molecule (H_2O) 	<ul style="list-style-type: none"> · one silver centre (Ag) · two ligand molecules ($2 \times \text{C}_{37}\text{H}_{28}\text{OP}_2$) · two water molecules ($2 \times \text{H}_2\text{O}$)

Table 1: ESI-MS signals and their interpretation in terms of chemical composition based on m/z values.

3.1.2.3. Ligand EPR analysis

To test the competence of the ligand molecule to accommodate an additional electron, an attempt was made to reduce the DPK ligand to the anionic DPK. Sample preparation was done in the glovebox under inert atmosphere. First, 1 mg of Na_(s) was submerged and stirred in 0.5 ml of THF. The reaction of the sodium with THF generated a very dark blue solution to which 1 mg of **5** was added. The resulting mixture was filtered. Electron Paramagnetic Resonance (EPR) analysis was used to analyse the sample, so the sample was transferred into a quartz EPR tube.

The EPR measurement can be seen in Figure 14 and shows that the reduction of the ligand molecule yields an organic radical stable in THF with a g-factor value of 2.004. The peak width amounts to a g-factor value of about 0.013. The obtained signal shows a multitude of hyperfine couplings, though retains the general curved shape corresponding to a singlet peak. Allocation of the peaks to the corresponding electron-nucleus couplings is complicated: due to overlap, the signals are heavily distorted. The observed hyperfine couplings arise from couplings of the uncoupled electron to nuclei with non-zero nuclear spin, which are in this case the both phosphorus atoms, the ¹³C carbon isotope atoms and all of the hydrogen nuclei. The isotope abundance of ¹³C is however low ($\pm 1.1\%$ ^[42]), so no hyperfine couplings originating from these nuclei are distinguishable from the noise in the EPR spectrum.

Theoretically, it would be possible to simulate the spectrum and approximate the couplings as generated by the EPR-active nuclei. For now, this measurement provides us with a fingerprint of the synthesized ligand.

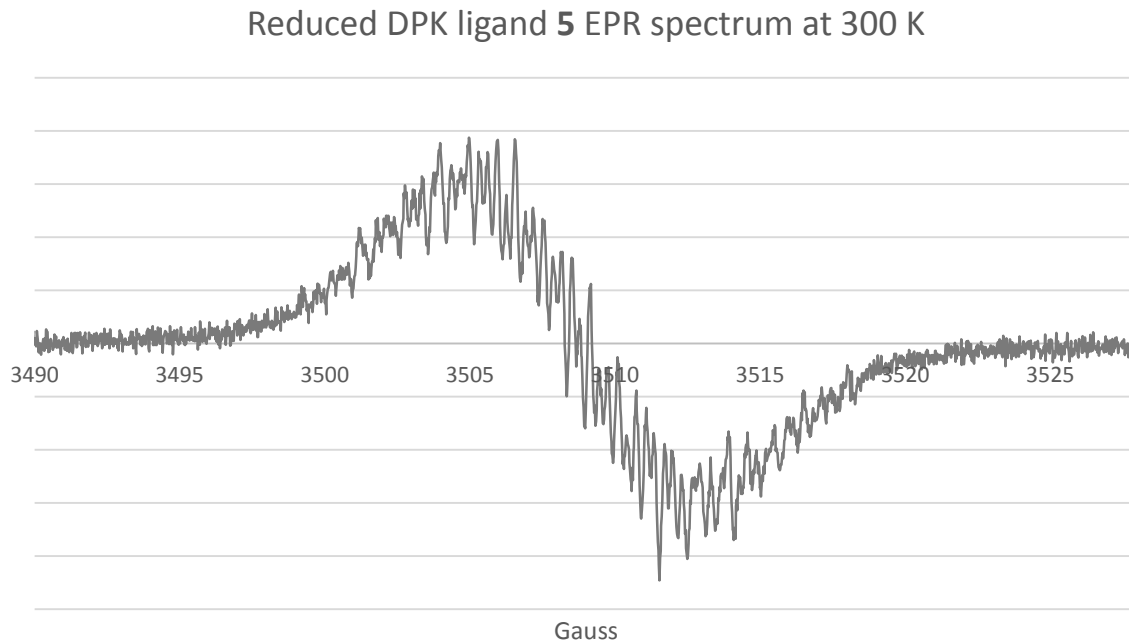


Figure 14: EPR spectrum of the radical anion form of ligand molecule **5** measured in C₇H₈ at 300 K.

Density Functional Theory (DFT) calculations have been used to optimize the geometries of the uncharged and radical anion form of ligand molecule **5**. From the calculation on the radical anion, a spin density plot could be generated. This plot shows differences in spin density in the molecule. Also, plots were calculated for the Highest Occupied Molecular Orbital (HOMO) and Lowest Unoccupied Molecular Orbital (LUMO) both of the uncharged and radical anion forms of **5**. The spin density plot for the radical anion shows correlation with both the LUMO plot obtained for the uncharged DPK molecule and with the HOMO plot obtained for the radical anion form. Conclusively, the additional electron in the radical anion form of the ligand occupies the LUMO of the uncharged molecule, turning this orbital into a Singly Occupied Molecular Orbital (SOMO). In the radical anion calculation, this singly occupied orbital can be regarded to be the HOMO of the molecule. The HOMO plot and spin density plot are shown in Figure 15. As can be seen, the free electron is mostly present around the carbonyl functionality and adjacent phenyl groups. This local presence shows that the uncoupled electron predominantly couples with the zero-spin abundant carbon and oxygen nuclei.

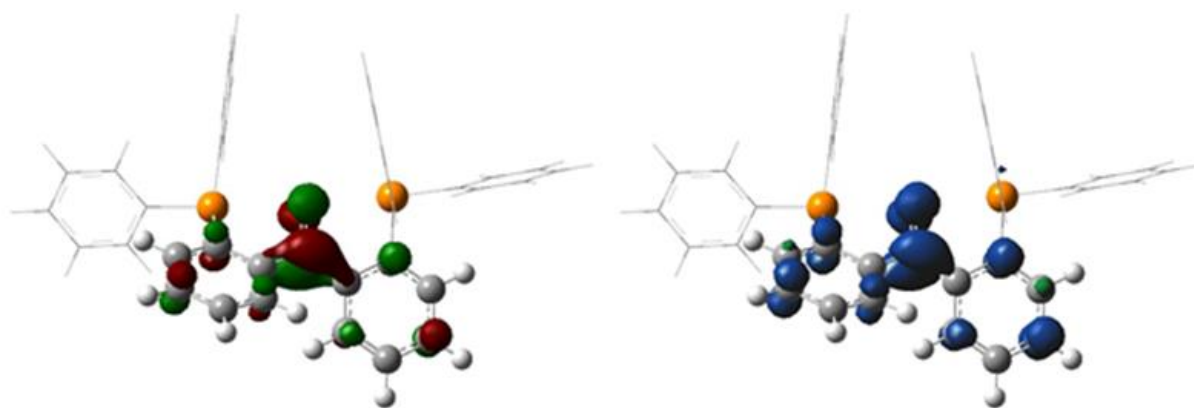


Figure 15: HOMO plot (left) and spin density plot (right) for the radical anion form of the DPK ligand (**5**) as generated after DFT calculations using Gaussian 09 and the GaussView 5.0.8 software. Calculations were performed using the Becke three-parameter Lee-Yang-Parr (B3LYP) functional and the 631-G** basis set. Phenyl rings on the phosphori are represented as wireframe to improve clarity. Hydrogen is shown in white, carbon in grey, phosphorus in orange. HOMO plot isovalues: MO=0.06; Density=0.004. LUMO plot isovalues: MO=0.02; Density =0.004. Pictures generated using GaussView 5.0.8.

3.2. Complexation reactions

Common synthesis procedures for the generated nickel-based complexes included working under inert $N_{2(g)}$ atmosphere in the glovebox and with dried and degassed solvent and reagents. More detailed synthesis procedures can be found in the experimental section.

3.2.1. Ni(0) complex synthesis

The DPK ligand as previously shown in Figure 8 was complexed with $[Ni(COD)_2]$ to generate two different complexes. Addition of the ligand to $[Ni(COD)_2]$ generates a dinickel-trisligand complex which can be converted to a monomeric Ni(0) complex by addition of triphenylphosphine. The bridging ligand molecule is then replaced by PPh_3 . The monomeric complex can also be generated directly by 1:1:1 combination of $[Ni(COD)_2]$, **5** and PPh_3 . Figure 16 shows these various complexation reactions more clearly.

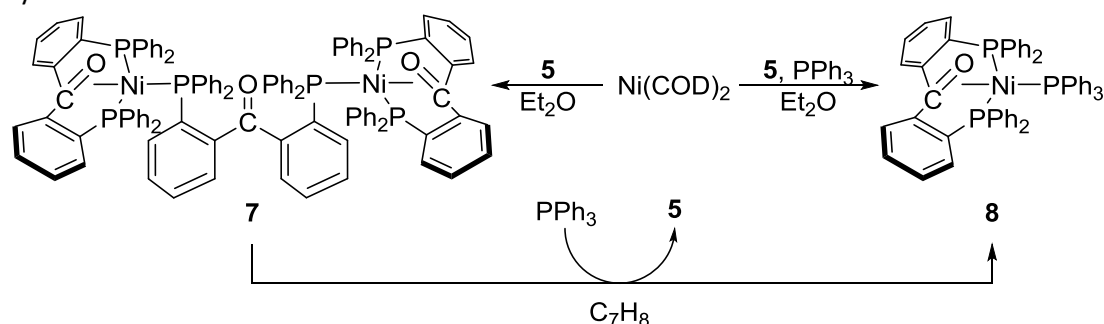


Figure 16: Summary of the different complexation reactions using $[Ni(COD)_2]$, DPK ligand **5** and PPh_3 . The pathway from **7** to **8** generates two equivalents of complex **8** per equivalent of complex **7**.

The synthesis of **7** was monitored in an in-situ NMR experiment; the DPK ligand was dissolved in C_6D_6 and added to solid $[Ni(COD)_2]$ at room temperature. ^{31}P -NMR was used to follow the progress of the reaction over time. No precipitation was observed in the NMR sample over time. A first measurement was performed 15 minutes after combination of the ligand solution and $[Ni(COD)_2]$, later measurements were performed at one hour after combination and at 18 hours after combination. In between and during the measurements, the sample was left unmodified under inert conditions at room temperature. Analysis showed that two different main products were being formed. Results of the NMR measurements have been compiled in table 2.

Reaction time (h)	Ratio 7 : main side product(s)
0.25	1.0 : 1
1	0.5 : 1
18	0.0 : 1

Table 2: Reaction times and corresponding ratios between the generated compound **7** and the main side products.

Over time, the amount of complex **7** in the air-tight sealed J. Young NMR tube diminished whilst the amount of main side product(s) increased. As there had not been made any (externally originating) change to the sample composition, it was concluded that complex **7** could and would undergo decomposition and be converted to the observed side product(s) under the applied conditions. Isolation and further analysis of this/these decomposition product(s) was not performed.

A consecutive experiment with the goal to provide an easy purification method for the compound was performed using Et₂O as solvent. Because of low solubility of both the [Ni(COD)₂] and **5** in this solvent, the reaction was proceeded under stirring in a suspension. The immediate colour change from brightly yellow to intense dark brown upon addition of the DPK (**5**) suspended in Et₂O to [Ni(COD)₂] indicated that some form of quick chemical reaction, presumably complexation, did occur. This reaction occurred despite that the reagents were only sparingly soluble. After 15 minutes of stirring, two different phases were synthesized and isolated (solid and liquid). ³¹P-NMR analysis showed that by using this synthesis method, complex **7** could be isolated as the solid and that main side product as observed in the previous experiment remained dissolved in the Et₂O together with other by products such as the COD that had dissociated from the Ni(0). Isolated as a solid, complex **7** degrades only slowly and is stable over the course of days under inert conditions at room temperature.

3.2.2. Ni(0) complex analysis

3.2.2.1. [Ni(0)₂(DPK)₃] NMR analysis

The ³¹P-NMR of **7**, as seen in Figure 17, shows three peaks with different chemical shifts. The integrals of the signals relate to each other as 1:1:1. As the ketone ligand **5** only has two phosphorus atoms, either two or one signal would be expected in ³¹P-NMR for any complex incorporating one ligand molecule. The presence of three peaks corresponding to the complex indicates that there must be three chemically different phosphorus atoms present in a 1:1:1 ratio that do not exchange on the ³¹P-NMR time scale. Three different signals for a complex based on a biphosphorus ligand could indicate the formation of a complex with six phosphorus atoms. This requires three molecules of **5** to be present in the complex.

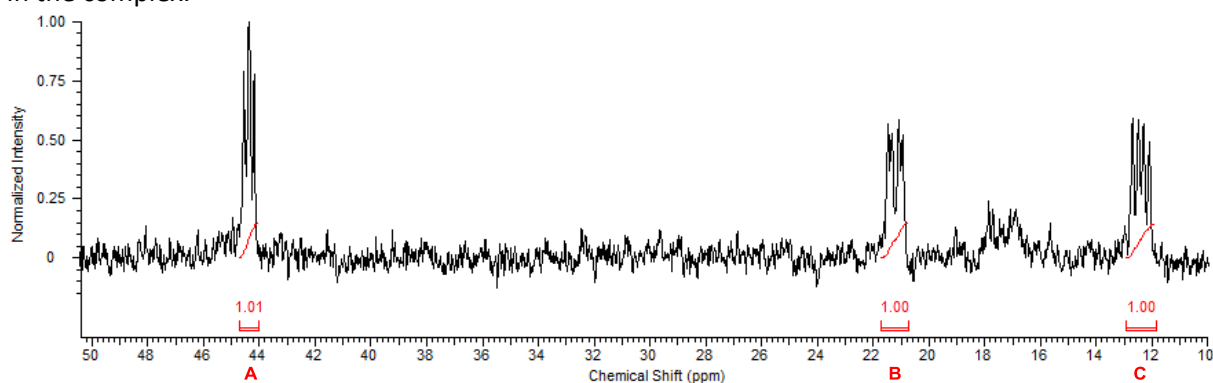


Figure 17: ³¹P-NMR of the solid material (**7**) obtained after reaction of [Ni(COD)₂] with **5** in Et₂O measured at 100°C.

The spectrum shows a doublet of a doublet (**A**) and two pairs of doublets (**B** and **C**). The couplings of **A** amount to 27.7 Hz and 30.6 Hz. The doublets as obtained for **B** and **C** show couplings of respectively 27.7 Hz and 30.6 Hz. It can thus be concluded that **A** corresponds to phosphori which couple with both **B** and **C** whilst the phosphori which cause the signals **B** and **C** only couple to **A** and not to each other. In addition, it can be seen that signals **B** and **C** are composed of pairs of doublets rather than single doublets. The relative shifts between the doublets in the signals are big (± 60 Hz). The splitting into doublets of doublets can arise from a coupling between **B** and **C**. The combined results indicate that three chemically significant different phosphori which all couple with each other are present in the complex and that there are some small differences to be found giving rise to the double nature of signals **B** and **C**.

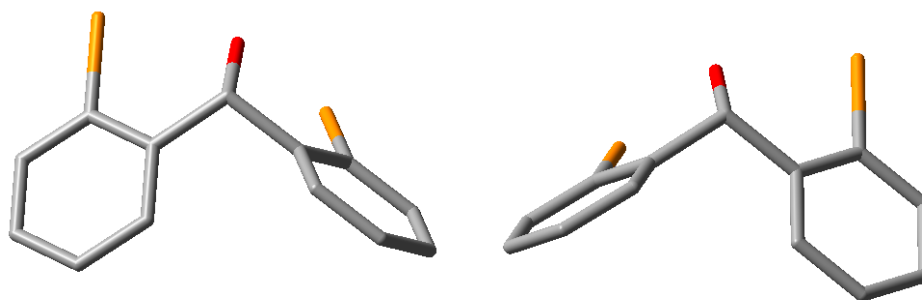


Figure 18: The syn- and anti- conformations of the benzophenone derived ligand molecules which could be converted into each other over a rotational energy barrier. The hydrogen atoms and phenyl groups on phosphorus atoms have been omitted to improve clarity. Phosphorus is shown in orange, oxygen in red, carbon in grey. Picture generated using GaussView 5.0.8.

The four doublet peaks could arise from a constrained rotational barrier in the molecule. Because of this barrier, the chemical environment of the phosphorus atoms from which peaks **B** and **C** originate could be different, causing a difference in chemical shift in NMR. If this were the case, two different isomers of the complex had been formed. This would also mean, that modification of either of the phenyl groups in the molecule might impose a preference for either the syn- or anti-conformation of the ligand, imposing chirality on the ligand. An approximation of the two different conformations can be seen in Figure 18. Such a constrained configuration could arise from coordination to a metal centre.

In order to test the hypothesis of the existence of such a conformational equilibrium, a series of variable temperature NMR (VT-NMR) measurements were done. By increasing the temperature, the equilibration is expected to go faster, decreasing the degree of distinctiveness of the two peaks belonging to the interchanging phosphori. By the same reasoning, the distance between the two doublet signals hypothetically increases upon lowering the temperature of the sample.

As the chemical properties of the phosphori are expected to become more alike, the signals **B** and **C** are expected to approach each other, with the extreme at the temperature where both signals resonate at an identical frequency right between the doublets as obtained in the ^{31}P -NMR spectrum earlier shown in Figure 17. When the thermal energy is high enough, the multiplicity of this signal would, theoretically, through quick interchange between the phosphori, be reduced to a triplet signal and be expected around 18 ppm. The expected sharpening arises from the fact that at higher temperatures, the reaction equilibration can be faster than the time scale at which NMR measurements are done and intermediate conformations are not detected anymore.

These intermediate conformations are what are expected to cause broadening of the signals. Lower temperatures would eventually freeze the equilibrium in place and in this way also lead to peak sharpening. Experimental work shows that this temperature has not yet been reached at -75°C .

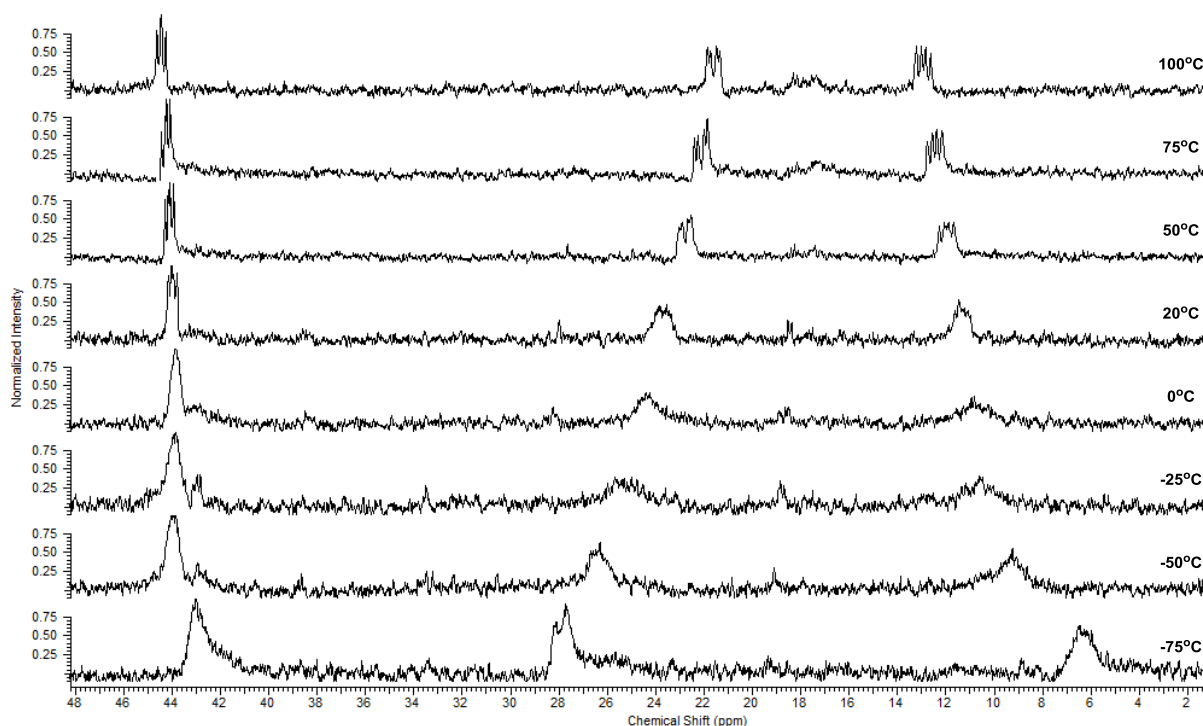


Figure 19: Zooms in the ^{31}P -NMR spectra of dimer compound **7** measured at a variety of temperatures.

The ^{31}P -VT-NMR was measured using purified dimer complex **7**. Obtained spectra have been compiled in Figure 19 and chemical shift and coupling results have been gathered in table 3. As expected, the peak sharpness is increased upon heating the sample; at 50°C and higher temperatures the signals split up in a pair of distinctive doublets. These doublets of doublets could indicate that the phosphori from which those signals originate, couple with two other phosphori. This way, the system contains three different phosphorus centres which all couple to each other.

Considering this altogether, the complex would include four phosphorus atoms that are interchangeable. All in all, this would result in two near-identical sets of three phosphori that all couple to each other within their own set.

Signal A				Signal B			Signal C	
Temp (°C)	Shift (ppm)	J_{AB} (Hz)	J_{AC} (Hz)	Temp (°C)	Shift (ppm)	J_{BC} (Hz)	Temp (°C)	Shift (ppm)
-75	42.9	-	-	-75	27.6	-	-75	5.6
-50	43.9	-	-	-50	26.1	-	-50	8.7
-25	43.8	-	-	-25	25.1	-	-25	10.0
0	43.8	-	-	0	24.0	-	0	10.4
20	44.0	21	36	20	23.2	60	20	10.9
50	44.1	23	36	50	22.4	62	50	11.5
75	44.2	25	35	75	21.7	64	75	11.9
100	44.4	28	31	100	21.3	62	100	12.5

Table 3: Chemical shifts and couplings for the three isolated signals obtained for the ^{31}P -VT-NMR of complex **7**. Indicated by - are values where the peak resolution is too low in quality to allow for a reliable coupling determination.

It can be assumed that all of the six phosphorus atoms would not find enough space around one nickel centre to coordinate on it. For nickel-triphenylphosphine complexes, of which the stereochemistry to some extent resembles that of the possibly formed complexes out of $[\text{Ni}(\text{COD})_2]$ and **5**, it is known that the maximum amount of nickel-coordinating triphenylphosphine ligands is four. This four-coordination yields the $[\text{Ni}(\text{PPh}_3)_4]$ complex^[43,44]. Based on this information, the structure as depicted in Figure 20 could be proposed. In this structure, the $[\text{Ni}(\text{COD})_2]$ and DPK ligand (**5**) have reacted in a 2:3 ratio. At the outward fringe of the molecule, the ligand molecules are expected to coordinate to the nickel in a tridentate way with both phosphori and the carbonyl moiety. The two identical residues are connected to each other by a bridging ligand. The carbonyl function of this molecule is not coordinated to a nickel centre.

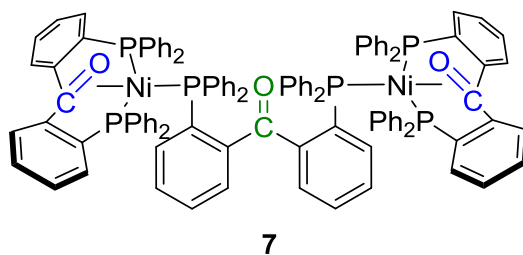


Figure 20: Representation of a possible structure of the formed complex **7**. The Ni-coordinating carbonyl functionalities are coloured blue, the uncoordinating carbonyl moiety is green.

However, the spectra shown in Figure 19 also show a change in chemical shifts for the signals **B** and **C**. In theory, the raise of temperature would only lead to sharpening of the peaks and not to a change in chemical shift. This change in shift might indicate that the system undergoes change in conformation upon temperature modification. It is difficult to correlate this result to the proposed static structure. Possibly, the formed structure on combination of $[\text{Ni}(\text{COD})_2]$ and the DPK ligand (**5**) is more complex. To test the hypothetical structure, different analysis methods were used.

3.2.2.2. $[\text{Ni}(\text{O})_2(\text{DPK})_3]$ FT-IR analysis

KBr FT-IR spectroscopy was used to measure the frequencies associated to the ketone entities in the formed $[\text{Ni}(\text{O})_2(\text{DPK})_3]$ complex. This measurement showed three peaks that are interesting; the first of those peaks is the one at 1679 cm^{-1} , which corresponds to a non-metal coordinated carbonyl functionality. This carbonyl moiety is coloured green in Figure 20. For reference, the free ligand shows a sharp carbonyl peak at 1652 cm^{-1} ^[38]. Besides this carbonyl peak, the spectrum also shows two small peaks at 1309 and 1292 cm^{-1} , which are not present in the spectrum of the uncomplexed ligand. This result confirms the theory that the isolated product contains a ligand molecule from which the carbonyl moiety is not coordinated to a metal centre. The two peaks at 1309 cm^{-1} and 1292 cm^{-1} might correspond to nickel-coordinated carbonyl stretch vibrations. Once again, a slight difference is observable for the two ligand molecules in tridentate coordination to the nickel. The two coordinated carbonyl functionalities are coloured blue in Figure 20. By linking the two nickel centres in Figure 20 together, the green coloured ketone functionality in the bridging ligand molecule would not be coordinated to nickel and would therefore give rise to a carbonyl peak in IR closely matching to the carbonyl vibration found for the uncomplexed ligand. The presence of these three peaks is in accordance with the hypothetical structure of the complex.

3.2.2.3. $[Ni(0)_2(DPK)_3]$ synthesis and NMR analysis

As the bridging ligand has close resemblance with triphenylphosphine (PPh_3) to the nickel centres to which it was supposed to be coordinated, a consecutive experiment was performed. In this experiment, PPh_3 was added to complex **7** to generate a monomeric complex. Theoretically, one equivalent of **7** could react with two equivalents of PPh_3 to generate two monomeric nickel(0)-complex molecules together with one free molecule of **5**. This reaction has been schematically summed in Figure 21.

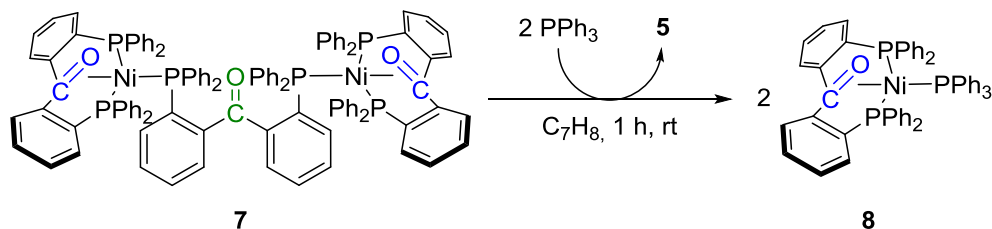


Figure 21: The synthetic route from complex **7** to complex **8** by use of PPh_3 .

The reaction was monitored in an in situ ^{31}P -NMR experiment. Instead of the generally used relaxation time of 1 second for ^{31}P -NMR measurements, a relaxation time of 23 seconds was used. This way, all of the chemically different phosphorus nuclei would have had enough time to relax back again to a collection with an overall random orientation; in other words, this change would omit the truncation usually encountered for ^{31}P -NMR measurements. Because of this, the NMR spectrum could be used in a quantitative way.

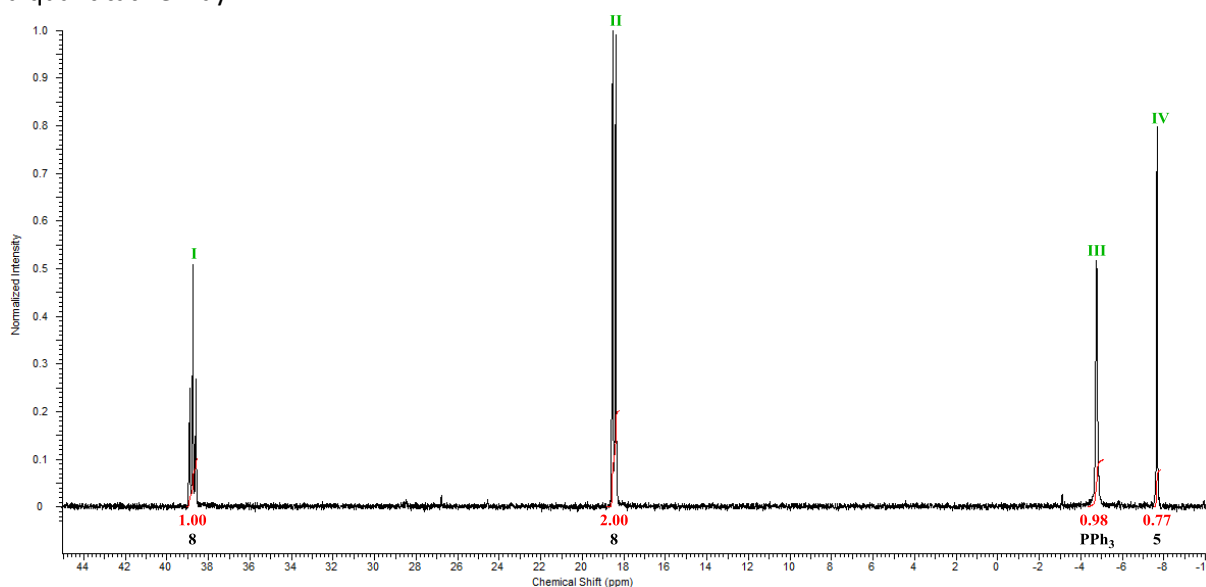


Figure 22: ^{31}P -NMR spectrum of the product in the reaction of **7** with PPh_3 . Peak assignment and integral values have been included below the peaks. The shifts of the signals vary slightly from the shifts acquired during earlier experiments; this is due to the fact that non-deuterated toluene had been used for the experiment making it impossible to fully tune the probe to the solvent. The spectrum has been referenced to the signal of H_3PO_4 which was recorded in a separate measurement using the exact same settings as for the obtained spectrum.

In the spectrum (Figure 22), no peaks originating from complex **7** can be observed. The peaks at 38.7 ppm (**I**) and 18.3 ppm (**II**) are peaks which have not been observed in earlier measurements. However, the triplet-doublet pattern and 1:2 integral ratio correlate well to the spectrum as expected for a monomeric complex: the triplet (**I**) has about the same chemical shift as the triplet in complex **7** and the two broad signals **B** and **C** in the spectrum of complex **7** seem to have converged to a single doublet (**II**). In addition, an excess of PPh_3 (**III**) is observed. The singlet peak at -7.9 ppm (**IV**) is close to the value of 8.2 ppm as observed for the free ligand molecule **5**. However, the integrals do not fully fit to the



expected values. Synthesis of a monomeric species out of **7** would yield two monomer molecules and one molecule of **5**. The ratio between the peaks **I**, **II** and **IV** was therefore expected to be 1:2:1 as peak **I** would correspond to the triphenylphosphine ligands in the two formed monomer molecules, peak **II** to the total of four phosphori in the nickel-coordinated DPK ligands in the monomers and peak **IV** to the two unbound DPK ligand phosphori. Whilst the experimental ratio between **I** and **II** fits to this theory, the ratio between signals **I** and **II** to **IV** does not. The reason for this may be artificial because of, for example, the aforementioned problem of truncation. Though, it is also all possible that complex **7** is in fact a more complicated cluster which decomposes into complex **8** and ligand **5** in a 4:3 ratio.

What is curious about this result is that the reaction leads to full conversion of the dimer into the monomer species. DFT calculations were performed on the compositions of the starting materials and product materials in this reaction. The performed reaction and related relative energies as calculated can be found in Figure 23. It should be realized that the calculated energy for complex **7** is to be regarded as an indication only; out of all the possible geometries of the complex, only one was optimized to a local minimum in energy. Besides, the proposed structure might not be the correct one for the complex. However, the relative energy is significantly lower for the products than that of the combined starting materials. Although the DFT calculations can axiomatically only provide an indication, it is not surprising that the reaction goes to full completion; according to the calculation, the reaction is energetically favourable.

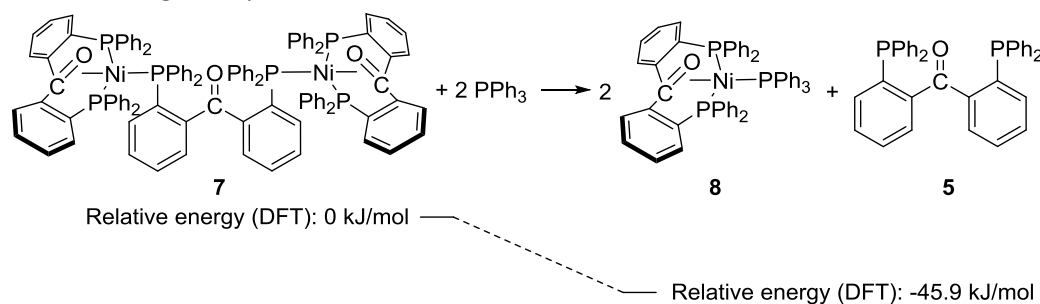


Figure 23: The reaction for the decomposition of **7** into **8** by PPh_3 and calculated relative energies in kJ/mol.

To verify the structure of complex **8**, an attempt was made to synthesise the PPh_3 -including monomer form of the complex directly by combination of $[\text{Ni}(\text{COD})_2]$, DPK ligand **5** and PPh_3 in a 1:1:1 ratio in C_6D_6 in an in-situ ^{31}P -NMR experiment. After a reaction time of 15 minutes at room temperature under inert conditions, ^{31}P -NMR was measured and the spectrum is shown in Figure 24. In subsequent synthesis experiments, the complex was formed by 1:1:1 combination of $[\text{Ni}(\text{COD})_2]$, compound **5** and PPh_3 in Et_2O to form a suspension. This suspension was then stirred for 15 minutes and the synthesised brown solid was isolated, washed with hexane and dried in vacuum to produce complex **8** as a brown powder in a 72% yield.

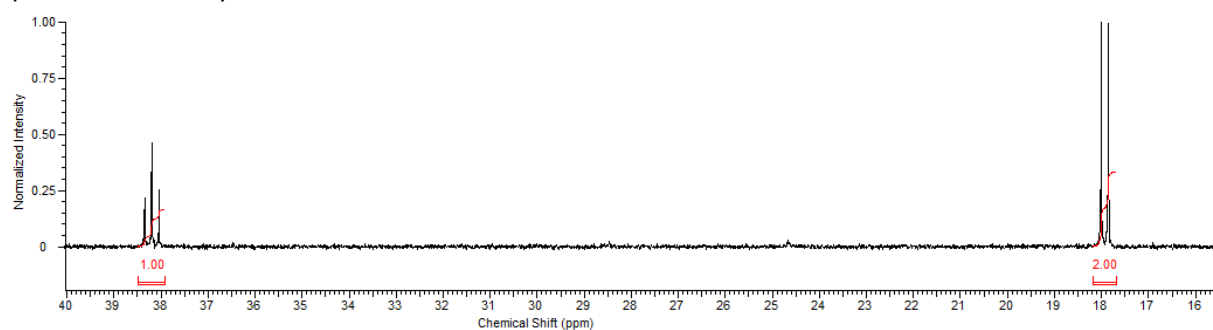


Figure 24: ^{31}P -NMR of the in-situ reaction with $[\text{Ni}(\text{COD})_2]$, compound **5** and PPh_3 in C_6D_6 .

The NMR spectrum shows two signals: one triplet at 38.2 ppm with a coupling of 25 Hz and an integral value of 1 and one doublet at 17.9 ppm also with a coupling of 25 Hz but an integral value of 2. The spectrum shows that the complex contains three phosphori of which two phosphori are equivalent. All of the phosphori couple with each other. The peaks in this spectrum correspond to the peaks shown earlier in Figure 22. For comparable Ni(0) complexes with a chelating biphosphine, similar chemical shifts are found^[45]. In addition, the two doublet peaks found in the spectrum for the coordination experiment with [Ni(COD)₂] and **5**, have merged to form a doublet peak at 17.9 ppm, which is in accordance with the expected shift of ±17 ppm for this signal at an elevated temperature where the measuring time exceeds the equilibration time. These results support the formation of complex **8** as shown earlier in Figures 21 and 23.

3.2.2.4. [Ni(0)(DPK)(PPh₃)] XRD & IR analysis

In order to further ascertain the structure of complex **8**, attempts were performed to grow crystals suited for an X-ray Diffraction (XRD) measurement. Dark red crystals of adequate quality were obtained through solution of the complex in Et₂O and subsequent vapour diffusion of hexane into the solution to grow crystals steadily.

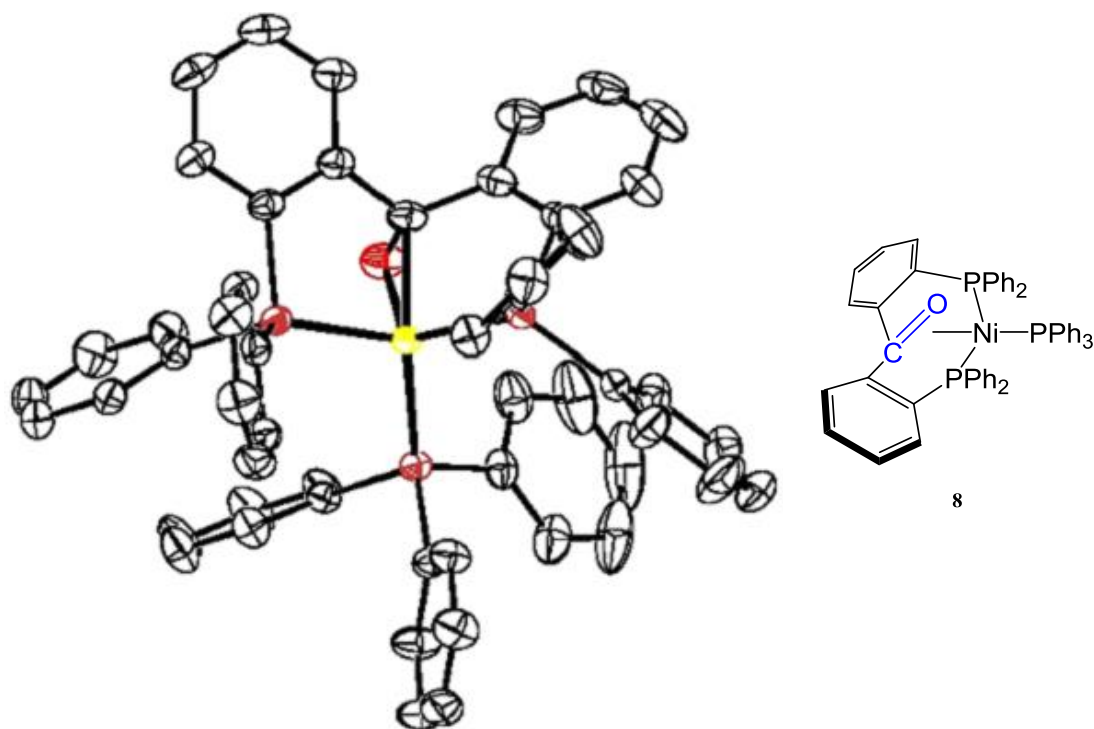


Figure 25: Picture of the crystal structure of [Ni(0)(DPK)(PPh₃)] complex **8** as measured of the obtained dark red crystals. Hydrogen atoms have been omitted for clarity. Carbon is shown in black, oxygen in red, phosphorus in violet and nickel in yellow.

As can be observed in Figure 25, the nickel assumes a tetrahedral geometry where ligand **5** is a tridentate ligand and the nickel centre is provided with an additional L-type ligand (PPh₃) to get to a total of 18 valence electrons. Comparison of this crystal structure to other crystal structures and more discussion can be found in chapter 3, subsection 2.5.1.

Also FT-IR supports the formation of a monomeric Ni(0) complex with coordinated ketone; the IR spectrum shows no carbonyl peak around 1650 cm⁻¹ but does show a peak which could correspond to a coordinated ketone at 1309 cm⁻¹, just as for one of the coordinated carbonyl moieties in the dimeric complex.

3.2.2. Ni(I) and Ni(II) synthesis

After the syntheses of the two Ni(0) complexes, several attempts were made at making Ni-based complexes with a different oxidation state on nickel. Initial attempts using dried NiCl₂ or NiBr₂ salts in various solvents (THF, Et₂O, DCM/MeOH) did not yield any product. When the salts were combined with [Ni(COD)₂] and ligand **5**, only the dimeric complex **7** was formed. As an alternative nickel(II) source [NiCl₂(DME)] was investigated. In presence of this coordinated dimethoxy ethylene, the nickel(II)chloride did dissolve in THF as well as in DCM. Conclusively, nickel sources with weakly coordinating organic ligands that improve solubility are more reactive towards complexation with **5**. The reaction equations for the syntheses of the Ni(I)- and Ni(II)- complex can be found in Figure 26.

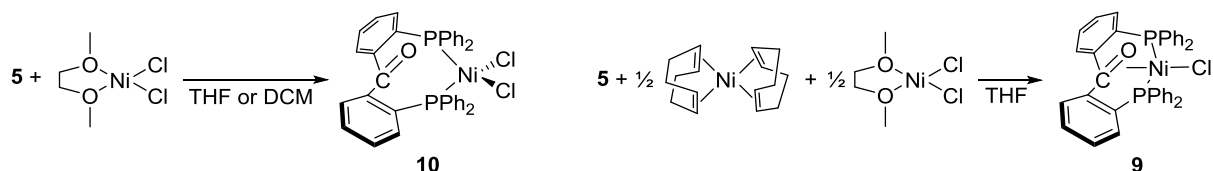


Figure 26: The two complexation reactions between ligand **5** and [NiCl₂(DME)] to generate the Ni(II) complex **10** and between ligand **5**, [Ni(COD)₂] and [NiCl₂(DME)] to yield the Ni(I) complex **9**. The two reactions were performed at room temperature under inert (N₂(g)) conditions.

The complexation reactions were performed under stirring at room temperature. Both the direct complexation from [NiCl₂(DME)] and the comproportionation reaction with [NiCl₂(DME)] and [Ni(COD)₂] occurred quickly after combination of the substrates; upon combination the colours of both reaction mixtures turned from yellow/orange to brown and NMR analysis indicated full conversion after 15 minutes of reaction time already. Crystals of both complexes were obtained by vapour diffusion crystallization where the Ni(I) and Ni(II) complexes were dissolved in C₆D₆ or C₇H₈ in the case of complex **9** and in DCM in the case of complex **10**. In both cases the used precipitant was hexane. The crystal structures will be discussed in the corresponding chapters and comparisons between the different structures will be made in chapter 3, subsection 5.2.1.



3.2.3. Ni(I) analysis

Analysis of the Ni(I) complex was composed of a multitude of methods. As can be seen in the crystal structure in Figure 27, the comproportionation of $[\text{Ni}(\text{COD})_2]$ and $[\text{NiCl}_2(\text{DME})]$ with the ligand yields together with ligand **5** a tetrahedral complex where the ketone is coordinated to the nickel metal centre.

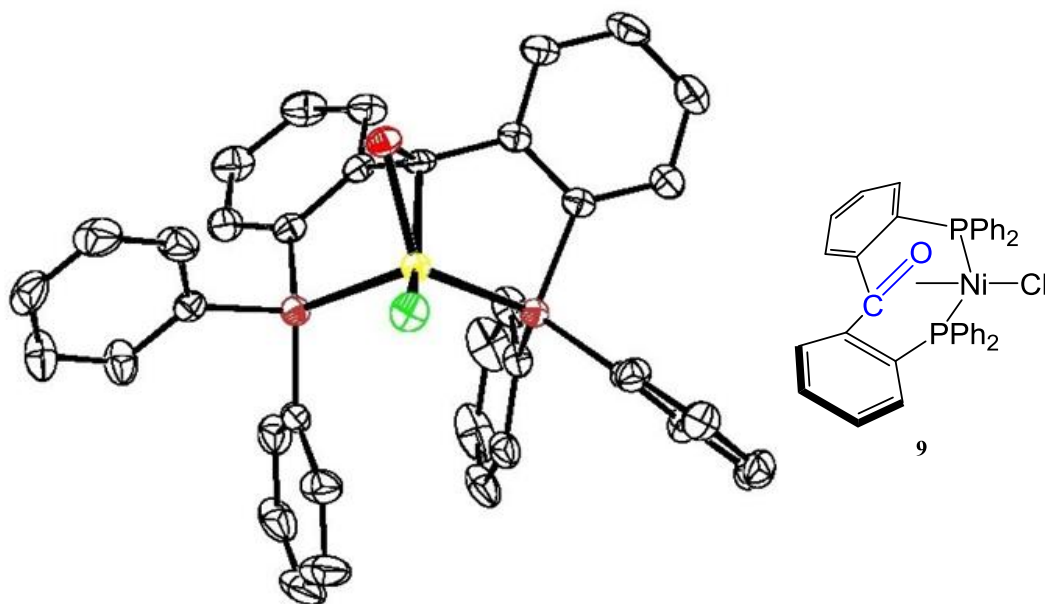


Figure 27: Picture of the crystal structure of $[\text{Ni}(\text{I})\text{Cl}(\text{DPK})]$ complex **9** as measured of the obtained red crystals. Hydrogen atoms have been omitted for clarity. Carbon is shown in black, oxygen in red, phosphorus in violet, chlorine in green and nickel in yellow.

3.2.3.1. $[\text{Ni}(\text{I})\text{Cl}(\text{DPK})]$ NMR analysis

Initial ^1H -NMR experiments showed that product material of the comproportionation of $[\text{Ni}(\text{COD})_2]$ and $[\text{NiCl}_2(\text{DME})]$ with ligand **5** contained paramagnetic material. This property of paramagnetism is expected for a Ni(I) complex, as both in the tetrahedral and square planar configuration the nickel(I)chloride complex possesses an uncoupled electron which causes the complex to be paramagnetic. However, the complex was expected to contain nothing but paramagnetic material aside from residual solvent peaks. Once the complex had been isolated in its crystalline form, some additional ^1H -NMR measurements were performed on dissolved crystals. One of the obtained spectra is shown in Figure 28. As can be observed, the spectrum also shows diamagnetic material apart from the residual THF solvent peaks at 1.8 ppm and 3.6 ppm and the laboratory grease peak at 0.2 ppm.

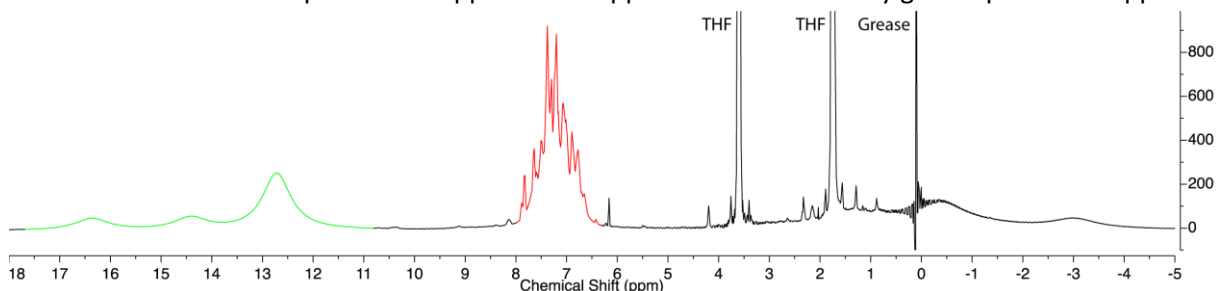


Figure 28: ^1H -NMR of crystalline $[\text{Ni}(\text{I})\text{Cl}(\text{DPK})]$ material. Used for the measurement are an acquisition time of 0.2 s and a relaxation time of 0.1 s to improve spectrum quality.

Possibly, the diamagnetic signals in the phenyl region originate from dimerization of the monomeric Ni(I) complex. As the coordination of the ligand to nickel(I)chloride yields a 17 VE complex, it would not be very surprising if the molecule reacts with another Ni(I)-monomer to equilibrate with an 18 VE dimer complex which is diamagnetic because of the trigonal bipyramidal geometry around the Ni(II) centres (**11**). It is known for some Ni(I)-complexes to form Ni(II) dimers^[21,23]. The monomer-dimer equilibrium has been visualized in Figure 29.

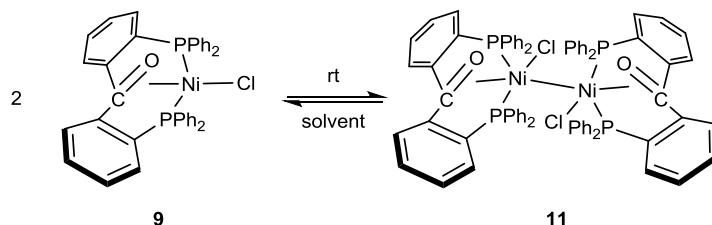


Figure 29: The 17 VE Ni(I)chloride diphosphine-ketone complex and its possible structure after dimerization to yield the 18 VE dinickel complex **11**.

Another result that supports the presence of diamagnetic material in the solution of the crystalline material is found in the ³¹P-NMR spectrum of the compound. Although no signals should be observed in this spectrum because of extreme peak broadening due to the paramagnetism of the complex, a sharp singlet peak is observed at a chemical shift of 32.2 ppm. Were it that only paramagnetic material was present in the sample, no peaks had been observed in the ³¹P-NMR spectrum. The fact that a singlet signal is present indicates that there is diamagnetic material present, which is in accordance with the ¹H-spectrum.

In order to establish this hypothesis further, ¹H-VT-NMR measurements were done on a sample that contained complex **9** dissolved in d-THF. If the dimerization happens spontaneously and the mixture is continually equilibrated, variation of the temperature would lead to variation in the composition of the mixture. This variation could then be observed by comparing the integrals of the corresponding peaks in the ¹H-NMR spectrum. The ratios between the diamagnetic and paramagnetic material at diverse temperatures have been compiled in table 4. An overlay of the measurements which were done at -75°C, -50°C and -30°C is shown in Figure 30

The relative amount of paramagnetic material increases as the temperature goes up. This observation was expected, as the paramagnetic part of the spectrum corresponds to the monomeric form of the complex. Not only does this measurement show that upon increasing the temperature more monomeric material is generated, it also shows that the paramagnetic material can be converted to diamagnetic material and vice versa.

<i>Temperature (°C)</i>	<i>Diamagnetic material</i>	<i>Paramagnetic material</i>
-75	1.00	1.13
-50	1.00	1.19
-30	1.00	1.24

Table 4: Relative integral values for the dia- and paramagnetic material present during the ¹H-VT-NMR experiment. Values for relative integrals correspond to the areas span the region from 6-8 ppm for the diamagnetic material shown in red in Figure 28 and from 10-26 ppm for the paramagnetic material shown in green in Figure 28. For these measurements, d-THF was used as solvent and measurement parameters were optimized for paramagnetic sample material (acquisition time 0.2 s, relaxation delay 0.1 s).

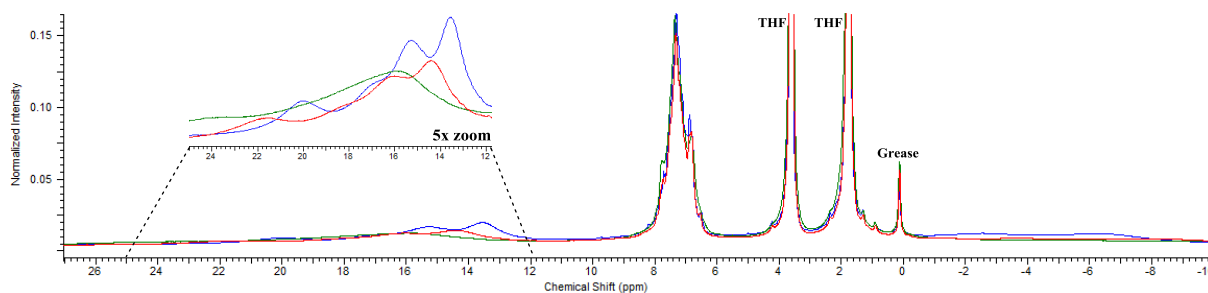


Figure 30: ^1H -NMR spectrum overlay of the VT-NMR experiment done on a d-THF solution of complex **9**. The measurement at -75°C is shown in green, the measurement at -50°C in red and the measurement at -30°C in blue. As can be seen, the spectrum remains mostly the same except for the paramagnetic signals from 12 to 18 ppm and -8 to -2 ppm.

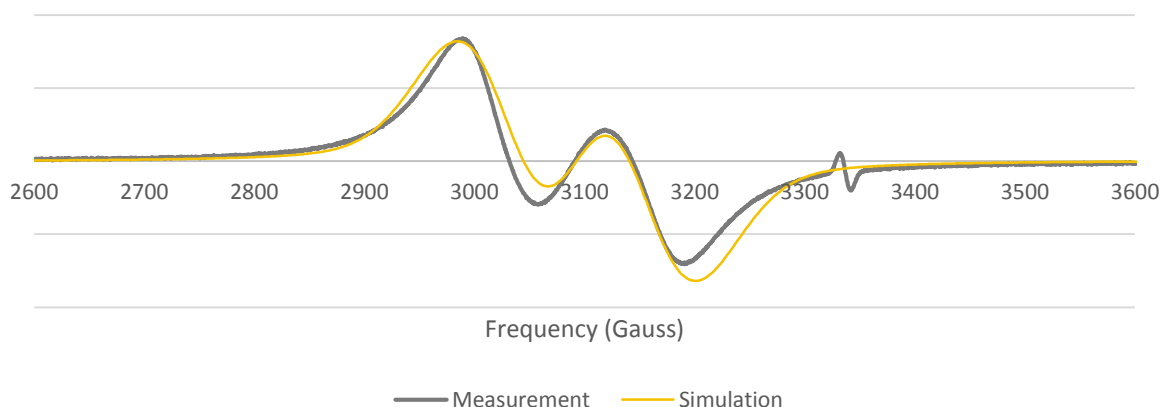
3.2.3.2. $[\text{Ni}(\text{I})\text{Cl}(\text{DPK})]$ IR analysis

Preparation of the sample for the FT-IR measurement was performed by grinding several milligrams into dried KBr and pressing a pellet out of this mixture under inert atmosphere. The IR measurement yielded a spectrum which does not include a sharp peak around 1650 cm^{-1} corresponding to an uncoordinated carbonyl vibration. The spectrum contains a broad peak around 1642 cm^{-1} , however. This peak may be caused by moisture present in the KBr or might arise from the diamagnetic complex formed. The spectrum also includes several peaks around 1300 cm^{-1} all of which may correspond to the energy of the C=O stretch vibration of a nickel-coordinated ketone. The peak at 1297 cm^{-1} may correspond to the carbonyl functionality, though the spectrum also shows two peaks close to each other at 1332 cm^{-1} and 1340 cm^{-1} . Possibly, the peak at 1297 cm^{-1} might correspond to the monomeric paramagnetic complex whilst the peaks at 1332 cm^{-1} and 1340 cm^{-1} might correspond to the two carbonyl stretch vibrations found in the dimeric diamagnetic form of the complex. However, this is all speculation; the most important information which can be extracted from the IR measurement is that the carbonyl moiety lies coordinated to the nickel centre. Other than that, the spectrum serves as a fingerprint of the complex.

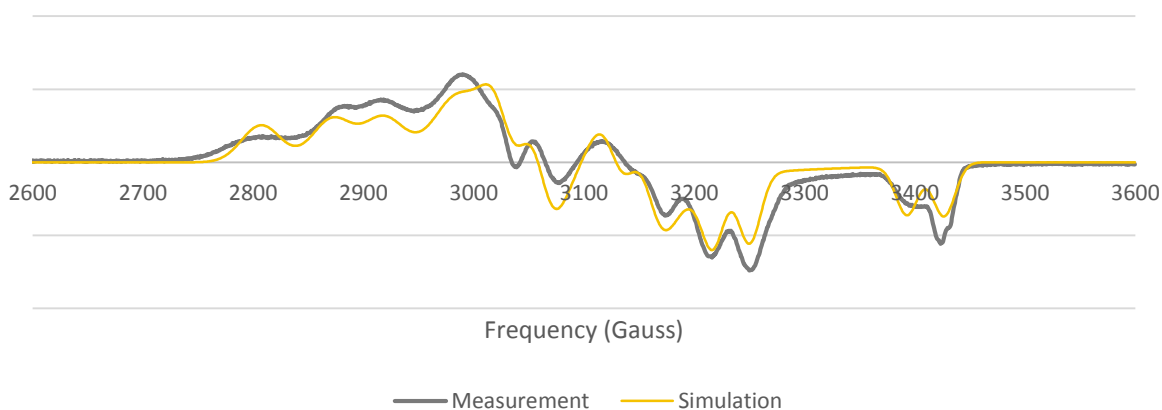
3.2.3.3. $[\text{Ni}(\text{I})\text{Cl}(\text{DPK})]$ EPR analysis

About 1 mg of **9** was dissolved in dry degassed C_7H_8 under inert conditions and the resulting solution was filtered to ensure no solid particles remained in the mixture. This sample was transferred to a quartz EPR tube and an EPR measurement was performed. The first measurement was done at room temperature (300 K). Thereafter, the sample was taken out of the EPR machine, the measurement cavity was cooled down to 100 K and the sample reinserted so that a frozen glassy toluene sample would be obtained. Under these conditions, another measurement was done. Both measurements and simulations can be seen in Figure 31.

[Ni(I)Cl(DPK)] (9) at 300 K



[Ni(I)Cl(DPK)] (9) at 100 K



The general shapes of the measurements at different temperatures differ greatly; this is due to anisotropy introduced by freezing the sample. The measurement at room temperature shows a broad doublet peak at a g -factor value of 2.17 (3075 Gauss) with a broadness of about 400 Gauss. The broadness and upward shift with regard to organic radical molecules correspond to an electron hosted in a metal d -orbital. The doublet multiplicity indicates that the free electron couples heavily with one of the present EPR-active nuclei. The nucleus to which the electron couples, is most likely a ^{31}P -nucleus.

DFT calculations were performed to rationalize the result of the electron only heavily coupling to one of the two phosphori. After Gibbs free energy optimization of the complex structure, the isotropic and anisotropic Fermi contacts were calculated for the atoms present in the molecule. Results of this calculation for the phosphorus nuclei are shown in table 5.

<i>Nucleus</i>	$^{31}\text{P}1$			$^{31}\text{P}2$		
	<i>Isotropic Fermi contact (MHz)</i>	419			45	
<i>Anisotropic spin dipole couplings (MHz)</i>	x	y	z	X	y	z
	-12	-12	24	-7	-5	12

Table 5: Isotropic Fermi contacts and anisotropic spin dipole couplings for the two phosphorus nuclei in Ni(I) complex 9 as calculated by means of DFT.

The results show a difference between the two phosphori. The order of magnitude with which the phosphori differ with regard to the isotropic Fermi contact is about 10. For the anisotropic spin dipole couplings, this order of magnitude equals approximately two. Clearly, the phosphori are chemically different.

Visualization of this difference was done by mapping a spin density plot of the complex. This plot can be seen in Figure 32. The plot shows that only one of the two phosphori has a strong interaction with the single electron occupying the SOMO of the complex. This explains the doublet structure as experimentally observed, as phosphorus is the only element in the complex that has a naturally abundant EPR-active isotope.

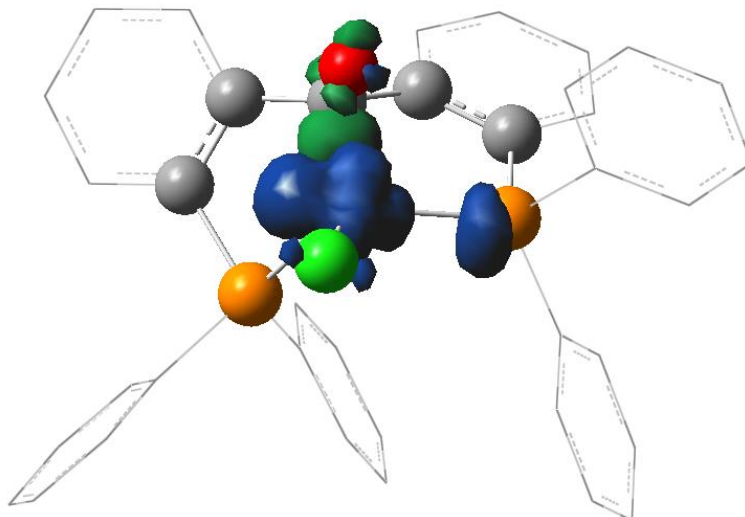


Figure 32: Surface density plot of Ni(I) complex 9 after optimization of the geometry by DFT. MO=0.02, Isovalue =0.004. To the plot non-relevant phenyl groups have been shown in wireframe and hydrogen atoms have been omitted for clarity. Carbon is shown in grey, oxygen in red, phosphorus in orange and nickel in green. Picture generated using GaussView 5.0.8.

The data acquired by doing the calculation could be used as initial values for simulations of the spectra. The EPR spectra and corresponding simulations can be found in the addendum. The simulated values for the g -factor of the signal, isotropic Fermi contacts and anisotropic spin dipole couplings through consequent optimization of the simulation are shown in table 6.

<i>Temperature (K)</i>	<i>100</i>			<i>300</i>
<i>g-factor</i>	<i>g(x)</i>	<i>g(y)</i>	<i>g(z)</i>	2.177
	2.325	2.175	2.026	
<i>Coupling $^{31}P^1$ (MHz)</i>	<i>A(x,x)</i>	<i>A(y,y)</i>	<i>A(z,z)</i>	380
	360	300	500	
<i>Coupling $^{31}P^2$ (MHz)</i>	<i>A(x,x)</i>	<i>A(y,y)</i>	<i>A(z,z)</i>	-
	210	100	95	

Table 6: Isotropic Fermi contacts and anisotropic spin dipole couplings for the two phosphorus nuclei in Ni(I) complex 9 as experimentally derived by means of optimization of simulated spectra. For the measurement at 100 K, where the sample is encapsulated in glassy toluene, the coupling specifies the anisotropic spin dipole coupling. For the measurement at 300 K, the coupling specifies the isotropic Fermi contact.

3.2.3.4. [Ni(I)Cl(DPK)] CV analysis

The cyclic voltammogram of **9** shows a quasi-reversible Ni(0)/Ni(I) couple with $E_{1/2}$ at -1.38 V versus [Cp₂Fe]⁺/[Cp₂Fe] with an oxidation-reduction distance of 0.33 V. The oxidation peak of this species is much less intense than the reduction feature, which possibly implies that the Ni(0) species reacts to redox non-active products. No other reduction or oxidation process was observed for complex **9**.

3.2.4. Ni(II) analysis

Besides using $[\text{NiCl}_2(\text{DME})]$ in a comproportionation with $[\text{Ni}(\text{COD})_2]$ and ligand **5**, the $[\text{NiCl}_2(\text{DME})]$ was also used on its own in a complexation with the diphosphine-ketone **5**. This reaction was proceeded in DCM and yielded the complex as shown earlier in Figure 26. The geometry as obtained from an X-ray diffraction measurement can be seen in Figure 33. The tetrahedral nickel(II)-complex **10** incorporates the ligand **5** as a bidentate ligand from which the carbonyl moiety is not coordinated to the nickel. This structure stands in sharp contrast to the structures of complexes **8** and **9** where the ketone function is coordinated to the nickel metal centre. Further results of this analysis can be found in chapter 3, subsection 5.2.1. Results of other analyses are discussed in this chapter.

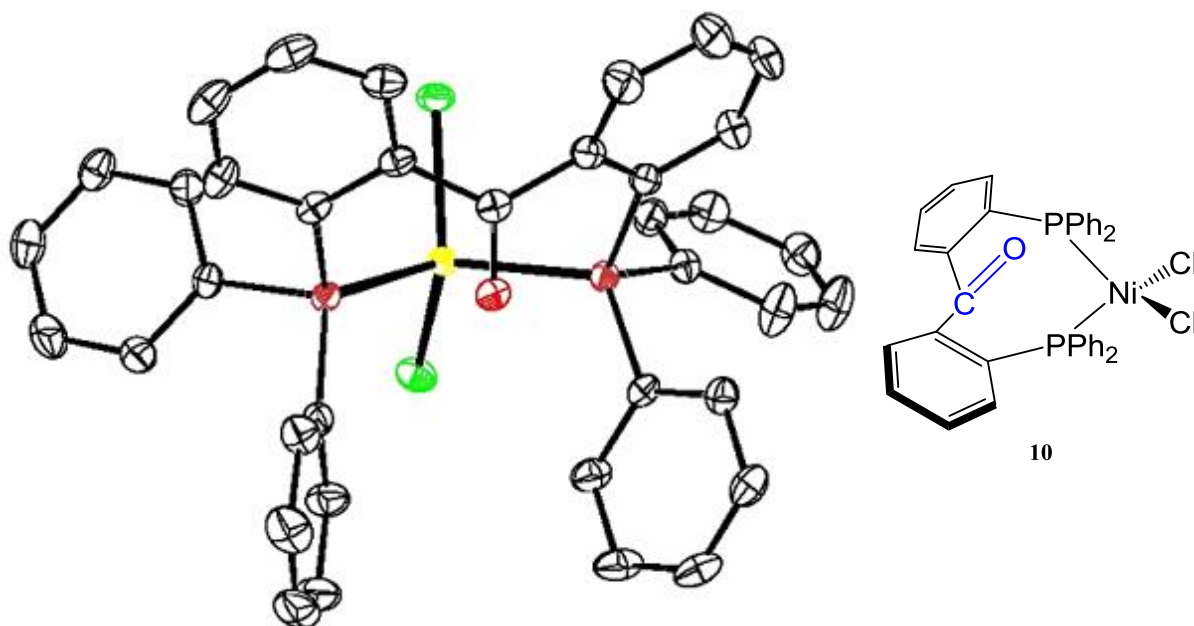


Figure 33: Picture of the crystal structure of $[\text{Ni}(\text{II})\text{Cl}_2(\text{DPK})]$ complex **10** as measured of the obtained brown crystals. Hydrogen atoms have been omitted for clarity. Carbon is shown in black, oxygen in red, phosphorus in violet, chlorine in green and nickel in yellow.

3.2.4.1. $[\text{Ni}(\text{II})\text{Cl}_2(\text{DPK})]$ ^1H -NMR analysis

Analysis by ^1H -NMR showed that the generated Ni(II) complex was paramagnetic. The ^1H -NMR of the complex is shown in Figure 34. For a Ni(II) d^8 complex, it is possible to access paramagnetic behaviour by assuming a tetrahedral or octahedral geometry. Of these geometries, the octahedral geometry can be considered implausible for the complex to assume because of the bulkiness of the ligand and small size of the nickel metal centre. Other than this observation, no other conclusions could be drawn from the paramagnetic NMR spectrum: the resonance signals have shifted significantly and have been broadened to such an extent that multiplicity is badly resolved. A tetrahedral configuration around the nickel centre would give a four-coordinate complex. As the $[\text{NiCl}_2(\text{DME})]$ contains two nickel(II)-bound chlorines, the ligand would provide two coordination sites. So, four-coordination implies that either one of the phosphori, one of the chlorines or the ketone $\text{C}=\text{O}$ would not be coordinated to the nickel centre. Due to the paramagnetism of the complex, no signals corresponding to **10** were found in the ^{31}P - and ^{13}C -NMR spectra.

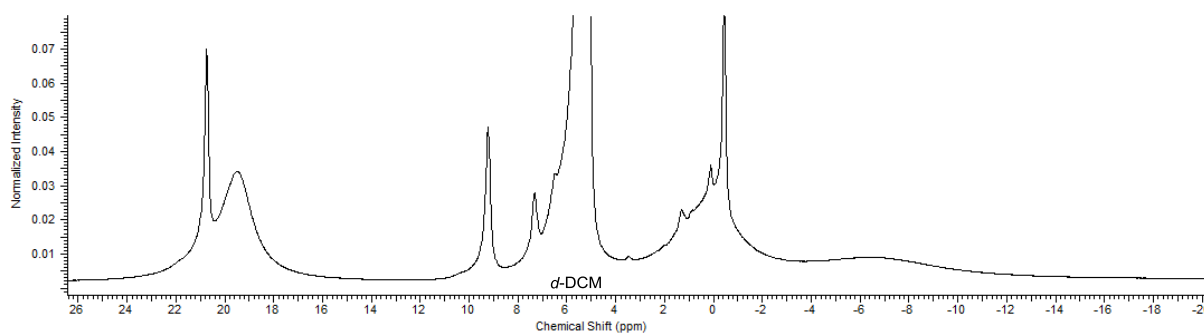


Figure 34: $^1\text{H-NMR}$ of the $[\text{Ni(II)Cl}_2(\text{DPK})]$ complex. For this measurement, 7.7 mg of complex was dissolved in 0.38 g 1:50 DCM/*d*-DCM solvent and measurement parameters were optimized for paramagnetic sample material (acquisition time 0.2 s, relaxation delay 0.1 s).

3.2.4.2. $[\text{Ni(II)Cl}_2(\text{DPK})]$ Evans Method

The amount of uncoupled electrons in a complex can be determined using the Evans Method. The sample from which the $^1\text{H-NMR}$ spectrum was recorded, was the same sample as used for this method. As the sample had been made with 1:50 DCM/*d*-DCM, it was supplied with a capillary filled with the same 1:50 DCM/*d*-DCM solution.

From the difference in chemical shifts between the solvent residual signals for the solvents inside and outside of the capillary, the magnetic susceptibility could be calculated using formulas (2) and (3)^[45]:

$$\chi_M = \frac{3\Delta f}{1000 \cdot f \cdot c} \quad (2) \quad \mu_{eff} = \sqrt{\frac{3k}{N_0 \cdot \mu_0 \cdot \mu_B^2} \cdot T \cdot \chi_M} = 798 \sqrt{T \cdot \chi_M} \quad (3)$$

where χ_M is the molar susceptibility of the sample in $\text{m}^3 \text{mol}^{-1}$, Δf is the difference in chemical shift of a set of protons in Hz, f is the frequency of operation of the spectrometer in Hz, c is the concentration of the sample in mol dm^{-3} and T is the temperature of the sample in K.

The chemical shift difference between the DCM signals of the inner and outer tubes was measured at room temperature. A zoom of the spectrum used for the Evans Method is shown in Figure 35. The difference in chemical shift for the two DCM solvent residue signals is 217 Hz. Using these formulas, the effective magnetic susceptibility for the complex was calculated and found to have a value of 2.8. The value of 2.8 corresponds to the theoretical value of 2.82 for complexes with two unpaired electrons.

3.2.4.3. $[\text{Ni(II)Cl}_2(\text{DPK})]$ IR analysis

As had been established that either one of the phosphori or the ketone is not coordinated to the nickel metal centre if the system is tetrahedral, a FT-IR analysis was performed. If a peak had been found at the vibrational frequency of about 1650 cm^{-1} and no peak corresponding to a coordinated ketone, as observed for the Ni(I) complex **9** around 1300 cm^{-1} , the ketone would have been the uncoordinated ligand part. Were it that the spectrum had not contained this distinctive vibration at about 1650 cm^{-1} but that it had contained a peak around 1300 cm^{-1} , it could have been concluded that the ketone was coordinated to the metal centre. This would require, for the complex to be in a tetrahedral configuration, that one of the phosphine groups was unbound to the nickel centre.

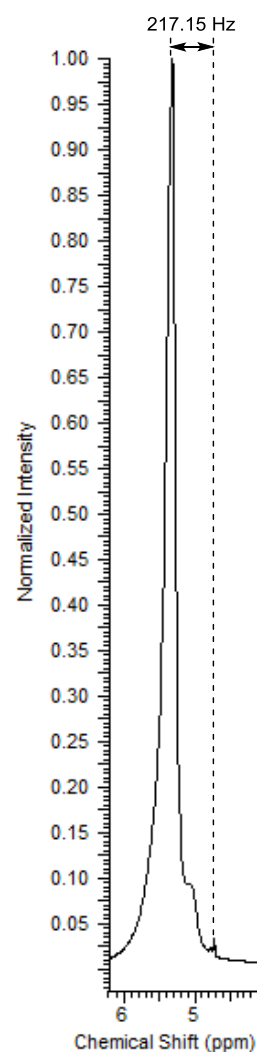


Figure 35: Zoom of the DCM solvent residual signals in the inner and outer tubes in the Evans Method $^1\text{H-NMR}$ measurement of complex 10.

The FT-IR spectrum showed a sharp peak at 1634 cm⁻¹ in accordance with a non-metal-coordinated carbonyl vibration. This is a clear indication that the carbonyl functionality of the ligand is not coordinated to the nickel metal centre. However, based on the addition of this result alone, it cannot be concluded that the complex has a tetrahedral 16 VE structure where both phosphori and the chlorines are coordinated to the Ni(II) centre. The XRD geometry determination provides the decisive conclusion on the true geometry around the metal centre in the crystals.

It might be surprising that a 16 VE Ni(II) species can exist whilst an additional ligand is within close proximity and can be coordinated to the nickel-centre without too much effort in a relatively uncrowded complex. But even though normally it is expected for organometallic complexes to prefer an 18 VE coordination, it has been established that *d*⁸ Pd(II) and *d*⁸ Pt(II) tend to avoid the 18 VE configuration^[33]. Also, the available carbonyl ligand is only a weak ligand which will mostly accept the electrons provided by the metal centre. For an oxidized Ni(II) centre whose electrons have already been withdrawn by other ligands, the energy gained from binding the carbonyl moiety might not be a lot. Amongst that line, it is not very surprising that the *d*⁸ Ni(II) centre prefers the four-coordinate 16 VE configuration over the 18 VE configuration under the by the chelating ligand imposed geometrical constraints.

3.2.4.4. [Ni(II)Cl₂(DPK)] CV analysis

Besides the proof obtained from the Evans Method measurement, another proof of complex **10** being a Ni(II) complex was found in Cyclic Voltammetry analysis. The cyclic voltammogram of **10** shows two redox couples within the solvent limit. The presence of the two subsequent redox couples indicates that the solution contains compounds that can be reduced at two different potentials. As it is very rare for nickel to access the Ni(III) or higher oxidation states, it can be assumed that the complex contains utmost Ni(II) and not any further oxidized nickel centres. Starting from Ni(II), quasi-reversible redox couple found with *E*_{1/2} at -1.50 V versus [Cp₂Fe]⁺/[Cp₂Fe] with an oxidation-reduction distance of 0.18 V can tentatively be assigned to a Ni(II)/Ni(I) couple. At a lower potential than that of the Ni(I)/Ni(II) couple, a non-reversible couple is found with *E*_{1/2} at -2.41 V versus [Cp₂Fe]⁺/[Cp₂Fe] with an oxidation-reduction distance of 0.70 V. This couple can tentatively be assigned to a Ni(I)/Ni(0) couple. Once again, the couples are at most only quasi-reversible leading to the conclusion that during the reaction formed products are being trapped in redox-non-active states. For the Ni(I) complex which is being generated, one of these redox-non-active products might be the dimerization product.

3.2.4.5. [Ni(II)Cl₂(DPK)] Elemental analysis

For Elemental Analysis, 10 mg of crystalline Ni(II) complex was placed in a small vial which was placed in a round-bottomed flask and put under vacuum overnight. Results are shown in table 7.

<i>Element</i>	<i>Calculated content (%)</i>	<i>Experimental content (%)</i>
<i>C</i>	65.46	65.21
<i>H</i>	4.77	4.19

Table 7: Calculated and experimental values for the carbon and hydrogen contents of the crystalline sample of complex 10 sent for Elemental Analysis.

3.2.5. Comparison between the various nickel-based complexes

The different synthesized nickel-based complexes make for a good comparison. Earlier discussed results already provide information for a comparison between the three synthesized complexes.

When compared using NMR, the complexes differ greatly from each other. Whilst the diamagnetic **8** and dimer form of **9** (**11**) both give signals in the phenyl region in $^1\text{H-NMR}$, it is difficult to compare the complexes based on the peaks found in this region. The peaks in the phenyl region are ill-defined for **11** and do not allow for a reliable comparison. Comparison between the $^{31}\text{P-NMR}$ measurements shows that it is possible that the phosphori in the complexes can be chemically distinct or equivalent on the NMR timescale. The $^1\text{H-NMR}$ spectra of complexes **9** and **10** can also be related to each other, but as the spectra do not yield a lot of information on the geometry or chemistry of the complexes by themselves, similarities between the spectra might not even be correlated to structural or chemical similarities between the Ni(I)- and Ni(II)-complexes.

IR analysis provides one distinct feature that can be compared throughout the complexes, however. Presence of an intense sharp peak around 1650 cm^{-1} in the spectrum of $[\text{Ni(II)Cl}_2(\text{DPK})]$ and the DPK indicates presence of an uncoordinated carbonyl functionality. Absence of this peak in the spectra of $[\text{Ni(0)(DPK)(PPh}_3)]$ and $[\text{Ni(I)Cl}(\text{DPK})]$ indicates that in complexes **8** and **9** the carbonyl group is not uncoordinated to the metal centre. In addition, the spectra of compounds **7**, **8** and **9** all show peaks at $\pm 1300\text{ cm}^{-1}$. These peaks have been tentatively assigned to the stretch vibrations of the nickel-coordinated ketones.

More comparative commentary can be given on the XRD crystal structures and UV-Vis spectra of the complexes and the free ligand.

3.2.5.1. Crystal structure comparison

Crystal structures of the three different complexes are shown in Figure 36. Relevant bond lengths and angles have been provided in table 8. More information has been provided in the addendum.

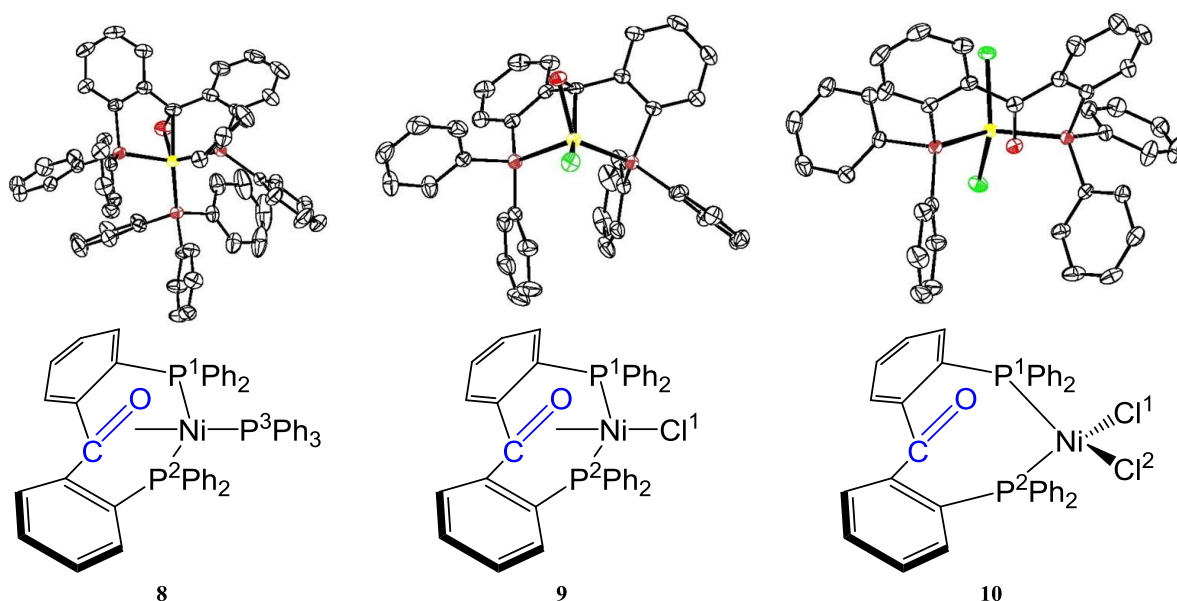


Figure 36: XRD crystal structures for the $[\text{Ni(0)(DPK)(PPh}_3)]$, $[\text{Ni(I)Cl}(\text{DPK})]$ and $[\text{Ni(II)Cl}_2(\text{DPK})]$ complexes. Hydrogen atoms have been omitted for clarity. Carbon is shown in grey, oxygen in red, phosphorus in violet, chlorine in green nickel in yellow. The deviation value for the structure determinations are respectively $R=0.04$; $R=0.04$; $R=0.02$.

<i>Complex</i>	<i>[Ni(0)(DPK)(PPh₃)]</i>	<i>[Ni(I)Cl(DPK)]</i>	<i>[Ni(II)Cl₂(DPK)]</i>
Bonds (Å)	Complex 8	Complex 9	Complex 10
<i>Ni-P¹</i>	2.158	2.257	2.346
<i>Ni-P²</i>	2.239	2.236	2.337
<i>Ni-X/L</i>	2.205	2.226	2.210
<i>Ni-Cl²</i>	-	-	2.234
<i>Ni-C</i>	2.000	2.005	3.403
<i>Ni-O</i>	2.009	1.973	3.101
<i>C=O</i>	1.330	1.309	1.230
Angles (°)	Complex 8	Complex 9	Complex 10
<i>P¹-Ni-P²</i>	120.6	107.6	113.0
<i>P¹-Ni-X/L</i>	110.1	115.5	108.5
<i>P²-Ni-X/L</i>	111.7	109.9	103.6
<i>P¹-Ni-Cl²</i>	-	-	97.6
<i>P²-Ni-Cl²</i>	-	-	100.6
<i>Cl¹-Ni-Cl²</i>	-	-	133.3
<i>P¹-Ni-CO</i>	101.1	102.1	59.2
<i>P²-Ni-CO</i>	91.2	91.5	58.5
<i>X/L-Ni-CO</i>	120.8	126.3	88.9
<i>Cl²-Ni-CO</i>	-	-	137.7
<i>P¹-C-P²</i>	82.3	76.6	79.5
<i>O-Ni-C</i>	38.7	38.4	21.1

Table 8: Comparison of several relevant bond lengths and angles for the comparison of the three crystal structures of the formed nickel-based monomers. C specifies the ketone carbon. X/L specifies the third ligand in the complex; for $[\text{Ni}(\text{O})(\text{DPK})(\text{PPh}_3)]$, this specifies the P^3 atom, for $[\text{Ni}(\text{I})\text{Cl}(\text{DPK})]$ and $[\text{Ni}(\text{II})\text{Cl}_2(\text{DPK})]$ this specifies the Cl^1 atom.

For the three different complexes, the nickel-phosphorus bonds deviate slightly; increased oxidation of the nickel metal centre increases the nickel-phosphorus bond distance. The nickel-phosphorus bond lengths are also dependant on other modifications that change the electronic structure around the nickel centre. For example, the presence of chlorine will also have an effect on the nickel-phosphorus bond lengths.

The change in oxidation state of the nickel seems to have another effect. In the Ni(0)- and Ni(I)-complexes the ketone function of the biphosphino-ketone ligand is coordinated to the nickel creating 18 VE and 17 VE complexes. It could be expected for the Ni(II)-complex that the ketone would also be coordinated to the metal centre to create an 18 VE complex. However, in line with the results from FT-IR, the XRD results show that the ketone is not coordinated to the nickel and that the Ni(II) complex assumes a tetrahedral coordination, just like the monomeric Ni(0)- and Ni(I) complexes.

The fact that the ketone is not coordinated to the nickel in **10** can be concluded from the significantly longer Ni-C and Ni-O distances (respectively 3.40 Å and 3.10 Å in $[\text{Ni}(\text{II})\text{Cl}_2(\text{DPK})]$ with respect to 2.00 Å and 2.01 Å in $[\text{Ni}(\text{O})(\text{DPK})(\text{PPh}_3)]$) and from the carbon-oxygen bond length in the different complexes: for the coordinated ketone, this distance has increased to 1.33 Å for complex **8** and to 1.31 Å for complex **9**. In complex **10** where the carbonyl functionality is not coordinated to the nickel, the distance is about 10% shorter, with a bond length of 1.230 Å. This value is closer to the value of 1.213 Å found by K. Ding et al.^[38] for the uncomplexed DPK molecule. As an example, compared to the bond length of 1.43 Å of the single-bonded carbon-oxygen in ethanol, the observed length of 1.33 Å lies just in between the two values.



It is known for fully tetrahedral compound, such as methane, that these angles have a value of 109.5°. The crystal structures show good correlation with this value and it can be assumed that the nickel centres have assumed a (distorted) tetrahedral configuration. The complexes can be regarded to be in a distorted tetrahedral configuration. For complex **8**, the crystal structure shows that the angle between the phosphori of the DPK ligand (120.6°) is larger than the angles between the triphenylphosphine phosphorus and the DPK ligand phosphori (110.1°; 111.7°). In contrast, the angle between the phosphorus and ketone is larger for the phosphorus in the PPh₃ ligand (120.8°) than for the phosphori of the DPK ligand (101.1°; 91.2°). This is a logical result, as the phosphori in ligand **5** are being pushed towards the ketone by being indirectly bound to it. Overall, this collection of angles approximates a distorted tetrahedral configuration. As the complex contains three different ligands, this result is in agreement with expectations.

In complex **9** the angle between the DPK phosphori (107.6°) is smaller than the phosphorus-nickel-chlorine angles (109.9°; 115.5°). This is in sharp contrast to the situation in complex **8** where the opposite was observed. An explanation for this is found in the difference in character between the L-type PPh₃ ligand and the X-type Cl ligand. Whereas the weakly bound PPh₃ ligand can accept electrons in its unoccupied σ^* orbital, the Cl ligand will bind more strongly and withdraw electrons from the nickel centre^[33]. Because of the presence of the chlorine, the DPK phosphori are bent away and the angle between them is decreased. It is remarkable that the angles between the DPK phosphori and the ketone remains about the same with the exchange of the PPh₃ ligand for a Cl ligand (91.5° and 102.1° for complex **9** compared to 91.2° and 101.1° respectively for complex **8**).

Complex **10** seems to be the tetrahedral complex with the strongest distortion. In this Ni(II)-complex, the two DPK phosphori and two chlorines are coordinated to the metal centre. Whilst this complex only includes two different ligands coordinated to nickel, the deviation in angles in this complex is greater than in the other complexes. The angle between the DPK phosphori (113.0°) is a bit larger than the value for a non-distorted tetrahedral geometry. The angle between the two chlorine ligands (133.3°) is extremely big for a tetrahedral configuration. This big angle shows that the chlorines repel each other significantly. The two big angles are compensated by the smaller angles between the phosphori and the chlorines which range from 97.6° to 108.5°.

The bond angles can also be used to determine whether the ketone is coordinated to the nickel in the complexes. Upon coordination, the carbonyl carbon rehybridizes from a trigonal planar sp^2 hybridization where the angles between three substituents are about 120° and the total sum of angles is 360° towards a tetrahedral sp^3 hybridization where the angles between the same three is 109.5° and the total sum of the angles is 328.5°. Angle magnitudes for the carbonyl functionality in the synthesized complexes can be found in table 9. For complex **10**, the sum of these angles equals 360°. In the other complexes, these angles are slightly smaller summing up to a total of 350.5° and 353.5° for the Ni(0)- and Ni(I)-complexes respectively. As the sums of the angles are somewhere in between the angle sums for sp^2 - and sp^3 -hybridization, it can be concluded that the carbon is neither sp^2 - or sp^3 -hybridized. This conclusion confirms that the coordination of the carbonyl moiety of the ligand in complexes **8** and **9** is in an intermediate state between the Dewar-Chatt-Duncanson π -bond and metalacycle extremes. As of such the nickel metal centres, formally regarded as Ni(0) and Ni(I) centres for the respective complexes, are in terms of chemical properties perhaps better approximated as Ni(I) and Ni(II) complexes instead.

Fragment	Angle α ($^\circ$)	Angle β ($^\circ$)	Angle γ ($^\circ$)	Sum of angles ($^\circ$)
sp^2 carbon	120	120	120	360
5	119.3	120.5	120.0	359.8
8	117.7	116.8	116.0	350.5
9	119.2	117.5	116.8	353.5
10	126.1	117.4	116.1	359.6
sp^3 carbon	109.5	109.5	109.5	328.5

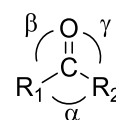


Figure 37: The annotation of the angles around the carbonyl functionality.

Table 9: Angles α , β and γ for the carbonyl moiety in sp^2 and sp^3 fragments and their values for **5**, **8**, **9** and **10**.

The P_1 -Ni- P_2 angle is of interest in another perspective too. The angle deviates significantly between the three complexes varying from 105.8° to 113.0° to 120.6° . The accessible variety in this angle is convenient in complex synthesis as the phosphori can not only adapt to one specific geometry like tetrahedral but can also be configured towards a range of geometries. It is important that the ligand allows for this geometrical accessibility, as it is possible that stabilization or modification of geometries is required to undergo the catalytic polar bond hydrogenation cycle. This configurational property generated in the ligand eight-membered ring can also be expressed in terms of the dihedral angle between the two ligand phenyl groups. An image with this specified dihedral angle (α , going from 1-2-3-4) is supplied in Figure 38.

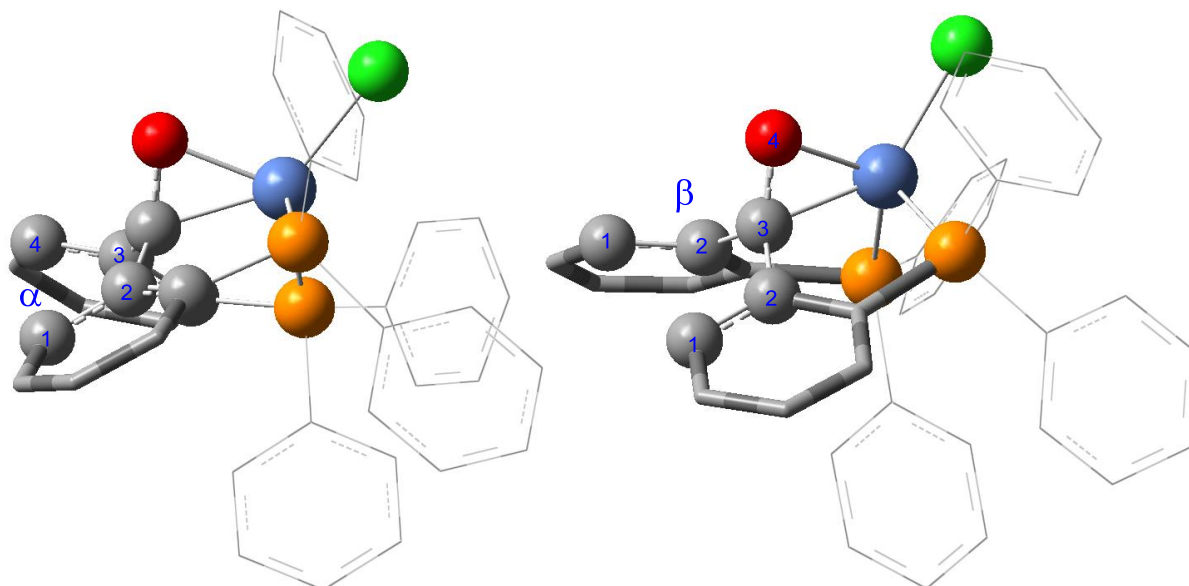


Figure 38: Specification of the dihedral angles α and β between the benzophenone chelating ligand's phenyl rings in Ni(II) complex **9**. The phenyl rings of the ligand have been depicted in tubes, the other phenyl rings in wireframe. Hydrogen atoms have been omitted for clarity. Carbon is shown in grey, oxygen in red, phosphorus in orange, chlorine in green, nickel in blue. The same angles were investigated in compounds **5**, **8** and **10**. Picture generated using GaussView 5.0.8.

Molecule	Angle α ($^\circ$)	Angle β_1 ($^\circ$)	Angle β_2 ($^\circ$)	Average $\beta_1\beta_2$ ($^\circ$)
5	73.7	128.2	143.4	135.8
8	31.5	68.0	108.0	88.0
9	35.7	69.5	115.4	92.5
10	9.1	138.4	148.9	143.7

Table 10: Values for dihedral angles α and β in molecules **5**, **8**, **9** and **10**.

This dihedral angle α varies significantly in the obtained crystal structures. Values for this angle in complexes **8**, **9** and **10** have been compiled in table 10. Important to note is that the uncomplexed ligand molecule only has a minor constraint on rotation around the ketone carbon-phenyl bonds. Angle

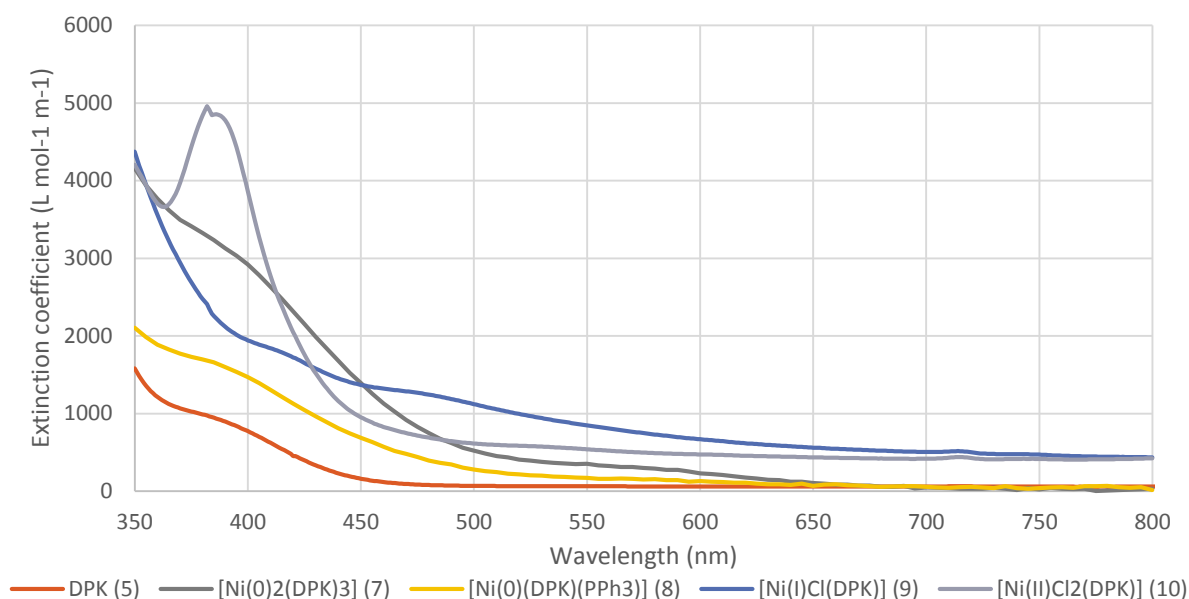
α is not fixed in solution for this molecule as all angle values will be accessible. Therefore, ligand **5** on its own has not been included in table 10. As can be seen from the data in table 10, the angle shows a significant difference between the complexes. Coordination to the nickel fixes the angle to $\pm 34^\circ$, but this angle drops to 9° when the ketone is not coordinated to the nickel. For a dihedral angle in an eight-membered ring, this shift of 25° is significant. Conclusively, a ligand was synthesised that binds to the nickel through the phosphori and, depending on the chemistry of the nickel centre, can opt to coordinate its ketone to the nickel or to refrain from carbonyl coordination.

However, the size of this angle for complexes **8** and **9** dictates that severe rearrangement of the molecule is needed to interchange between the anti- to the syn- conformations as described in chapter 3, subsection 2.2.1. By use of another ligand framework or introducing substituents on the phenyl rings, transposition between the two conformers at elevated temperatures can be locked and chiral catalysts can be synthesised.

Besides from the dihedral angle α , the dihedral angles β_1 and β_2 (going from 1-2-3-4) are also of interest. In the compound, two of these structurally similar angles are present; one on either side of the ketone. The reason of interest in this angle is that it describes how well developed the conjugated π -system of the benzophenone derived residue is. In a completely flat molecule where these dihedral angles both have a value of 180° , π -orbital overlap and conjugation are maximized. The flat configuration is restrained by the protons attached to the carbons labelled **1** in Figure 38. In a fully flat geometry, the nuclei of these protons would overlap.

In complexes **8** and **9** the values for angles β_1 and β_2 are approximately 70° and 110° respectively. In complex **10** where the ketone is not coordinated to the nickel and in the free ligand, these angles have values of 138° and 149° respectively for complex **10** and of 128° and 143° respectively for ligand **5**. These results show that the ketone, if not coordinated to the metal, maintains the conjugated π -system to some extent. In contrast, the nickel-coordinated ketones of complexes **8** and **9** seem to have broken up the π -system completely. The oxygen atoms of the carbonyls in these molecules stand nearly perpendicular to the phenyl rings, which is another indication that the carbonyl carbon atoms have shifted away from sp^2 -hybridizations towards sp^3 -hybridizations when coordinated to the nickel.

3.2.5.2. UV-Vis comparison



The complexes and ligand were compared in UV-Vis analysis as can be seen in Figure 39. For these measurements, a minor amount (1-4 mg) of complex/compound was dissolved in dried degassed C_7H_8 under inert conditions and the sample diluted to a concentration in the order of $\pm 50 \mu\text{M}$. The concentrations have been expressed in the extinction coefficient so that the spectra are normalized against each other. As can be observed, all of the molecules adsorb light in the visual part of the spectrum. Their adsorbance ranging from 350-450 nm explains their common yellow/orange/brown shade.

Ligand **5** and complexes **7** and **10** all show a peak at around 390 nm, which might be partially caused by the uncoordinated ketone moiety. This supports the earlier obtained results, which show that the $[\text{Ni}(\text{O})_2(\text{DPK})_3]$ complex **7** and the $[\text{NiCl}_2(\text{DPK})]$ complex **10** both contain an uncoordinated ketone. The $[\text{Ni}(\text{II})\text{Cl}_2(\text{DPK})]$ complex shows a sharp peak at 390 nm compared to the peaks of molecules **5** and **7**. This distinctive peak might originate from a charge-transfer transition from the organometallic d-electrons to unfilled higher bands in the molecule. If so, the band should be subject to concentration, temperature and solvent dependencies. Strikingly, this distinct transition is only observed for the Ni(II)-complex **10** and not for complex **9** which also contains an uncoupled electron in its ligand-hybridized d-orbital set. Possibly, this band requires the carbonyl functionality not to be coordinated to the nickel metal centre. Further research towards the origin of this band has not been performed.

It is remarkable that this result was obtained for in specific the Ni(II) complex **10** in combination with the results obtained from XRD showing that the metal assumes a tetrahedral configuration. This is because it is described in literature that in the chemistry of nickel(II) complexes with four ligands that orange and red complexes are square planar and diamagnetic, whilst the green and blue complexes are tetrahedral and paramagnetic^[46].

4. Conclusions

A convenient method for the synthesis of the benzophenone derived chelating ketone-diphosphine ligand **5** has been developed with an overall reaction yield of 48%. The product could be isolated successfully and was analysed by means of NMR, FT-IR, EPR, UV-Vis and ESI-MS. Elemental composition and structural configuration corresponded to the ligand structure as it was to be synthesised.

Ligand **5** was combined with various nickel sources in order to form three monomeric tetrahedral nickel-based diphosphine-ketone complexes. In addition, the dimeric complex **7** was isolated. The structures of these complexes were, where applicable, elucidated by means of various NMR techniques, FT-IR, UV-Vis, EPR, CV, EA and XRD. The complexations between $[\text{Ni}(\text{COD})_2]$ and **5** yielded two complexes (complexes **7** and **8**), depending on whether PPh_3 was present in the reaction mixture or not. The complexes were established to have the chemical formulas $\text{C}_{111}\text{H}_{84}\text{Ni}_2\text{O}_3\text{P}_6$ and $\text{C}_{55}\text{H}_{43}\text{NiOP}_3$ respectively. Addition of PPh_3 to complex **7** allows for conversion to complex **8**. Use of the $[\text{NiCl}_2(\text{DME})]$ salt in comproportionation to $[\text{Ni}(\text{COD})_2]$ gave paramagnetic Ni(I)-complex **9** with the chemical formula $\text{C}_{37}\text{H}_{28}\text{ClNiOP}_2$ which is believed to be in equilibrium with its dimeric form **11**. The equilibrium between the monomer and dimer is believed to be reliant on the generation of an 18 VE Ni(I) dimer opposed to a monomeric 17 VE Ni(I)-complex. This equilibrium has been shown to exist by means of VT- ^1H -NMR. Use of $[\text{NiCl}_2(\text{DME})]$ alone instead of the $[\text{Ni}(\text{COD})_2]$ resulted in synthesis of Ni(II)-complex **10** with the chemical formula $\text{C}_{37}\text{H}_{28}\text{Cl}_2\text{NiOP}_2$. This is the only complex for which it is observed through various analysis techniques that the carbonyl function is not coordinated to the nickel centre. Coordination of the ligand to the nickel metal centre seems to be oxidation-state dependant. The carbonyl functionality in the ketone is the most labile ligand to the nickel in complexes: oxidation of the nickel metal centre to Ni(II) causes the carbonyl functionality to shift away from the nickel centre.

As of yet, attempts at the hydrogenation of polar bonds in substrate molecules have not been performed. An investigation of the catalytic activity of the synthesised complexes in polar bond hydrogenation should be the next step in this research. Even though the direct hydrogenation of CO_2 has not been achieved, a foundation for the synthesis of variously oxidized diphosphine-ketone ligated nickel complexes and conceivable polar bond hydrogenation catalysts based on a first-row transition metal has been established.

5. Future Outlook

The application of the synthesized Ni(0)- Ni(I)- and Ni(II)- complexes in (polar bond) hydrogenation has to be further investigated. Addition of H₂ to the complexes could show in NMR if the complexes are to be hydrogenated if a stable species is generated through hydrogenation. A substrate scope can be tested to see to what extent the synthesized complexes are useful for hydrogenation of different functional groups. Possible unsaturated model substrates are simple ketones, imines, aldehydes or alkenes containing polar or non-polar bonds with varying extents of steric hindrance around the unsaturated reaction site. In this context, table 12 shows exemplary usable model substrates for functional groups which can be examined. Ultimately, carbon dioxide should be used as a substrate to fulfil the goal of CO₂ conversion to commodity chemicals and fuel catalysed by a cheap and abundant first-row transition metal based catalyst system.

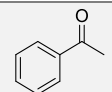
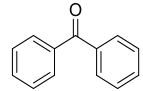
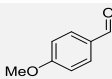
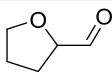
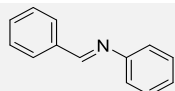
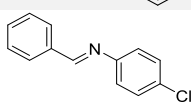
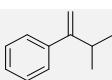
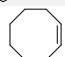
<i>Substrate</i>	<i>Functionality</i>	<i>Structure</i>
<i>acetophenone</i>	ketone	
<i>benzophenone</i>	ketone	
<i>4-methoxybenzaldehyde</i>	aldehyde	
<i>tetrahydrofuran-2-carbaldehyde</i>	aldehyde	
<i>N,1-diphenylmethanimine</i>	imine	
<i>(E)-N-(4-Chlorobenzylidene)aniline</i>	imine	
<i>(1-isopropylvinyl)benzene</i>	alkene	
<i>cyclooctene</i>	alkene	

Table 11: Various substrates to probe in hydrogenation reactions with corresponding functionalities and structures.

If catalytic conversion of these substrates is unsuccessful, the catalyst structure may need to be modified to improve catalytic hydrogenation capabilities. Catalytic test results might more specifically point out which direction to take. In general, the effect on the carbonyl coordination to the nickel should play a significant part in catalyst modification. Options to keep in mind are the inclusion of atoms or molecules that either vastly or finely change the electronic structure around the supposedly active site of the catalyst.

Ventures towards useful catalysis might also be enhanced by improvement of knowledge about the hydrogen coordination to the complexes. Combination of the synthesised complexes with polar σ -bonded diatomic molecules like HCl or HBr rather than the non-polar diatomic H₂ can show the effect of heterolytic coordination and allows for distinguishability between the anionic and cationic species. The information obtained through this experiment could also serve as being a model in establishing the reaction mechanism of optionally encountered hydrogenation reactions.

Also, it could be useful to synthesize the alcohol obtained from reduction of the ketone **5**. Complexation of this alcohol to the $[\text{Ni}(\text{COD})_2]$ and $[\text{NiCl}_2(\text{DME})]$ salts might yield the structure as earlier proposed in Figures 3 and 7 and depicted in Figure 40. Analysis of this structure in its isolated form might provide information very useful in the research towards an efficient catalyst.

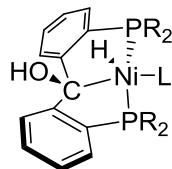


Figure 40: Structure of the complexes derived from complexation between the alcohol as possibly obtained from reduction of DPK ligand **5** and various nickel salts.

As has been investigated by R. Langer et al^[47] for iridium and by B. J. Coe et al^[48] for octahedral transition metal complexes based on Cr(0), Fe(II) and Co(II) amongst others and as calculated and shown for Ru(III) complexes^[35], the *trans*-influence of the ligand opposite the hydride has a major effect on the favourability of CO₂ insertion into M-H bonds. If CO₂ insertion into the metal-hydride bonds proves to be the challenging step in the homogeneously catalysed hydrogenation of CO₂, research can be directed to the *trans*-influence of the ligand opposite the hydride and the complex structure can be modified to promote CO₂ insertion.

Catalytic hydrogenation by first-row transition metal complexes is not only of interest for CO₂ conversion. Selective hydrogenation steps are useful in fields like medicine synthesis as well, where selectivity and chirality may play important roles. The formed complexes can also be modified and be useful in such fields of study; the two ketone-bound phenyl rings in the ligand are chemically non-equivalent, but may interchange their chemical properties in a small timescale. NMR shows splitting of signals for the protons bound to these phenyl rings for complexes **7** and **8**, EPR shows a distinct difference between the nickel-bound phosphori in complex **9**, and XRD exhibits a twist in the nickel-incorporating eight-membered ring. Modification of the functional group as shown in Figure 41 could lead to preference for either one of both conformers. This way, a possibility for synthesis of a chiral catalyst has opened up. Synthesis of such a catalyst requires a considerable amount of additional research however not only towards synthesis, but also isolation through stereo selective synthesis or resolution of a racemic mixture of the produced catalyst.

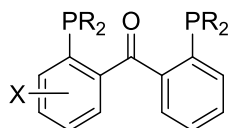


Figure 41: The general DPK ligand and indication of the ring position where modification of functionality leads to a prochiral ligand. X = -Me/-OMe/-OH/-NH

For future syntheses, modification of the biphenyl functionality on the ligand might be possible by using a different phosphine during the first reaction step. Alternative substituents on the phosphine can be used to alter the stereochemistry near the nickel metal centre, thereby altering the chemical properties around the nascent active site of the complex. Interesting substituents which can be considered are, for example, more the bulky $-\text{P}(\text{tert-butyl})_2$ or $-\text{P}(\text{C}_6\text{H}_{11})_2$. Use of such bulky substituents is meant to disallow the dimerization of complexes, generating less saturated complexes which are higher in energy and conceivably more prone to additions of small molecules like H₂.

6. Experimental

6.1. General working procedures

All reagents were purchased from commercial sources and used as received unless stated otherwise. Dichloromethane (DCM), triethylamine (Et₃N), N-isopropylidimethylamine (*i*-PrEt₂N) and N,N-dimethylformamide (DMF) were degassed by bubbling N_{2(g)} through the liquid for at least 30 minutes and subsequently stored over molecular sieves. The trifluoromethanesulfonic anhydride ((CF₃SO₂)₂O), deuterated benzene (C₆D₆) and deuterated toluene (C₇D₈) were degassed using the freeze-thaw-pump cycle according to the procedure found in literature^[49] and subsequently stored over molecular sieves. Tetrahydrofuran (THF) was distilled over sodium/benzophenone before use, degassed by bubbling N_{2(g)} through it and stored over molecular sieves. Dry diethylether (Et₂O) and toluene (C₇H₈) were acquired from a MBRAUN MB SPS-80 solvent purification system and dried before use using N_{2(g)}. Diphenyl- and triphenylphosphine (HPPH₂/PPh₃) were checked for oxidation by use of ³¹P NMR before use.

6.2. Analysis methods

¹H-, ¹³C-, ¹⁷F- and ³¹P-NMR-spectra (resp. 400, 100, 400 and 161 MHz) were recorded on an Agilent MRF400 spectrometer at 25°C. Chemical shifts are reported relative to TMS using the residual solvent resonance as internal standard. Infrared spectra were recorded using a Perkin Elmer Spectrum One FT-IR spectrometer equipped with a general liquid cell accessory. For air-sensitive complexes, KBr-FT-IR was used. The KBr used for making pellets was predried in the oven for at least 72 hours at 140°C and stored under inert atmosphere. UV-Vis spectra were measured using a Lambda 35 UV-Vis spectrometer. The UV-Vis samples were synthesised in the glovebox under N_{2(g)} and sealed with a Teflon cap. Thereafter, the samples were expressed from the glovebox and the spectra recorded. Toluene (C₇H₈) was used as solvent for all spectra to generate solutions with compound/complex concentrations of ±50 μM. CV measurements were performed using a reference 0.1M TBAPF₆ (tetra-*n*-butylammonium hexafluorophosphate) electrolyte in dried and degassed THF under inert atmosphere. A three-electrode cell connected to an external IVIUM Standard 100mA/10V Vertex potentiostat run by a personal computer with IVIUMsoft software. A glassy carbon electrode (0.5 mm diameter) was employed as the working electrode, with a 0.01M Ag/AgNO₃ reference electrode and Pt wire as the counter electrode. The working electrode was cleaned between experiments using a dry tissue. The potentials are reported versus the [Cp₂Fe]/[Cp₂Fe]⁺ reference potential. EPR analyses were carried out by dissolving several milligrams of substrate in an appropriate solvent under inert conditions followed by filtration of the sample to ensure no solids were present. The sample was transferred to a quartz EPR tube and spectra were recorded on a Bruker EMX Plus 6000 Gauss machine with ER 041 XG X-Band Microwave Bridge. In X-ray diffraction, reflections were measured on a Bruker Kappa ApexII diffractometer with sealed tube and Triumph monochromator (λ = 0.71073Å). X-ray intensities were integrated using the Eval15 software^[50]. Absorption correction was performed with SADABS^[51]. The structures were solved with direct methods using SHELXS-97^[52] ([Ni(0)(DPK)(PPh₃)], complex **8**) or with Patterson overlay methods using SHELXT^[53] ([Ni(I)Cl(DPK)] complex **9**, and the two measurements on [Ni(II)Cl₂(DPK)], complex **10**). Least-squares refinement was performed with SHELXL-2014^[52] against *F*² of all reflections. Non-hydrogen atoms were refined freely with anisotropic displacement parameters. Hydrogen atoms of the metal complex molecules were located in difference Fourier maps. Hydrogen atoms of the solvent molecules were included in calculated positions. All hydrogen atoms were refined with a riding model. Structure calculations and checking for higher symmetry were performed with PLATON^[54].

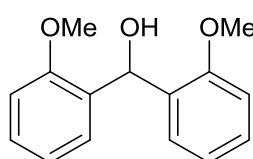


6.3. DFT

DFT results were obtained using the Gaussian 09 software package^[55], using the B3LYP (Becke, three-parameter, Lee-Yang-Parr) functional and the 6-31g(d,p) basis set on all atoms. For EPR calculations, IGLO III basis sets were obtained from the EMSL basis set exchange^[56]. The structures were optimized without any symmetry restraints. Frequency analyses were performed on all calculations. DFT calculation-derived pictures have been generated using the GaussView 5.0.8. software.

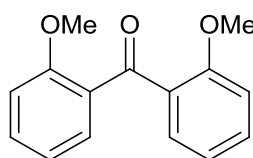
6.4 Syntheses procedures

Bis(2-methoxyphenyl)methanol (1)



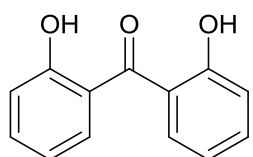
Procedure based on literature^[57]. Magnesium (2.01 g, 82.59 mmol) was suspended in THF (100 ml). A small amount of I₂ was added to activate the magnesium giving the suspension an orange colour, which faded away. The mixture was heated to 70°C up to reflux. To this suspension, 2-bromo-anisole (14.82 g, 79.21 mmol) dissolved in THF (50 ml) was added drop wise over 1 hour. The solution became black and contained solid Mg. After having refluxed for 1 hour, o-anisaldehyde (10.79 g, 79.218 mmol) dissolved in THF (25 ml) was added in 1 hour at room temperature. This addition gave a white precipitate. After the mixture had been stirred overnight, the suspension was pale white and turbid. The resulting suspension was poured out over an ice bath. HCl (4M, 30 ml) was added until the mixture was acidic. DCM (30 ml) was used to extract the product. The product was dried with anhydrous MgSO₄ and, filtered, the solvent evaporated. The crude product was recrystallized from hexane/toluene 1:20 (10 ml), filtered, washed and concentrated in vacuum. The resulting white crystals were obtained in 14.9 g (60.95 mmol, 77%) yield, and was pure enough for further reactions. ¹H-NMR (400 MHz, (CD₃)₂CO): δ 7.27 (d, 2H, J_{HH}=7.4 Hz, Ar), 7.20 (t, 2H, J_{HH}=8.2 Hz, Ar), 6.92 (d, 2H, J_{HH}=8.2 Hz, Ar), 6.87 (t, 2H, J_{HH}=7.4 Hz, Ar), 6.39 (d, 1H, J_{HH}=5.9 Hz), 4.25 (d, 1H, J_{HH}=4.7, -OH), 3.76 (s, 6H, -OMe). FT-IR: ν = 3554, 3003, 2938, 2837, 1601, 1588, 1489, 1463, 1438, 1391, 1289, 1239, 1185, 1162, 1108, 1050, 1027, 937, 869, 794, 753 cm⁻¹.

Bis(2-methoxyphenyl)methanone (2)



Procedure based on literature^[58]. Bis(2-methoxyphenyl)methanol (14.89 g, 60.95 mmol) was dissolved in toluene (125 ml). MnO₂ (6.19 g, 71.22 mmol) was added resulting in a black suspension. The mixture was heated to reflux (110°C) and stirred for six hours. Purification was done by filtration over celite and removal of solvent. This afforded 11.7 g (48.17 mmol, 79%) of white crystalline product pure enough for further reactions. ¹H-NMR (400 MHz, (CD₃)₂CO): δ 7.49 (d, 2H, J_{HH}=7.4 Hz, Ar), 7.46 (t, 2H, J_{HH}=7.8 Hz, Ar), 7.04 (d, 2H, J_{HH}=7.8 Hz, Ar), 7.00 (t, 2H, J_{HH}=7.4 Hz, Ar), 3.61 (s, 6H, -OMe). FT-IR ν: 2964, 1641, 1596, 1485, 1463, 1435, 1306, 1284, 1259, 1154, 1104, 1045, 119, 926, 796, 751 cm⁻¹.

Bis(2-hydroxyphenyl)methanone (3)

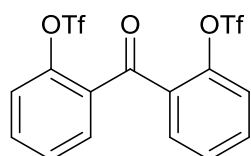


Procedure based on literature^[59,60]. Bis(2-methoxyphenyl)methanone (118 mg, 0.49 mmol) was dissolved in dry DCM (1 ml) under inert atmosphere. Boron tribromide (1.5 ml of an orange 1M solution in DCM) was added drop wise under constant stirring turning the solution orange brown. The mixture was



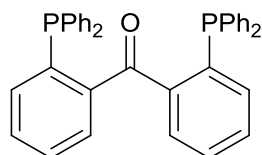
stirred overnight at room temperature. The solution was poured out on ice generating gas fumes. The organic layer was isolated and solvent evaporated. Further purification of the now yellow solution was done using silica gel column chromatography using hexane as eluent. The product was obtained as yellow crystalline powder (106 mg, 0.49 mmol, >99%). $^1\text{H-NMR}$ (400 MHz, CDCl_3): δ 10.57 (s, 2H, -OH), 7.61 (d, 2H, $J_{\text{HH}}=8.2$ Hz, Ar), 7.50 (dd, 2H, $J_{\text{HH}}=8.2$ Hz, $J_{\text{HH}}=7.4$ Hz, Ar), 7.08 (d, 2H, $J_{\text{HH}}=8.2$ Hz, Ar), 6.93 (dd, 2H, $J_{\text{HH}}=8.2$ Hz, $J_{\text{HH}}=7.4$ Hz, Ar). FT-IR: $\nu=$ 3277, 2963, 1612, 1572, 1479, 1456, 1438, 1337, 1307, 1220, 1146, 1036, 952, 934, 860, 840, 796, 755, 701 cm^{-1} .

Bis(2-trifluoromethanesulfoxyphenyl)methanone (4)



Procedure based on literature^[38]. Before use, the $(\text{CF}_3\text{SO}_2)_2\text{O}$ was degassed using the freeze-pump-thaw technique. Bis(2-hydroxyphenyl)methanone (2.40 g, 11.20 mmol) was dissolved in dry anhydrous DCM (66 ml) and dry anhydrous Et_3N (6.6 ml) giving a yellow solution which was cooled down to -84°C using an EtOAc ice bath. Degassed $(\text{CF}_3\text{SO}_2)_2\text{O}$ (8 ml) was added drop wise over the course of 1 hour turning the solution red brown. The product was heated to room temperature and extracted in EtOAc (40 ml) and washed with 1M HCl (15 ml), saturated HCO_3^- in water (15 ml) and brine (15 ml). Anhydrous MgSO_4 was used to dry the organic phase. The solvent was removed at the rotary evaporator and the product concentrated. Silica gel column chromatography was used to further purify the product using a 1:5 EtOAc / hexane eluent to afford 3.1 g (6.57 mmol, 59%) pure yellow product crystals. $^1\text{H-NMR}$ (400 MHz, CDCl_3): δ 7.67 (m, 4H, Ar), 7.49 (t, 2H, $J_{\text{HH}}=7.4$ Hz, Ar), 7.38 (d, 2H, $J_{\text{HH}}=8.6$ Hz, Ar). $^{19}\text{F-NMR}$ (376 MHz, CDCl_3): δ -73.18 (s, 6F, -OTf). FT-IR ν : 2988, 1678, 1609, 1486, 1421, 1303, 1269, 1249, 1210, 1194, 1142, 1108, 1084, 946, 859, 766, 687 cm^{-1} .

DPK (bis(2-diphenylphosphinophenyl)methanone) (5)

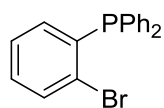


O-bromophenyldiphenylphosphine (4.0 g, 11.72 mmol) was combined with dry Et_2O (40 ml). The yellow suspension was cooled down to -50°C using an acetone ice bath. A 1.6 M n-BuLi in hexane solution (0.77 g, 12 mmol, 7.5 ml) was added drop wise under stirring. Over 30 minutes of stirring, the reaction mixture was heated up to room temperature. The reaction mixture became red and turbid upon the addition. This red colour faded away to become a less intense red terracotta-like colour. Then, after cooling down the reaction mixture again to -50°C a 0.3 M N,N-dimethylcarbonylchloride in dry Et_2O solution (20 ml, 672.5 mg, 6.24 mmol) was added drop wise over 5-10 minutes. During the addition, the temperature of the bath was kept between -30°C and -40°C . Then the bath was brought to -50°C again and the suspension stirred overnight, allowing the mixture to heat up to room temperature. The reaction was then cooled down again and treated at 0°C with 2.5M NH_4Cl solution in water (30 ml, 4.00 g, 90 mmol NH_4Cl) turning the suspension yellow. Various Et_2O washes were used to further purify the product, obtaining it as a yellow powder (2.5 g, 4.54 mmol, 77%). $^1\text{H-NMR}$ (400 MHz, C_6D_6): δ 7.33 (t, 4H, $J_{\text{HH}}=7.4$ Hz, Ph), 7.32 (t, 4H, $J_{\text{HH}}=7.0$ Hz, Ph), 7.21 (t, 2H, $J_{\text{HH}}=7.4$ Hz, Ph), 7.20 (t, 2H, $J_{\text{HH}}=7.0$ Hz, Ph), 7.00 (m, 14H, Ar/Ph), 6.84 (t, 1H, $J_{\text{HH}}=7.8$ Hz, Ar), 6.84 (t, 1H, $J_{\text{HH}}=7.4$ Hz, Ar), 6.74 (t, 1H, $J_{\text{HH}}=7.4$ Hz, Ar), 6.74 (t, 1H, $J_{\text{HH}}=7.4$ Hz, Ar). $^{13}\text{C-NMR}$ (100 MHz, C_6D_6): δ 196.8 (t, 1C, $J_{\text{CC}}=3.1$ Hz, C=O), 144.2 (s, unassigned), 144.0 (s, unassigned), 139.7 (d, $J_{\text{CC}}=2.3$ Hz, unassigned), 139.5 (d, $J_{\text{CC}}=3.1$ Hz, unassigned), 138.3 (t, $J_{\text{CC}}=3.1$ Hz, unassigned), 138.2 (t, $J_{\text{CC}}=3.8$ Hz, unassigned), 134.7 (s, unassigned), 133.9 (d, $J_{\text{CC}}=21.4$ Hz, unassigned), 130.6 (t, $J_{\text{CC}}=3.1$ Hz, unassigned), 130.4 (s, unassigned), 128.2 (m,



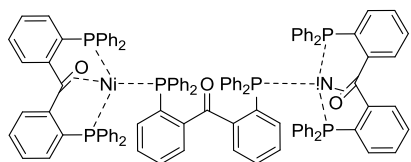
unassigned), 127.7 (s, unassigned). ^{31}P -NMR (161 MHz, C_6D_6): δ -8.3 (s, 1P). FT-IR ν : 3051, 1734, 1657, 1584, 1478, 1433, 1298, 1245, 1089, 1026, 928, 740, 693 cm^{-1} . ESI-MS m/z : 657 [M^+], 657.

o-bromophenyldiphenylphosphine (6)



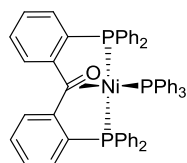
Procedure based on literature^[41]. Dry Et_3N (3.1 ml, 22 mmol), $\text{Pd}(\text{PPh}_3)_4$ (100.2 mg, 0.09 mmol), *o*-bromo-iodobenzene (2 ml, 15.4 mmol), diphenylphosphine (2.85 ml, 15.4 mmol) and dry degassed toluene (40 ml) were combined under inert conditions giving an orange solution. After the mixture had been heated to 80°C for 12 hours, the deep red organic layer was washed with brine (2 x 20 ml). The aqueous phase was washed twice with Et_2O and the Et_2O fractions were combined. The solvent was evaporated on the rotary evaporator. Cold MeOH (3 x 4 ml) was used to wash the crude product. The product was dried in vacuo and isolated as pale yellow powder (3.0 g, 8.8 mmol, 57%). ^1H -NMR (400 MHz, C_6D_6): δ 7.29 (m, 5H, Ar), 6.98 (m, 6H, Ar), 6.83 (dt, 1H, $J_{\text{HH}}=7.8$ Hz; $J_{\text{HH}}=2.2$ Hz, Ar), 6.70 (dt, 1H, $J_{\text{HH}}=7.4$ Hz; $J_{\text{HH}}=1.2$ Hz, Ar), 6.61 (dt, 1H, $J_{\text{HH}}=7.8$ Hz; $J_{\text{HH}}=2.0$ Hz, Ar). ^{31}P -NMR (161 MHz, C_6D_6): δ -4.83 (s, 1P). FT-IR ν : 3049, 1554, 1475, 1423, 1248, 1094, 1014, 750, 742, 693 cm^{-1} .

[Ni(O)₂(DPK)₃] (7)



$[\text{Ni}(\text{COD})_2]$ (26.3 mg, 0.096 mmol) and DPK (**5**, 78.8 mg, 0.143 mmol) were combined in a vial under inert atmosphere. Et_2O (3 ml) was added and the created dark brown suspension was stirred for 15 minutes. The suspension was filtered and the light brown solid phase washed with Et_2O (3 ml). Toluene (4 ml) was used to dissolve the solid phase and the dark brown solution was concentrated and dried under vacuum to yield the product as a light brown powder (54 mg, 0.03 mmol, 65%). ^1H -NMR (400 MHz, C_6D_6): δ 8.78 (s, broad, 3H), 7.79 (d, 3H, $J_{\text{HH}}=7.0$ Hz), 7.57 (m, 6H), 7.28 (m, 3H), 7.20 (t, 6H, $J_{\text{HH}}=8.2$ Hz), 7.07-6.73 (m, broad, 34H), 6.68 (t, 12H, $J_{\text{HH}}=7.4$ Hz), 6.54 (t, 6H, $J_{\text{HH}}=7.4$ Hz), 6.48 (d, 2H, $J_{\text{HH}}=7.4$ Hz), 6.34 (t, 4H, $J_{\text{HH}}=7.0$ Hz), 6.18 (d, 2H, $J_{\text{HH}}=7.4$ Hz). ^{31}P -NMR (100 MHz, 300 K, C_6D_6): δ 44.06 (dd, 2P, $J_{\text{PP}}=36.9$ Hz, $J_{\text{PP}}=22.2$ Hz, Ni-P), 22.93 (broad d, 2P, $J_{\text{PP}}=36.9$ Hz, **5**-P-NiP-**5**), 11.22 (broad d, 2P, $J_{\text{PP}}=35.6$ Hz, **5**-P-NiP-**5**). ^{31}P -NMR (100 MHz, 373 K, C_7D_8): δ 44.4 (dd, 2P, $J_{\text{PP}}=28$ Hz, $J_{\text{PP}}=31$ Hz, Ni-P), 21.3 (dd, 2P, $J_{\text{PP}}=28$ Hz, $J_{\text{PP}}=62$ Hz, **5**-P-NiP-**5**), 5.6 (dd, 2P, $J_{\text{PP}}=31$ Hz, $J_{\text{PP}}=62$ Hz, **5**-P-NiP-**5**). FT-IR (KBr pellet) ν : 3437, 3051, 1679, 1585, 1481, 1459, 1433, 1261, 1184, 1157, 1092, 1027, 921, 802, 775, 739, 691, 658, 626, 514 cm^{-1} .

[Ni(O)(DPK)(PPh₃)] (8)



PPh_3 (120.9 mg, 0.46 mmol), DPK (**5**, 250.0 mg, 0.45 mmol) and $[\text{Ni}(\text{COD})_2]$ (124.9 mg, 0.45 mmol) were combined in one vial and 3 ml dry degassed Et_2O was added. The obtained suspension immediately turned brown. After 45 minutes of stirring, the solid was separated from the liquid, dissolved in THF and concentrated in vacuo to obtain the product **8** as a brown powder (284 mg, 0.33 mmol, 72%). ^1H -NMR (400 MHz, C_6D_6): δ 7.84 (d, 2H, $J_{\text{HH}}=7.8$ Hz, Ar), 7.59 (t, 6H, $J_{\text{HH}}=8.2$ Hz, Ph), 7.21-7.31 (broad m, 10H, $J_{\text{HH}}=19.2$), 6.98 (t, 3H, $J_{\text{HH}}=7.4$, Ph), 6.85-6.95 (m, 7H, Ph/Ar), 6.77-6.85 (m, 11H, Ph/Ar), 6.72 (t, 4H, $J_{\text{HH}}=7.4$ Hz, Ph). ^{13}C -NMR (100 MHz, C_6D_6): δ 154.6 (dd, 2C, $J_{\text{CC}}=19.1$ Hz, $J_{\text{CC}}=16.0$ Hz, CCO_{Ar}), 141.6 (dt, 2C, $J_{\text{CC}}=8.4$ Hz, $J_{\text{CC}}=16.8$ Hz, CP_{Ar}), 137.9 (t, 4C, $J_{\text{CC}}=14.5$ Hz, PC_{Ph_2}), 137.0 (dt, 2C, $J_{\text{CC}}=29.8$ Hz, $J_{\text{CC}}=4.6$ Hz, CCP_{Ar}), 136.2 (t, 3C, $J_{\text{CC}}=11.4$ Hz, PC_{Ph_3}), 133.8 (d, 8C, $J_{\text{CC}}=13.7$ Hz, PCC_{Ph_2}), 133.4 (t, ?C, $J_{\text{CC}}=7.6$ Hz), 132.3 (t, ?C, $J=6.1$ Hz), 132.0 (s, ?C), 128.5-127 (m, ?C), 126.5 (s, ?C), 120.4 (dt, 1C, $J_{\text{dt}}=13.7$ Hz, $J_{\text{t}}=9.2$ Hz, CO_{Ar}). ^{31}P -NMR (161 MHz,

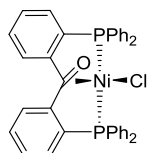


C₆D₆): δ 38.2 (t, 1P, J_{PP}=25 Hz, PPh₃), 17.9 (d, 2P, J_{PP}=25 Hz, P-5-P). FT-IR (KBr pellet) v: 3447, 3052, 2346, 1585, 1480, 1459, 1434, 1309, 1262, 1092, 1027, 914, 777, 740, 680, 660, 625, 517 cm⁻¹.

Synthesis out of **7**

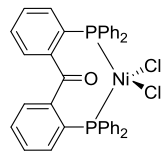
[Ni(O)₂(DPK)₃] (**7**, 5.7 mg, 3.22 μmol) and PPh₃ (3.4 mg, 12.96 μmol) were combined in the glovebox and dissolved in C₇H₈ at room temperature. In situ NMR showed full conversion to **9**, generation of 1 eq of **5** with regard to the amount of **7** and an excess of PPh₃.

[Ni(I)Cl(DPK)] (**9**)



[Ni(COD)₂] (25.0 mg, 0.09 mmol), [NiCl₂(DME)] (20.0 mg, 0.09 mmol) and DPK (**5**, 100.0 mg, 0.18 mmol) were combined in a vial in the glovebox at room temperature. Dry degassed THF (3 ml) was added and the brown solution with yellow solids was stirred for 45 minutes. The mixture was filtered and the solid phase washed with THF (2 x 0.3 ml). The light brown solid was washed with hexane (3 x 0.3 ml) and the solid dried under vacuum. The solid (±100 mg) was again dissolved in THF (3 ml), the mixture stirred for 30 minutes and insoluble particles filtered off. To initiate precipitation from the solvent, hexane (5 ml) was added and the suspension was kept in the freezer for 3 days. The solid was filtered off and dried in vacuo to obtain the product as a dark brown powder (45 mg, 0.07 mmol, 38%). ¹H-NMR (400 MHz, d₈-THF): δ 16.32 (s, broad), 14.41 (s, broad), 12.71 (s, broad), 7.25 (m, diamagnetic material), -0.36 (s, broad), -3.00 (s, broad). ³¹P-NMR (161 MHz, d₈-THF): δ 32.4 (s, 2P). FT-IR (KBr-Pellet) v: 3421, 3053, 1643, 1481, 1459, 1435, 1340, 1332, 1298, 1262, 1240, 1098, 1028, 919, 778, 746, 694, 520, 505 cm⁻¹

[Ni(II)Cl₂(DPK)] (**10**)



[NiCl₂(DME)] (101.4 mg, 0.46 mmol) and DPK (**5**, 260.4 mg, 0.47 mmol) were mixed together in a vial in the glovebox at room temperature. Dry degassed DCM (2ml) was added and the obtained solution was stirred for 1 hour. From this solution, the product was obtained as dark brown crystalline material from crystallization against hexane (259 mg, 0.38 mmol, 83%).

¹H-NMR (400 MHz, d₂-DCM): δ 20.67 (s, sharp), 19.38 (s, broad), 9.25 (s, sharp), 7.37 (s, sharp), 5.88 (s, sharp), 5.01 (s, sharp), -0.47 (s, sharp), -6.63 (s, broad). ¹H-NMR Evans Method (400 MHz, d₂-DCM): Δδ=217 Hz. FT-IR (KBr-Pellet) v: 3394, 3058, 1963, 1634, 1579, 1560, 1482, 1455, 1435, 1294, 1185, 1163, 1132, 1094, 1029, 998, 932, 805, 753, 744, 693, 641, 529, 504 cm⁻¹ EA: calculated: 65.46% C; 4.77% H. experimentally found: 65.21% C; 4.19% H.



7. Acknowledgements

It gives me a lot of joy to conclude that I have had a great time at the Organic Chemistry and Catalysis group. This is mostly because of all the lovely people around at the group. I have learned a lot from a lot of different people and would therefore like to thank everyone for their help.

Of course, some people deserve a bit more thanks than others. The one person I would like to thank the most is Doctor Marc-Etienne Moret. Thank you for the daily supervision from which interesting discussions frequently emerged. I hope that in your view the energy you spent on me has been rewarded by the work done by me and that last year was very resourceful not only for me but also for you.

Also, I would like to thank Professor Bert Klein Gebbink for allowing me to work in his research group. I have learned a lot just by being surrounded by people who actually did perform the chemistry which I learned about during my previous years in college. I can only thank you for enabling me to be part of this and to join the lunch lectures, work discussions and other meetings.

Other people I would like to give a special mention, are the people who were working on (almost) the same project as me. Dide and Richt, you were two enthusiastic colleagues whom I would gladly bring to an interview for a new job: it would please me to look forward to some more years of innovative and productive research. Also, you bring the right balance between productivity and distraction.

Finally, I would like to thank the remainder of the people at the OCC group. Even though we did not share a lot in research grounds, we have had a lot of good moments together. Thank you for the interesting research talks and work-related exchanges of knowledge. In contrast to this seriousness, I would also like to give my thanks for the plethora of chemistry jokes, extremely implausible stories and other nonsense. All in all, just thanks for giving me the chance to be part of a group where I felt at home.

8. References

- [1] W. Leitner, *Angew. Chem. Int. Ed.*, **1995**, *34*, 2207–2221
- [2] A. D. Getty, C. C. Tai, J. C. Linchan, P. G. Jessop, M. M. Olmstead, A. L. Rheingold, *Organometallics*, **2009**, *28*, 5466-5477
- [3] M. S. Jeletic, M. L. Helm, E. B. Hulley, M. T. Mock, A. M. Appel, J. C. Linehan, *ACS Catal.*, **2014**, *4*, 3755-3762
- [4] Z. Jiang, T. Xiao, V. L. Kuznetsov, P. P. Edwards, *Phil. Trans. R. Soc. A*, **2010**, *368*, 3343-3364
- [5] D. W. Ball, *Physical Chemistry*, Ch.1-3, **2002**, ISBN-13: 978-0534266585
- [6] R. Noyori, T. Ohkuma, M. Kitamura, *J. Am. Chem. Soc.*, **1987**, *Vol. 109*, *No. 19*, 5856-5858
- [7] R. Noyori, T. Ohkuma, *Angew. Chem. Int. Ed.*, **2001**, *40*, 40-73
- [8] E. Balaraman, C. Gunanathan, J. Zhang, L. J. W. Shimon, D. Milstein, *Nature Chemistry*, **2011**, *3*, 609-614
- [9] T. Burgemeister, F. Kastner, W. Leitner, *Angew. Chem.*, **1993**, *105*, 781-783
- [10] H. Wiener, J. Blum, H. Feilchenfeld, Y. Sasson, N. Zalmanov, *J. Catal.*, **1988**, *110*, 184-190
- [11] S. Ge, R. A. Green, J. F. Hartwig, *J. Am. Chem. Soc.*, **2014**, *136*, 1617-1627
- [12] S. Ge, J. F. Hartwig, *J. Am. Chem. Soc.*, **2011**, *133*, 16330-16333
- [13] T. M. Figg, T. R. Cundari, *Organometallics*, **2012**, *31*, 4998-5004
- [14] K. Koo, G. L. Hillhouse, A. L. Rheingold, *Organometallics*, **1995**, *14*, 456-460
- [15] P. T. Matsunaga, J. C. Mavropoulos, G. L. Hillhouse, *Polyhedron*, **1995**, *14*, 175-185
- [16] K. Koo, G. L. Hillhouse, *Organometallics*, **1998**, *17*, 2924-2925
- [17] J. J. Curley, K. D. Kitiachvili, R. Waterman, G. L. Hillhouse, *Organometallics*, **2009**, *28*, 2568-2571
- [18] D. V. Gutsulyak, W. E. Piers, J. Borau-Garcia, M. Parvez, *J. Am. Chem. Soc.*, **2013**, *135*, 11776-11779
- [19] T. T. Tsou, J. C. Huffman, J. K. Kochi, *Inorganic Chemistry*, *Vol. 18*, *No. 8*, **1979**, 2311-2317
- [20] A. L. Iglesias, J. J. García, *Journal of Molecular Catalysis A: Chemical*, **2009**, *298*, 51-59
- [21] A. L. Iglesias, M. Muñoz-Hernández, J. J. García, *Journal of Organometallic Chemistry*, **2007**, *692*, 3498-3507
- [22] A. Arévalo, J. J. García, *Eur. J. Inorg. Chem.*, **2010**, 4063-4074
- [23] A. Flores-Gaspar, P. Pinedo-González, M. G. Crestani, M. Muñoz-Hernández, D. Morales-Morales, B. A. Warsop, W. D. Jones, J. J. García, *J. Mol. Cat.*, **2009**, 1-11



- [24] T. J. Mooibroek, E. C. M. Wenker, W. Smit, I. Mutikainen, M. Lutz, E. Bouwman, *Inorg. Chem.*, **2013**, *52*, 8190-8201
- [25] W. H. Harman, J.C. Peters, *J. Am. Chem. Soc.*, **2012**, *134*, 5080-5082
- [26] D. Milstein, W. C. Fultz, J. C. Calabrese, *J. Am. Chem. Soc.*, **1986**, *108*, 1336-1338
- [27] E. Balaraman, B. Gnanaprakasam, L. J. W. Shimon, D. Milstein, *J. Am. Chem. Soc.*, **2010**, *132*, 16756-16758
- [28] C. A. Huff, M. S. Sandford, *ACS Catal.*, **2013**, *3*, 2412-2416
- [29] G. Zeng, S. Sakaki, *Inorg. Chem.*, **2013**, *52*, 2844-2853
- [30] G. J. Kubas, *Journal of Organometallic Chemistry*, **2014**, *751*, 33-49
- [31] S. M. Kuang, D. G. Cuttell, D. R. McMillin, P. E. Fanwick, R. A. Walton, *Inorg. Chem.*, **2002**, *41*, 3313-3322
- [32] Y.-H. Huang, J. A. Gladysz, *J. Chem. Educ.*, **1988**, *Vol. 65, No. 4*, 298-303
- [33] R. H. Crabtree, *The Organometallic Chemistry of the Transition Metals*, **2009**, ISBN 978-0-470-257-62-3
- [34] J. F. Hartwig, *Organotransition Metal Chemistry - From Bonding to Catalysis*, **2010**, ISBN 978-1-891389-53-5, p. 8-9; 266-267
- [35] Y.-Y. Ohnishi, T. Matsunaga, Y. Nakao, H. Sato, S. Sakaki, *J. Am. Chem. Soc.*, **2005**, *127*, 4021-4032
- [36] P.J. Chirik, K. Wieghardt, *Science*, **2010**, *327*, 794-795
- [37] J. Cámpora, P. Palma, E. Carmona, *Coordination Chemistry Reviews*, **1999**, *193-195*, 207-281
- [38] Q. Jing, C.A. Sandoval, Z. Wang, K. Ding, *Eur. J. Org. Chem.*, **2006**, 3606-3616
- [39] P. Lucas, N. E. Mehdi, H. Anh Ho, D. Bélanger, L. Breau, *Synthesis*, **2000**, *9*, 1253-1258
- [40] Y. A. Getmanenko, C. Risko, P. Tongwa, E. G. Kim, H. Li, B. Sandhu, T. Timofeeva, J. L. Brédas, S. R. Marder, *J. Org. Chem.*, **2011**, *76*, 2660-2671
- [41] F. Zhang, L. Wang, S. H. Chang, K. L. Huang, Y. Chi, W. Y. Hung, C. M. Chen, G. H. Lee, P. T. Chou, *Dalton Trans.*, **2013**, *42*, 7111-7119
- [42] Vogel's Textbook of Practical Organic Chemistry, B. S. Furniss, A. J. Hannaford, P. W. G. Smith, A. R. Tatchell, Fifth Edition, ISBN: 0-582-46236-3, **1989**, p. 1436
- [43] V. V. Smirnov, D. W. Brinkley, M. P. Lanci, K. D. Karlin, J. P. Roth, *J. Mol. Cat.*, **2006**, 100-107
- [44] S. D. Ittel, *Inorg. Synth.* **1990**, *28*, 98.
- [45] G. J. P. Britovsek, V. C. Gibson, S. K. Spitzmesser, K. P. Tellman, A. J. P. White, D. J. Williams, *J. Chem. Soc., Dalton Trans*, **2002**, 1159-1171



- [46] M. Schultz, P. N. Plessow, F. Rominger, L. Wiegel, *Acta Cryst.*, **2013**, C69, 1437-1447
- [47] R. Langer, Y. Diskin-Posner, G. Leitus, L. J. W. Shinon, Y. Ben-David, D. Milstein, *Angew. Chem. Int. Ed.*, **2011**, 50, 9948-9952
- [48] B. J. Coe, S. J. Glenwright, *Coord. Chem. Rev.*, **2000**, 203, 5
- [49] W. L. F. Armarego, C. L. L. Chai, *Purification of Laboratory Chemicals*, **2009**, ISBN 978-1-85617-567-8, pg. 31
- [50] A. M. M. Schreurs, X. Xian, L. M. J. Kroon-Batenburg, *J. Appl. Cryst.*, **2010**, 43, 70-82
- [51] G. M. Sheldrick, **1999**, SADABS: Area-Detector Absorption Correction, Universität Göttingen, Germany
- [52] G. M. Sheldrick, *Acta Cryst.*, **2008**, A64, 112-122
- [53] G. M. Sheldrick, **2014**, SHELXT, Universität Göttingen, Germany
- [54] A.L. Spek, *Acta Cryst.*, **2009**, D65, 148-155
- [55] M. J. Frish, G. W. Trucks, H. B. Schlegel, G. E. Scuseria, M. A. Robb, J. R. Cheeseman, G. Scalmani, V. Barone, B. Mennucci, G. A. Petersson, H. Nakatsuji, M. Caricato, X. Li, H. P. Hratchian, A. F. Izmaylov, J. Bloino, G. Zheng, J. L. Sonnenberg, M. Hada, M. Ehara, K. Toyota, R. Fukuda, J. Hasegawa, M. Ishida, T. Nakajima, Y. Honda, O. Kitao, H. Nakai, T. Vreven, J. A. Montgomery, Jr., J. E. Peralta, F. Ogliaro, M. Bearpark, J. J. Heyd, E. Brothers, K. N. Kudin, V. N. Staroverov, R. Kobayashi, J. Normand, K. Raghavachari, A. Rendell, J. C. Burant, S. S. Iyengar, J. Tomasi, M. Cossi, N. Rega, J. M. Millam, M. Klene, J. E. Knox, J. B. Cross, V. Bakken, C. Amado, J. Jaramillo, R. Gomperts, R. E. Stratmann, O. Yazyev, A. J. Austin, R. Cammi, C. Pomelli, J. W. Ochterski, R. L. Martin, K. Morokuma, V. G. Zakrzewski, G. A. Voth, P. Salvador, J. J. Dannenberg, S. Dapprich, A. D. Daniels, Ö. Farkas, J. B. Foresman, J. V. Ortiz, J. Cioslowski, D. J. Fox, "Gaussian 09 Revision A.02".
- [56] <https://bse.pnl.gov/bse/portal>, **The Role of Databases in Support of Computational Chemistry Calculations**, Feller, D., *J. Comp. Chem.*, **1996**, 17(13), 1571-1586, **Basis Set Exchange: A Community Database for Computational Sciences** Schuchardt, K.L., Didier, B.T., Elsethagen, T., Sun, L., Gurumoorthi, V., Chase, J., Li, J., and Windus, T.L., *J. Chem. Inf. Model.*, **2007**, 47(3), 1045-1052, doi:10.1021/ci600510j. Website last visited on 9/10/2014.
- [57] C. Faerman, H. Negri, G. Punte, *Can. J. Chem.*, **1983**, 61, 2001-2005
- [58] A. Kamimura, H. Komatsu, T. Moriyama, Y. Nozaki, *Tetrahedron*, **2013**, 69, 5068-5072
- [59] P.R. Brooks, M.C. Wurtz, M. G. Vetelino, D. M. Rescek, G. F. Woodworth, B. P. Morgan, J. W. Coe, *J. Org. Chem.*, **1999**, 64, 9719-9721
- [60] J. F. W. McOmie, M. L. Watts, D. E. West, *Tetrahedron*, **1968**, 24, 2289-2292
- [61] S. Parsons, H.D. Flack, T. Wagner, *Acta Cryst.*, **2013**, B69, 249-259

9. Addendum

Contents

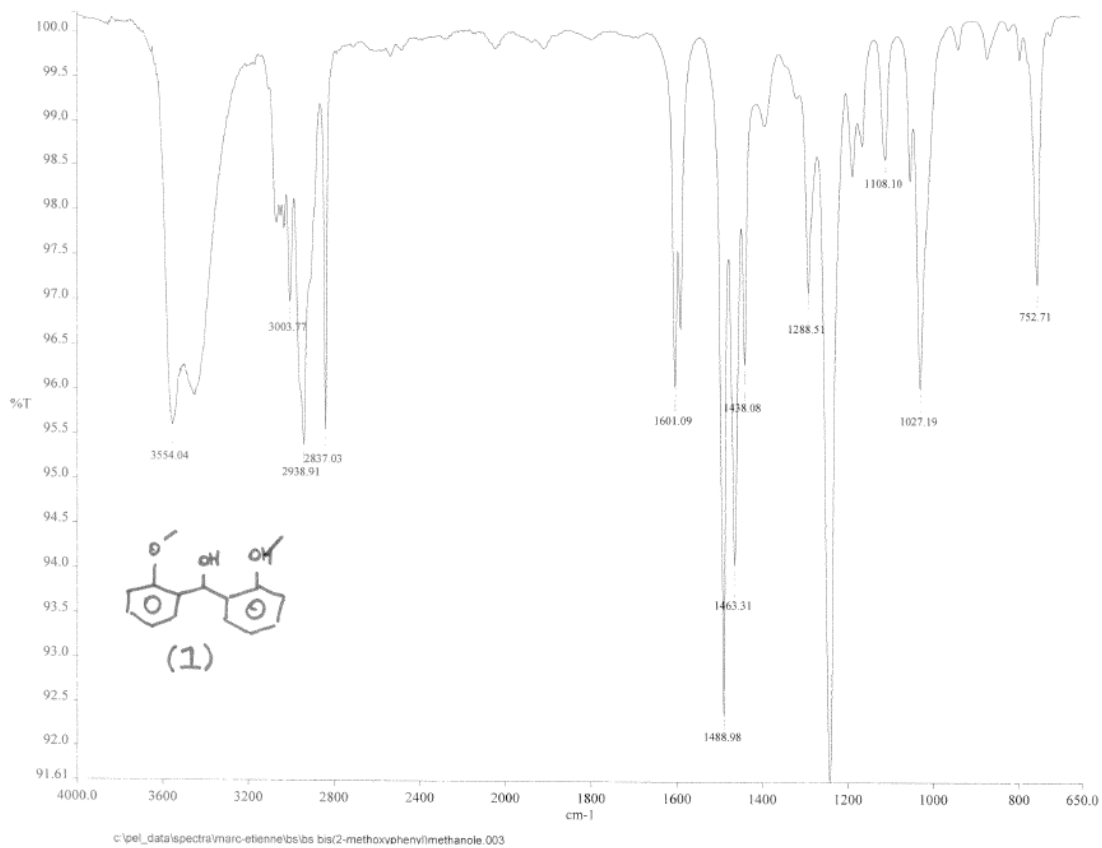
ATR-FT-IR - bis(2-methoxyphenyl)methanole (1)	59
ATR-FT-IR - bis(2-methoxyphenyl)methanone (2)	59
ATR-FT-IR - bis(2-hydroxyphenyl)methanone (3)	60
ATR-FT-IR - bis(2-triflatephenyl)methanone (4)	60
ATR-FT-IR - DPK (5)	61
ATR-FT-IR - o-bromophenyldiphenylphosphine (6)	61
KBr-FT-IR - [Ni ₂ (DPK) ₃] (7)	62
KBr-FT-IR - [Ni(0)(DPK)(PPh ₃)] (8)	62
KBr-FT-IR - [Ni(I)Cl(DPK)] (9)	63
KBr-FT-IR - [Ni(II)Cl ₂ (DPK)] (10)	63
¹ H-NMR - bis(2-methoxyphenyl)methanole (1)	64
¹ H-NMR - bis(2-methoxyphenyl)methanone (2)	64
¹ H-NMR - bis(2-hydroxyphenyl)methanone (3)	65
¹ H-NMR - bis(2-triflatephenyl)methanone (4)	65
¹⁷ F-NMR - bis(2-triflatephenyl)methanone (4)	66
¹ H-NMR - DPK (5)	66
¹³ C-NMR - DPK (5)	67
¹³ C-NMR - DPK zoom (5)	67
³¹ P-NMR - DPK (5)	68
¹ H-NMR - o-bromophenyldiphenylphosphine (6)	68
³¹ P-NMR - o-bromophenyldiphenylphosphine (6)	69
¹ H-NMR - [Ni ₂ (DPK) ₃] (7)	69
¹ H-NMR - [Ni ₂ (DPK) ₃] (7) zoom	70
¹³ C-NMR - [Ni ₂ (DPK) ₃] (7)	70
³¹ P-NMR - [Ni ₂ (DPK) ₃] (7)	71
³¹ P-VT-NMR - [Ni ₂ (DPK) ₃] (7)	72
¹ H-NMR - [Ni(0)(DPK)(PPh ₃)] (8)	73
¹ H-NMR - [Ni(0)(DPK)(PPh ₃)] (8) zoom	73
³¹ P-NMR - [Ni(0)(DPK)(PPh ₃)] (8)	74
¹ H-NMR - [Ni(I)Cl(DPK)] (9)	75
¹ H-NMR, Paramagnetic measurement settings - [Ni(I)Cl(DPK)] (9)	75



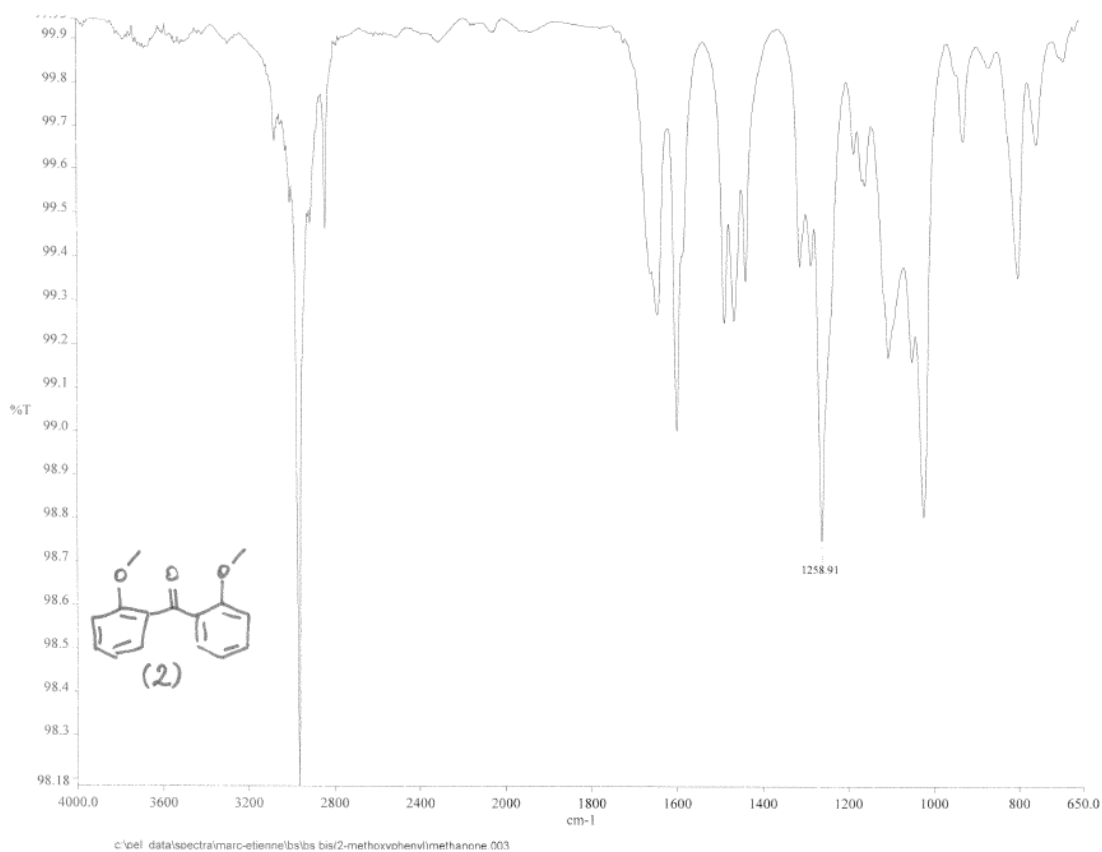
¹H-VT-NMR , Paramagnetic measurement settings - [Ni(I)Cl(DPK)] (9).....	76
³¹P-NMR - [Ni(I)Cl(DPK)] (9).....	76
¹H-NMR - [Ni(II)Cl ₂ (DPK)] (10)	77
¹H-NMR , Paramagnetic measurement settings - [Ni(II)Cl ₂ (DPK)] (10)	77
¹H-NMR , Evans method - [Ni(II)Cl ₂ (DPK)] (10).....	78
UV-Vis - DPK (5), [Ni ₂ (DPK) ₃] (7), [Ni(O)(DPK)(PPh ₃)] (8), [Ni(I)Cl(DPK)] (9), [Ni(II)Cl ₂ (DPK)] (10)	78
CV - NBu ₄ PF ₆ in THF electrolyte reference spectrum	79
CV - [Ni(I)Cl(DPK)] (9).....	79
CV - [Ni(I)Cl(DPK)] (9) zoom -1.8V to -0.75V.....	80
CV - [Ni(II)Cl ₂ (DPK)] (10)	80
CV - [Ni(II)Cl ₂ (DPK)] (10) zoom -1.5 V to -0.5 V	81
CV - [Ni(II)Cl ₂ (DPK)] (10) zoom -3 V to -1.5 V.....	81
EPR - bis(2-diphenylphosphinophenyl)methanone (DPK, 5).....	82
EPR - [Ni(I)Cl(DPK)] – 300 K (9)	82
EPR - [Ni(I)Cl(DPK)] – 100 K (9)	83
XRD - Crystallographic results for complexes 8 , 9 and 10	84
XRD - [Ni(O)(DPK)(PPh ₃)] (8)	85
XRD - [Ni(I)Cl(DPK)] (9)	86
XRD - [Ni(II)Cl ₂ (DPK)] (10).....	87



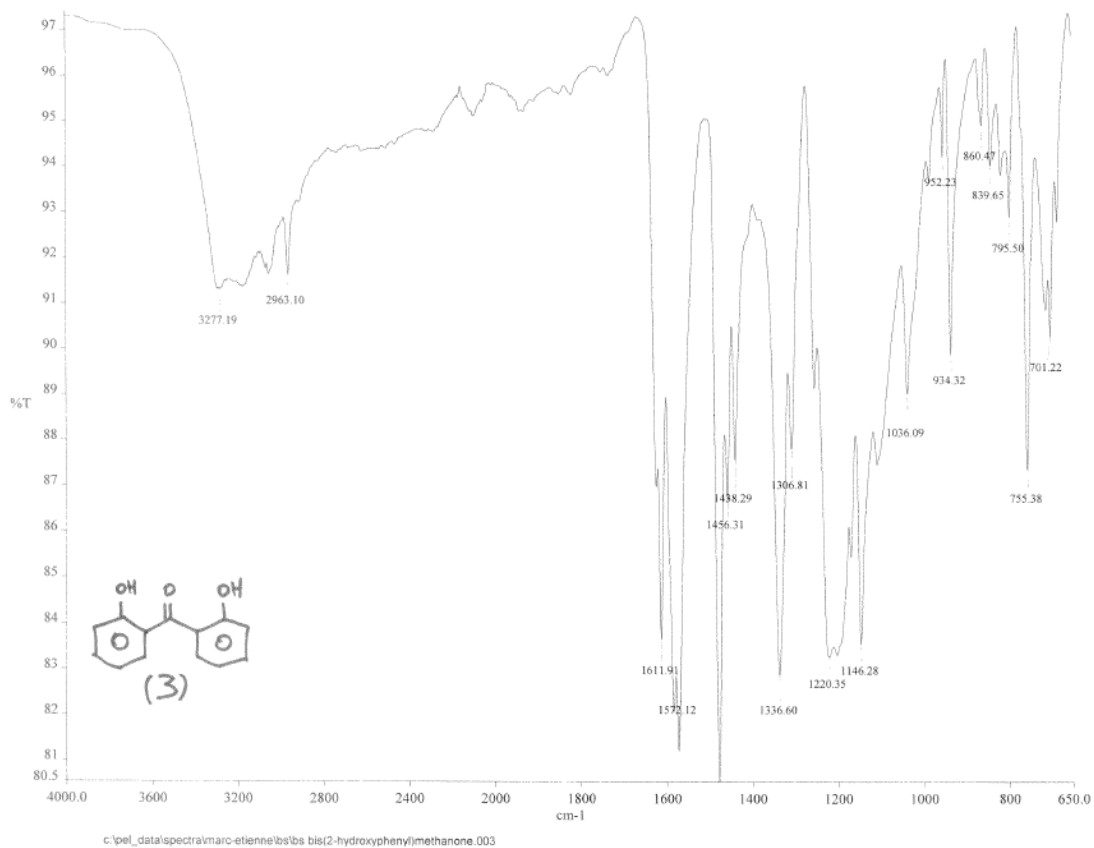
ATR-FT-IR - bis(2-methoxyphenyl)methanole (1)



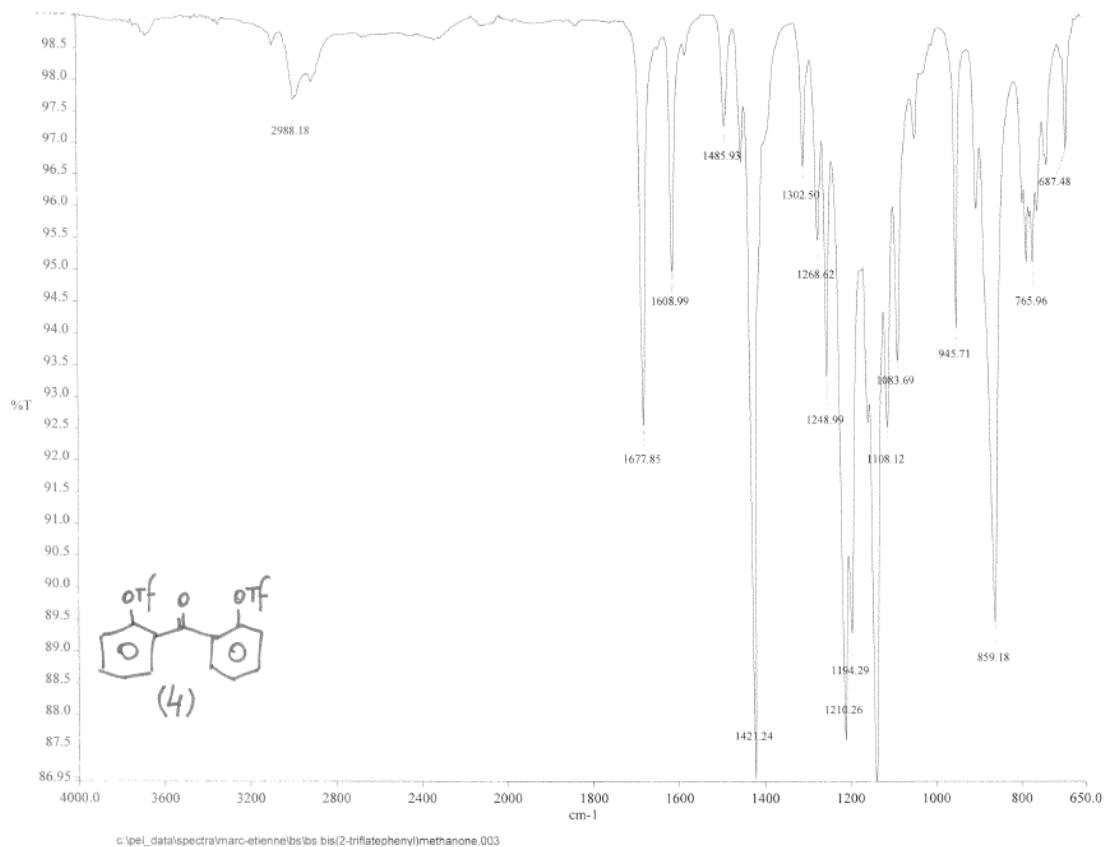
ATR-FT-IR - bis(2-methoxyphenyl)methanone (2)



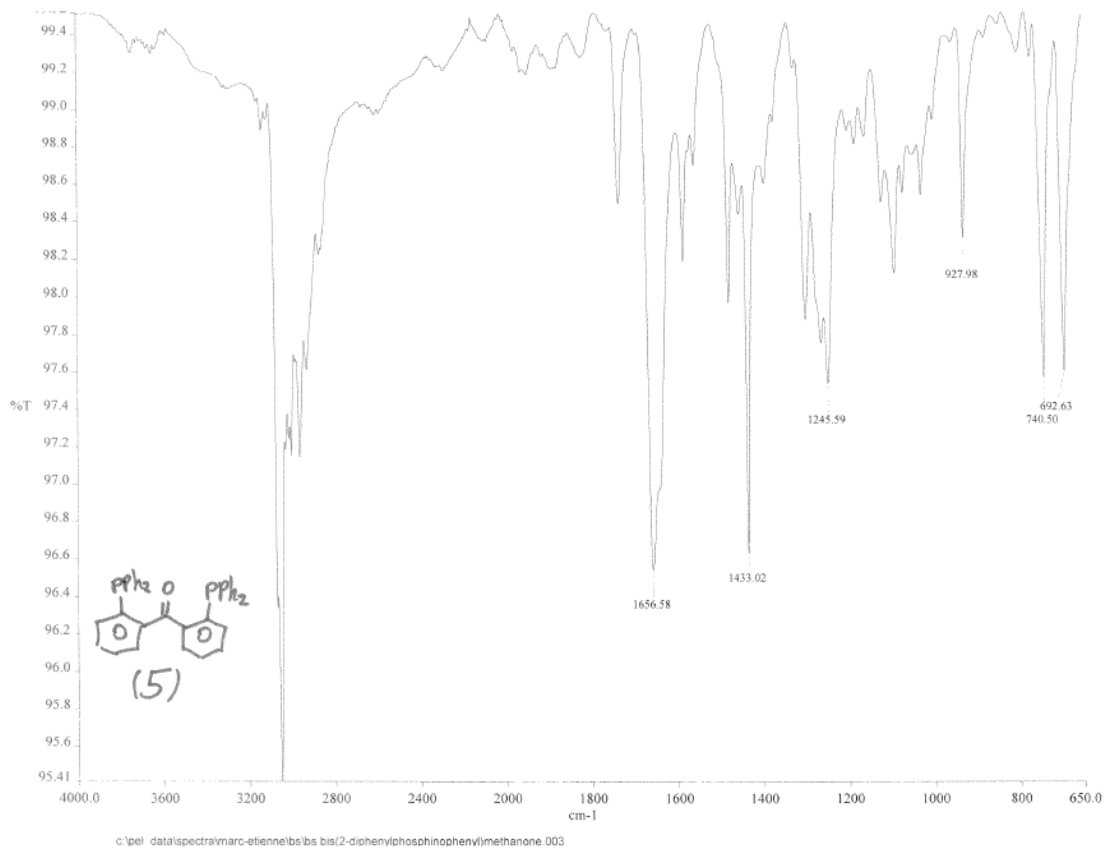
ATR-FT-IR - bis(2-hydroxyphenyl)methanone (3)



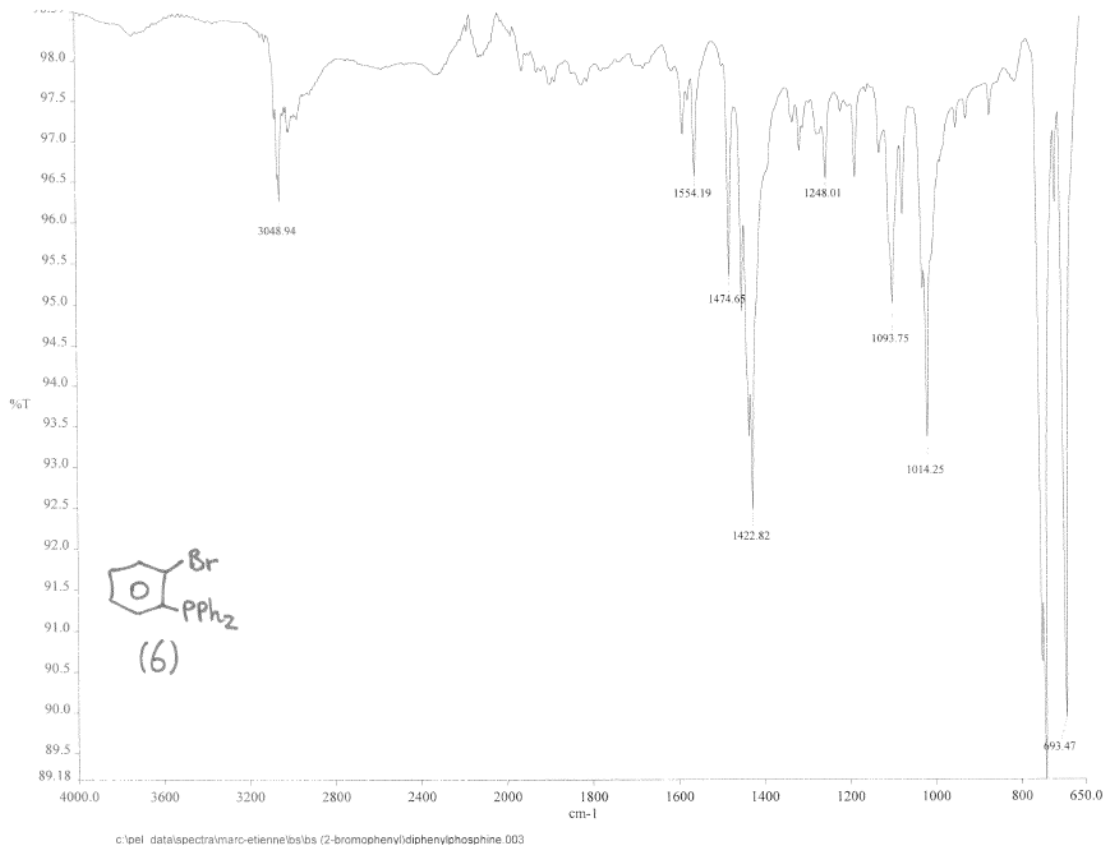
ATR-FT-IR - bis(2-triflatephenyl)methanone (4)



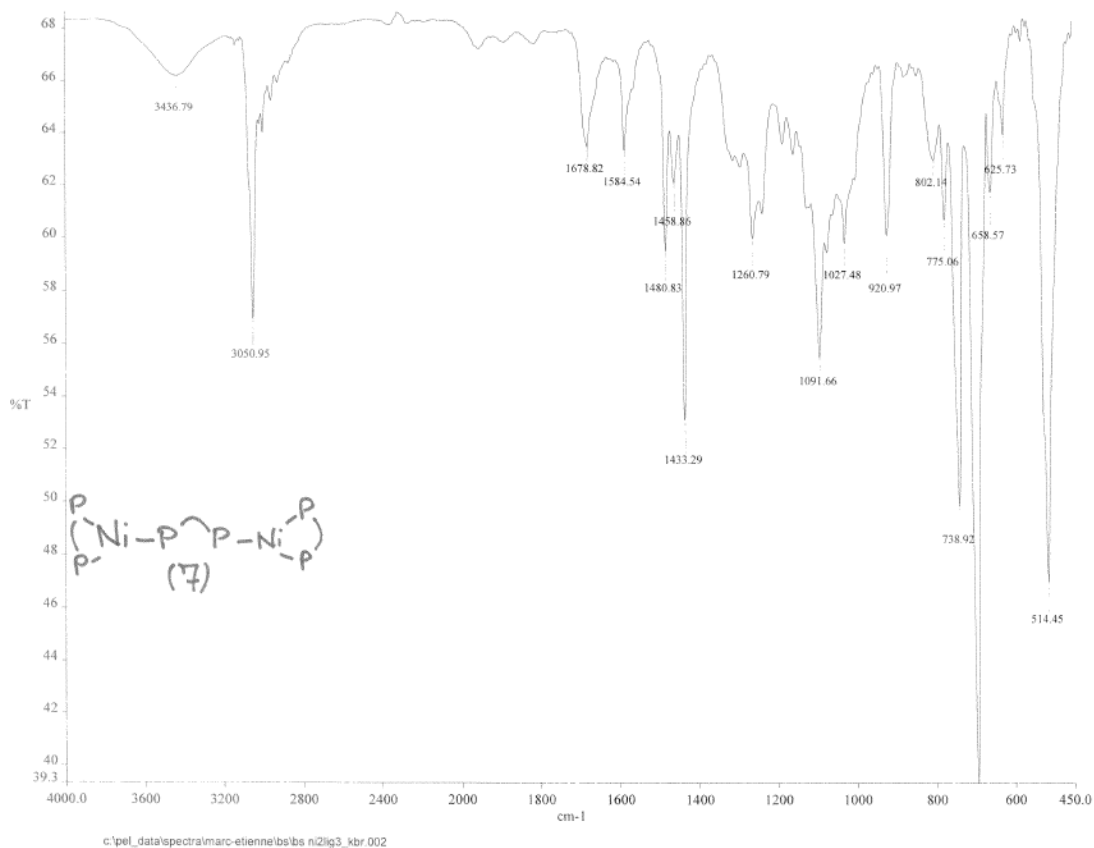
ATR-FT-IR - DPK (5)



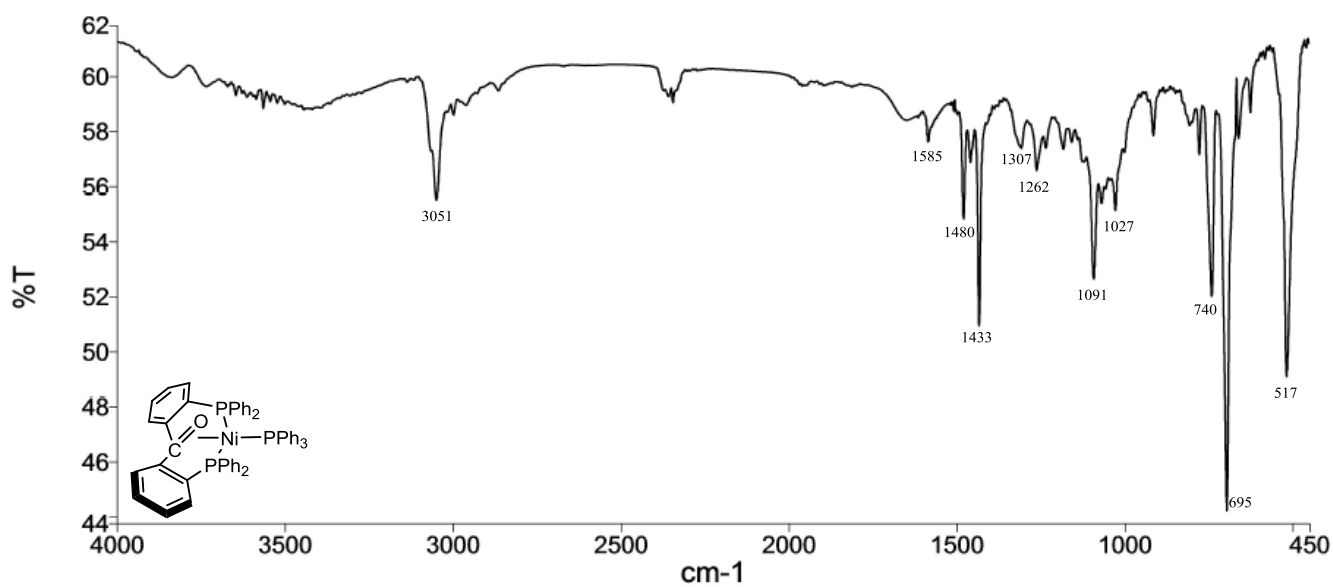
ATR-FT-IR - o-bromophenyldiphenylphosphine (6)



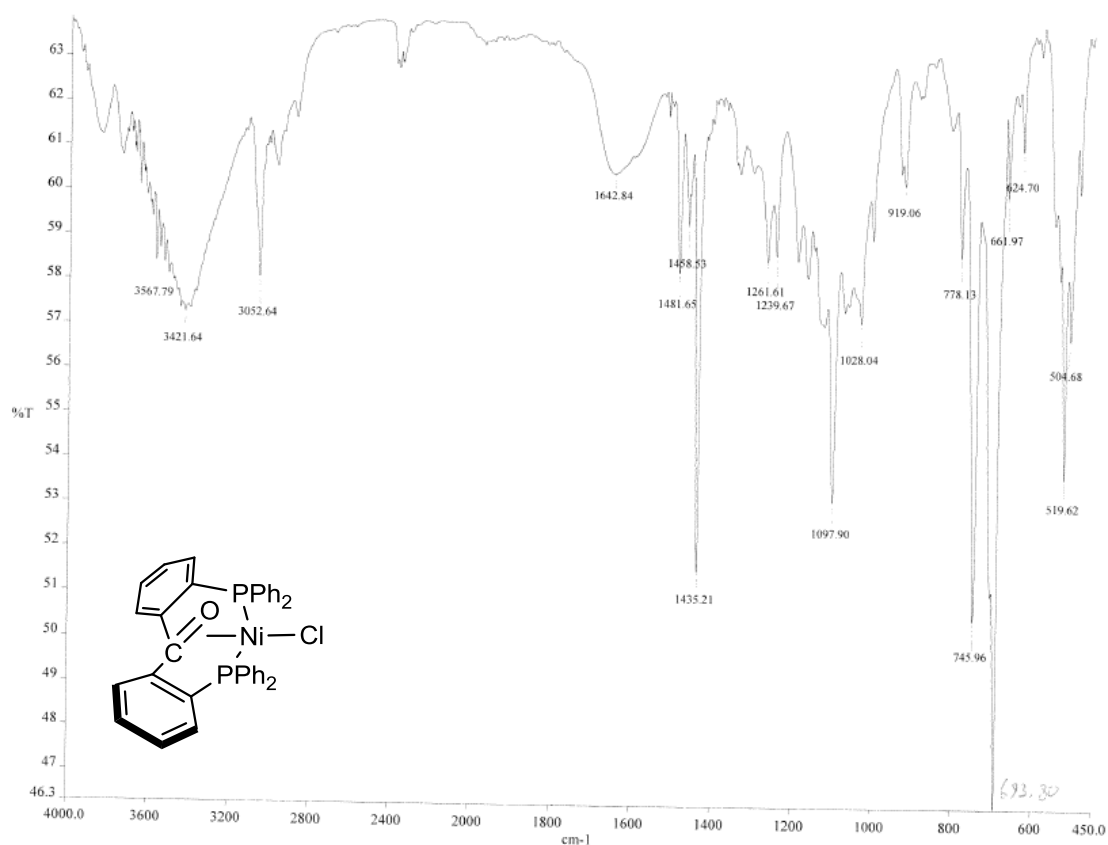
KBr-FT-IR - [Ni₂(DPK)₃] (7)



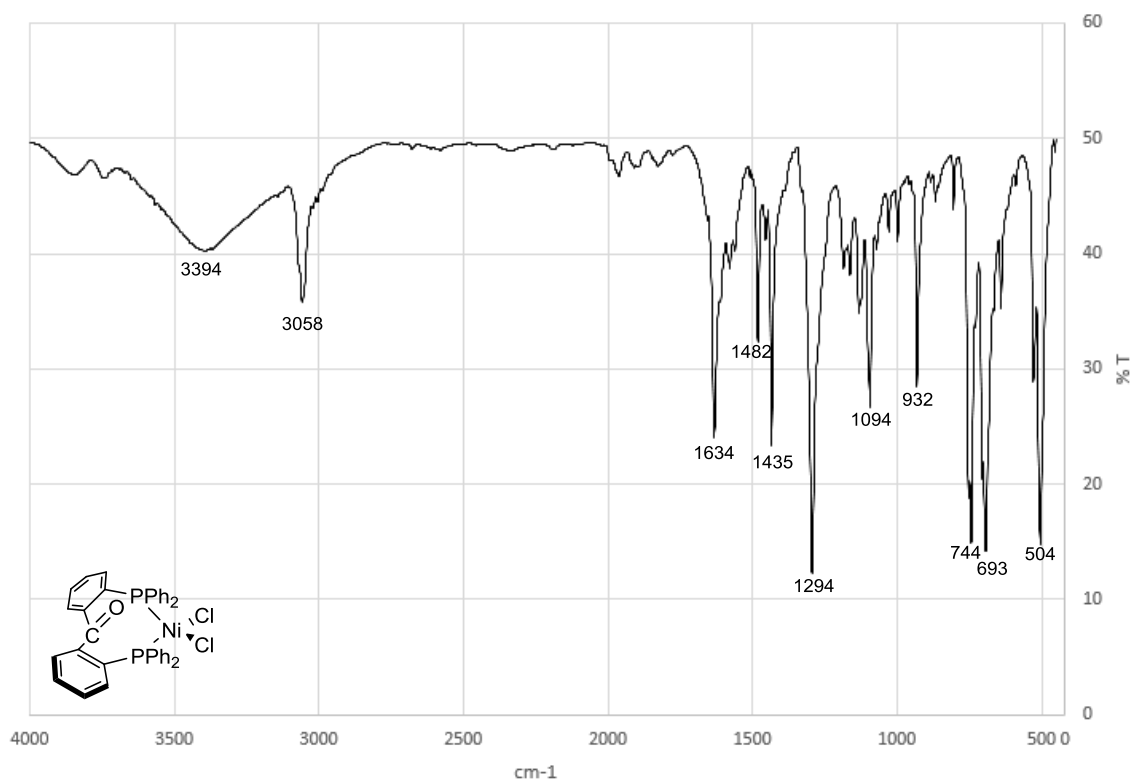
KBr-FT-IR - [Ni(0)(DPK)(PPh₃)] (8)



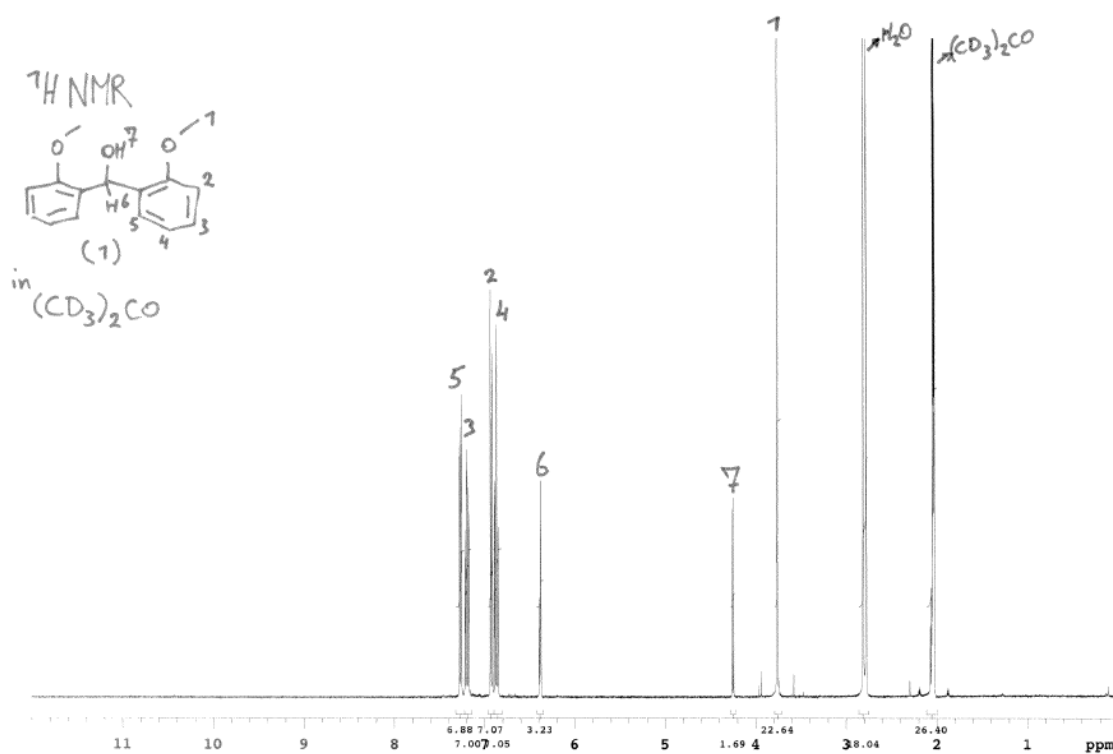
KBr-FT-IR - [Ni(I)Cl(DPK)] (9)



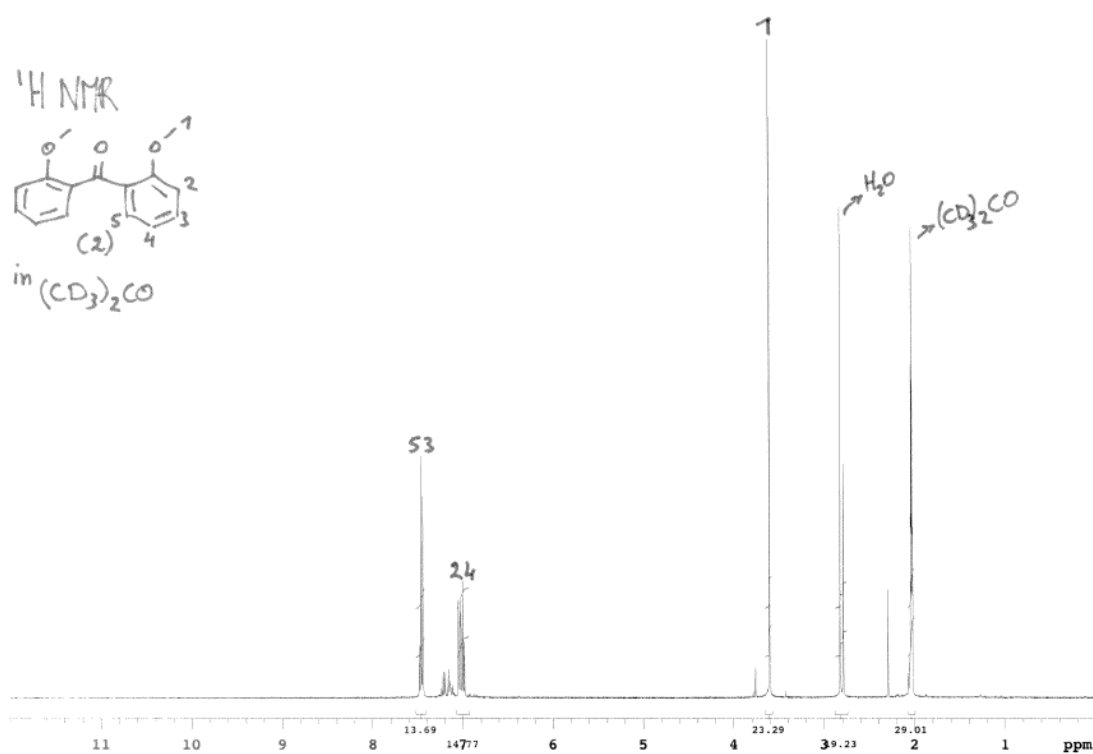
KBr-FT-IR - [Ni(II)Cl₂(DPK)] (10)



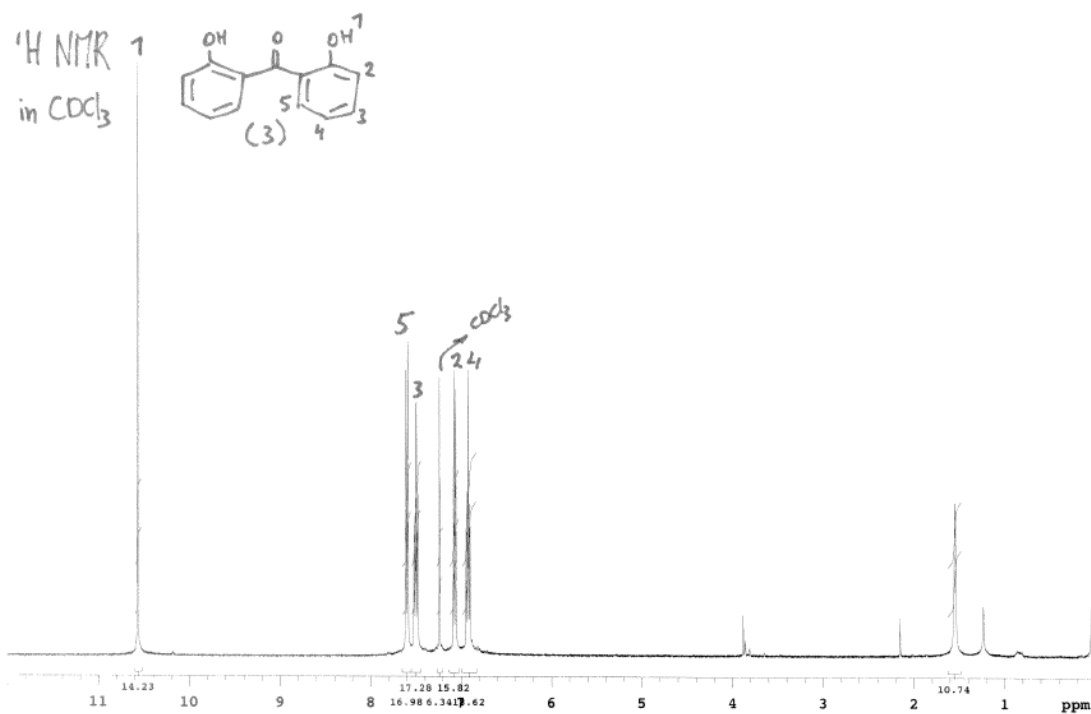
$^1\text{H-NMR}$ - bis(2-methoxyphenyl)methanole (1)



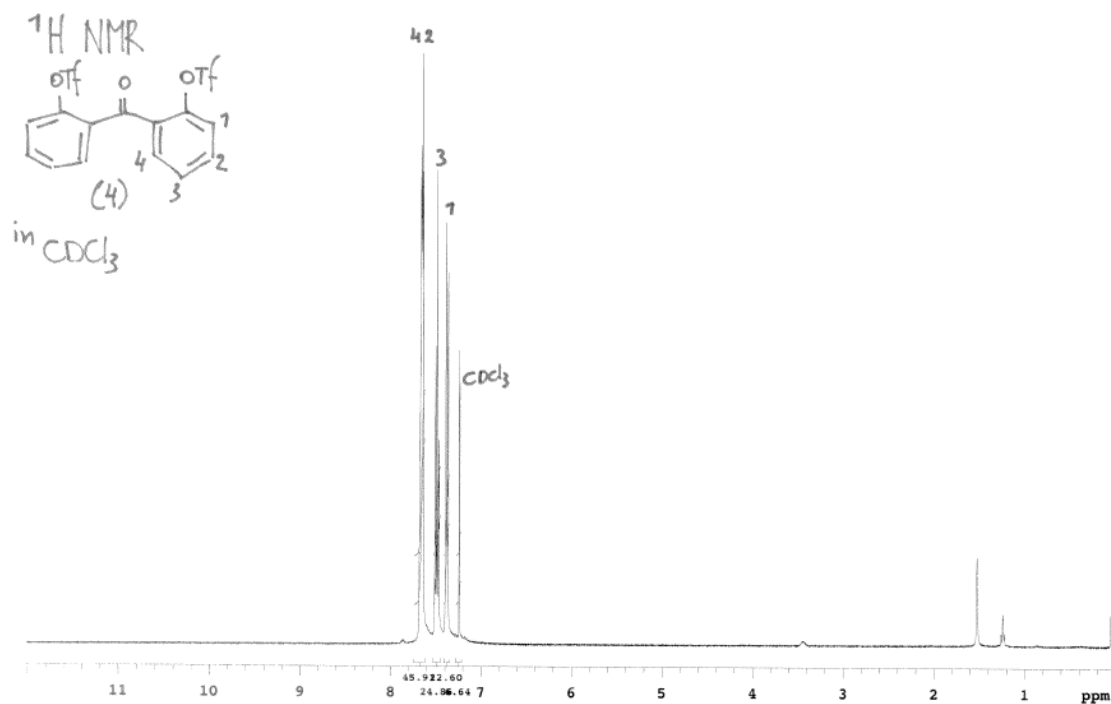
$^1\text{H-NMR}$ - bis(2-methoxyphenyl)methanone (2)



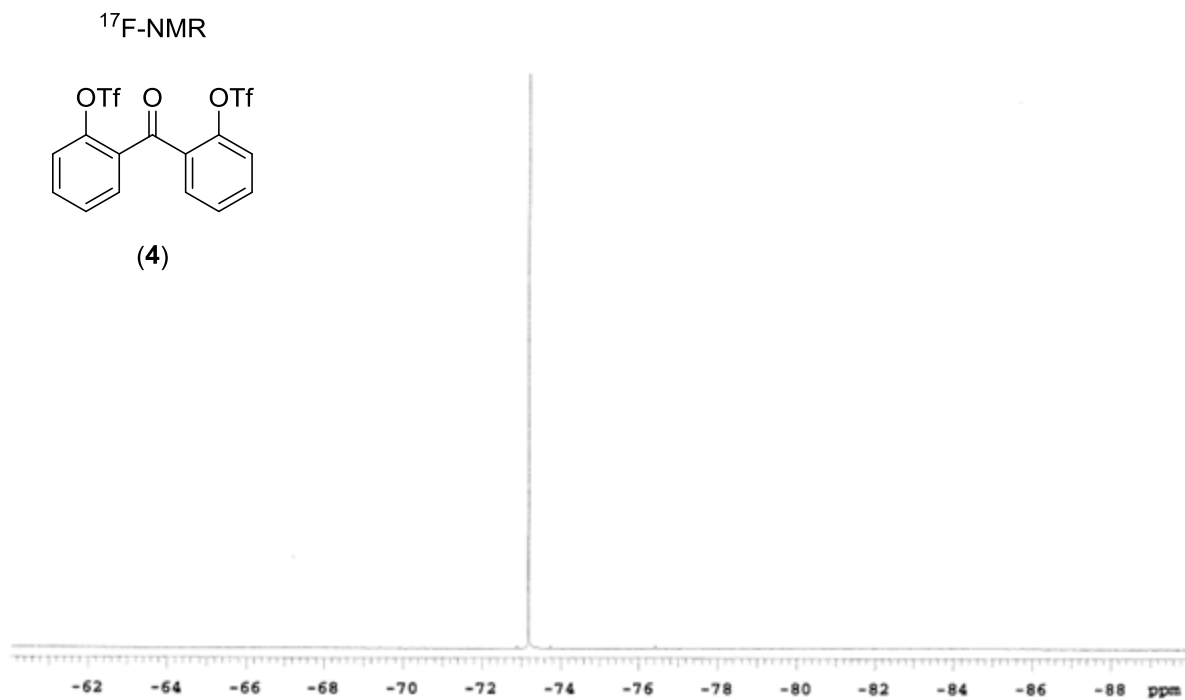
$^1\text{H-NMR}$ - bis(2-hydroxyphenyl)methanone (3)



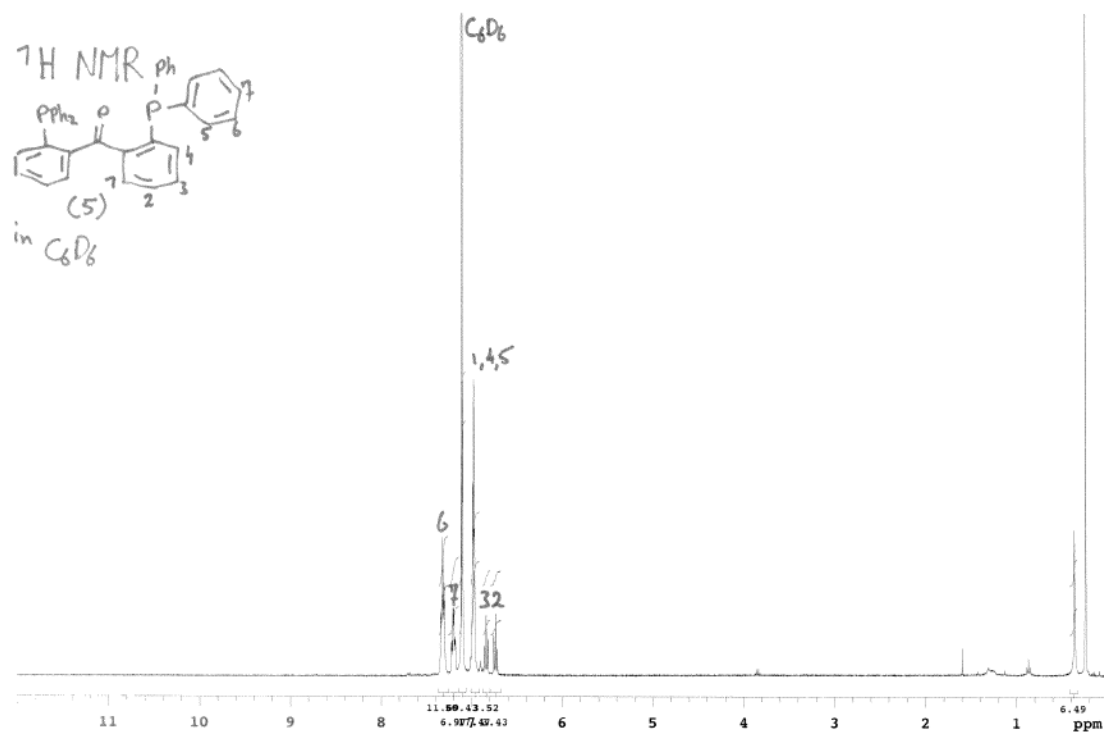
$^1\text{H-NMR}$ - bis(2-triflatephenyl)methanone (4)



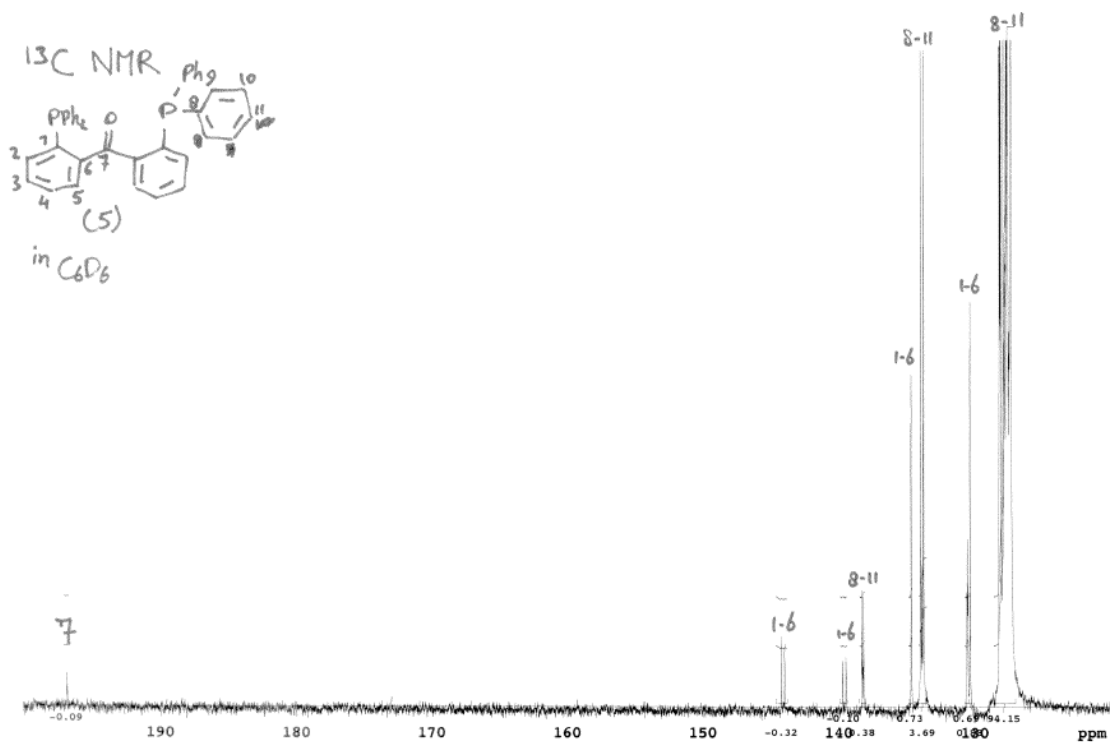
^{17}F -NMR - bis(2-triflatephenyl)methanone (4)



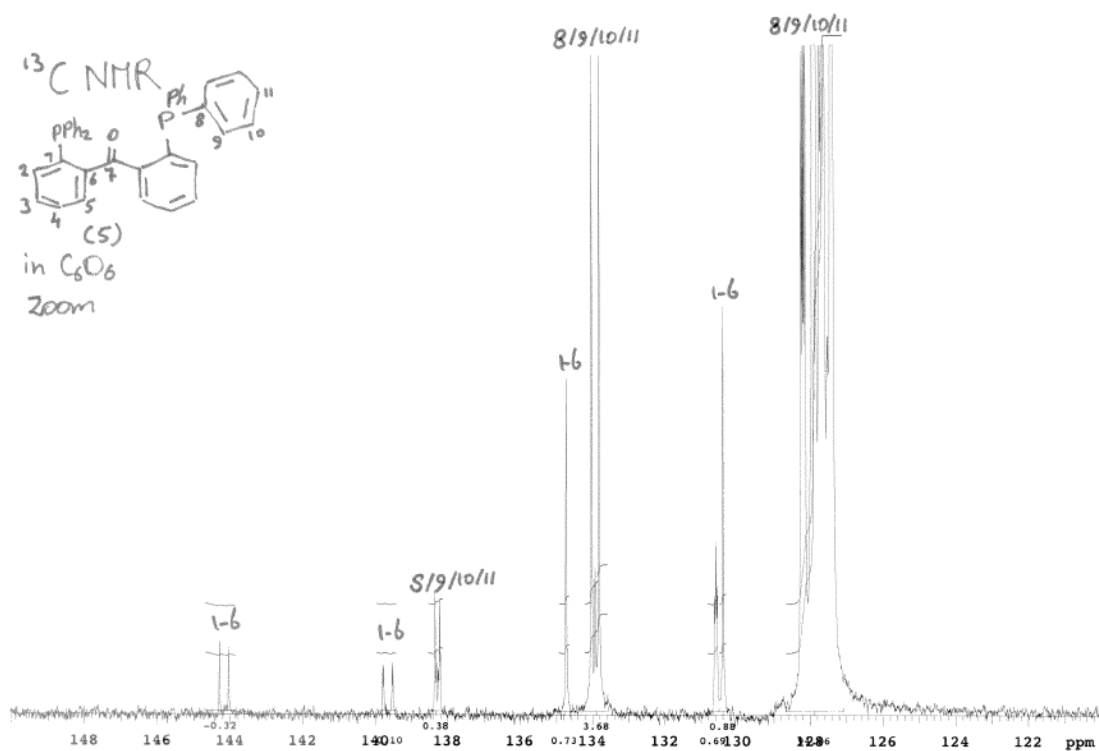
^1H -NMR - DPK (5)



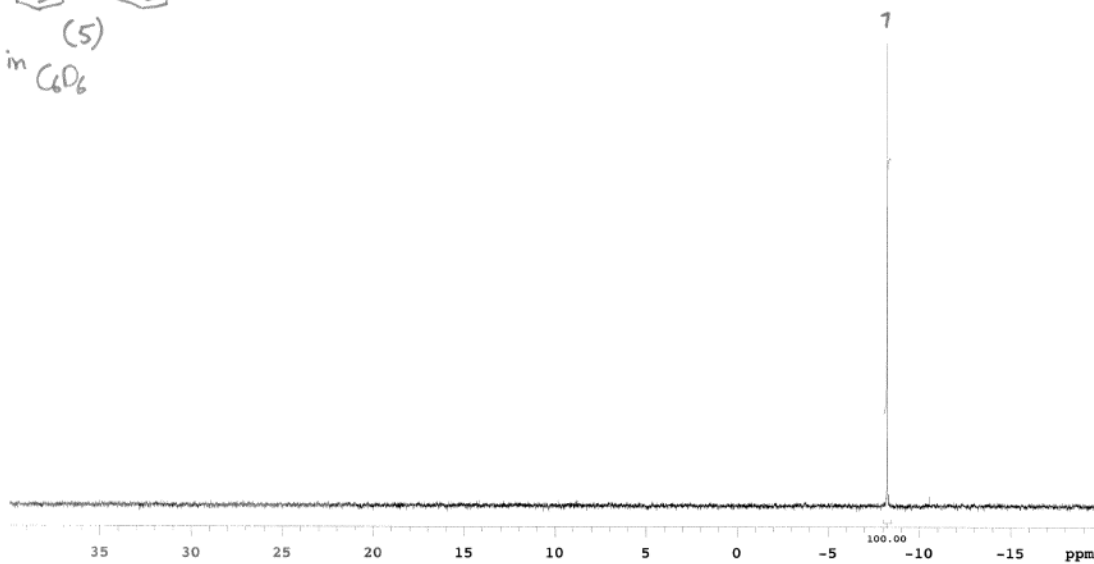
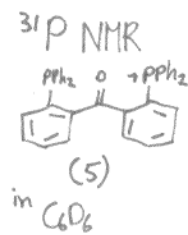
^{13}C -NMR - DPK (5)



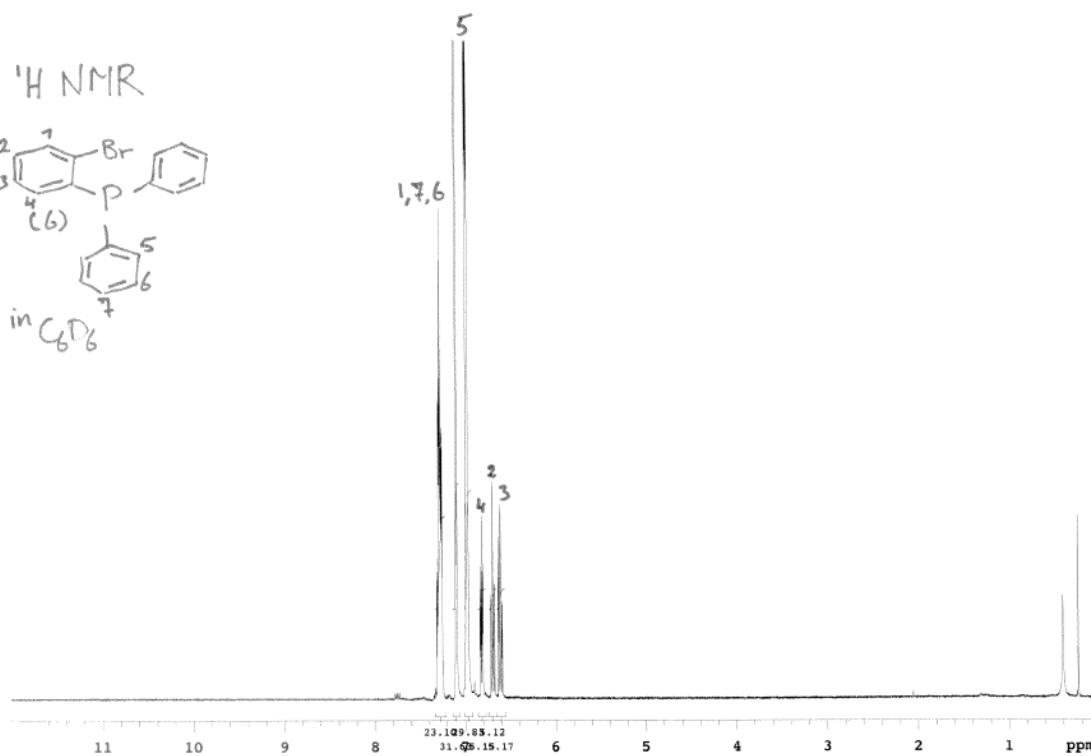
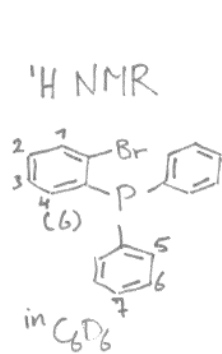
^{13}C -NMR - DPK zoom (5)



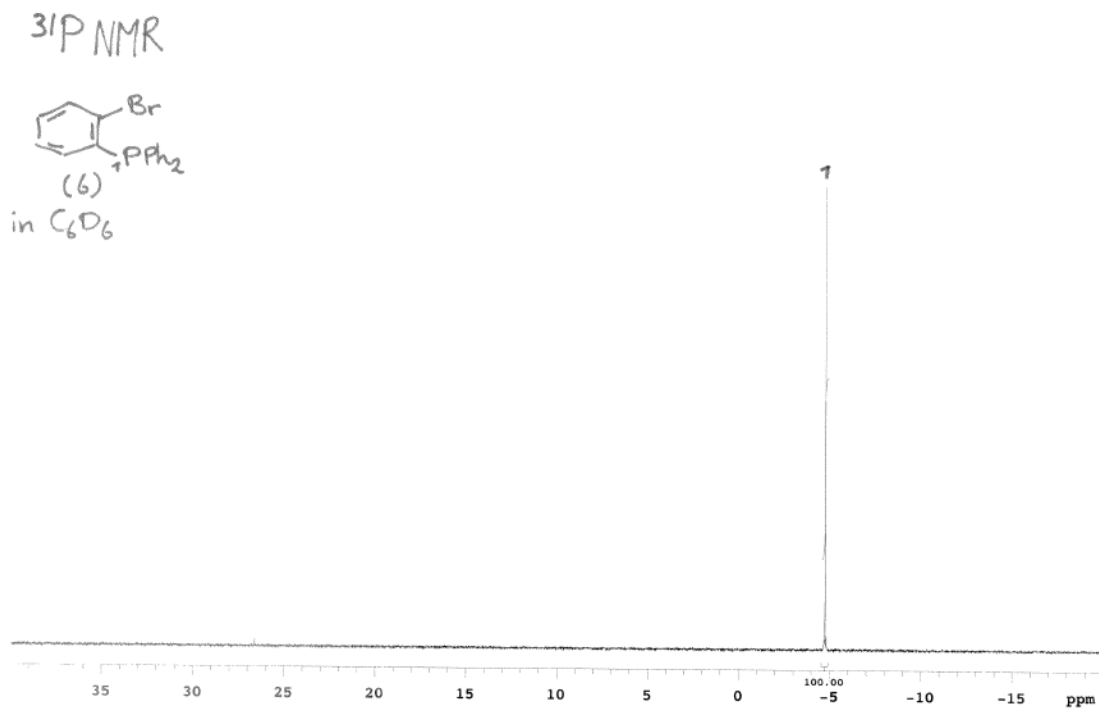
^{31}P -NMR - DPK (5)



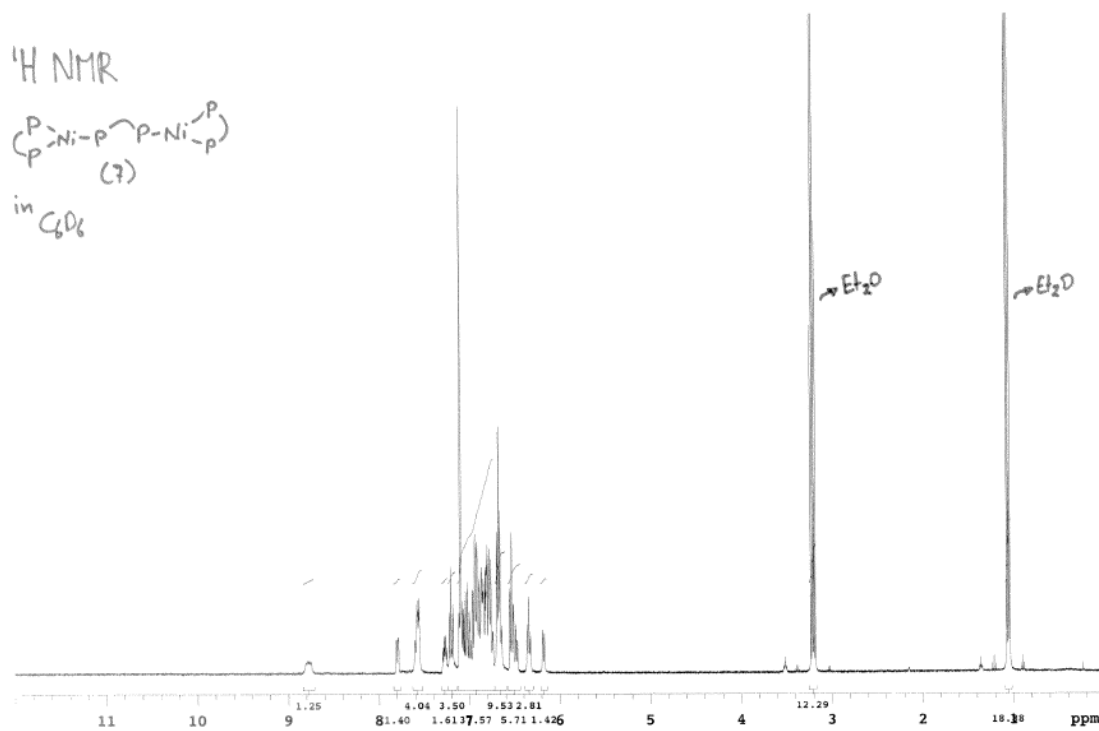
^1H -NMR - o-bromophenyldiphenylphosphine (6)



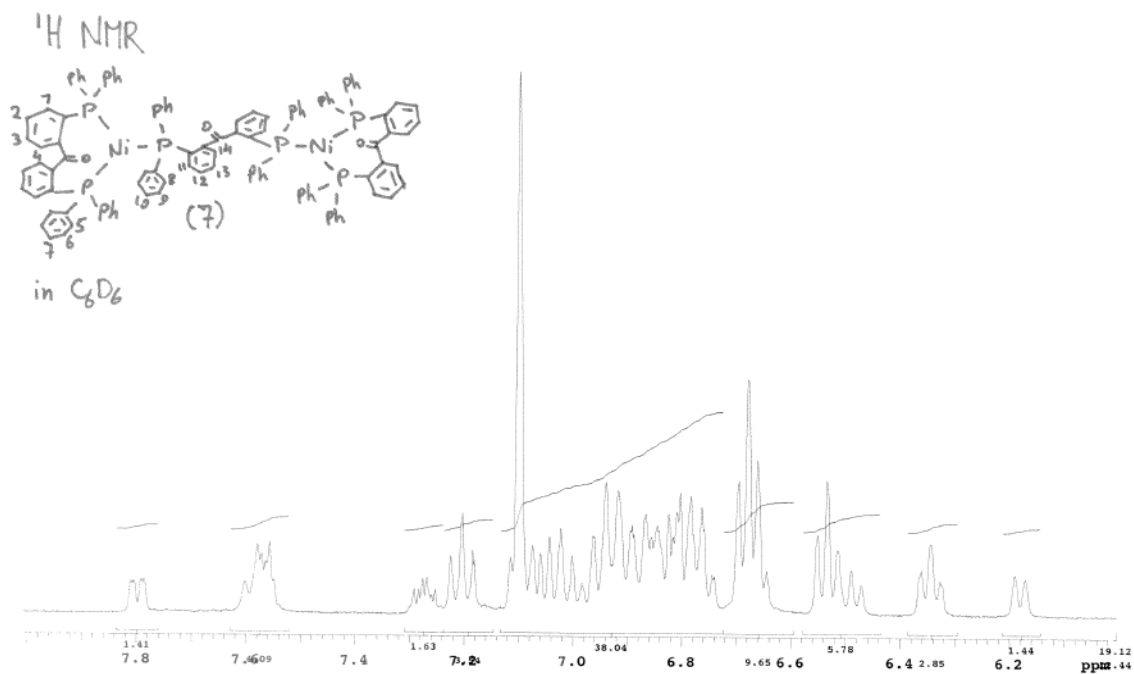
^{31}P -NMR - o-bromophenyldiphenylphosphine (6)



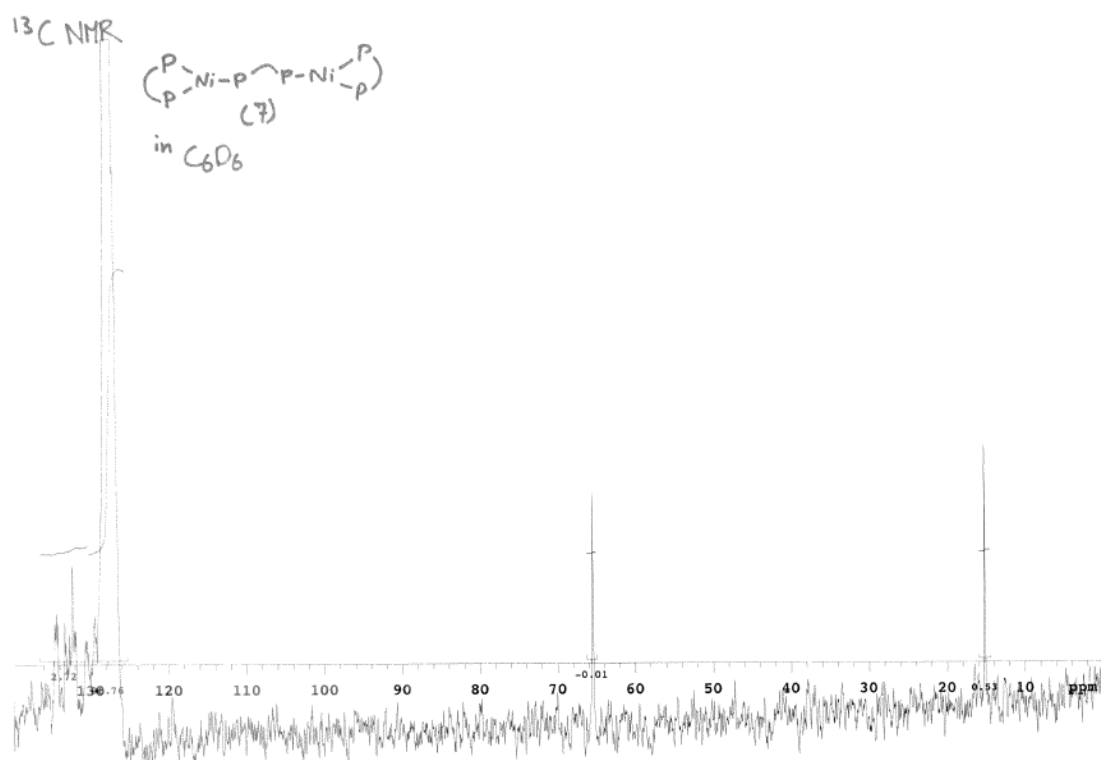
^1H -NMR - $[\text{Ni}_2(\text{DPK})_3]$ (7)



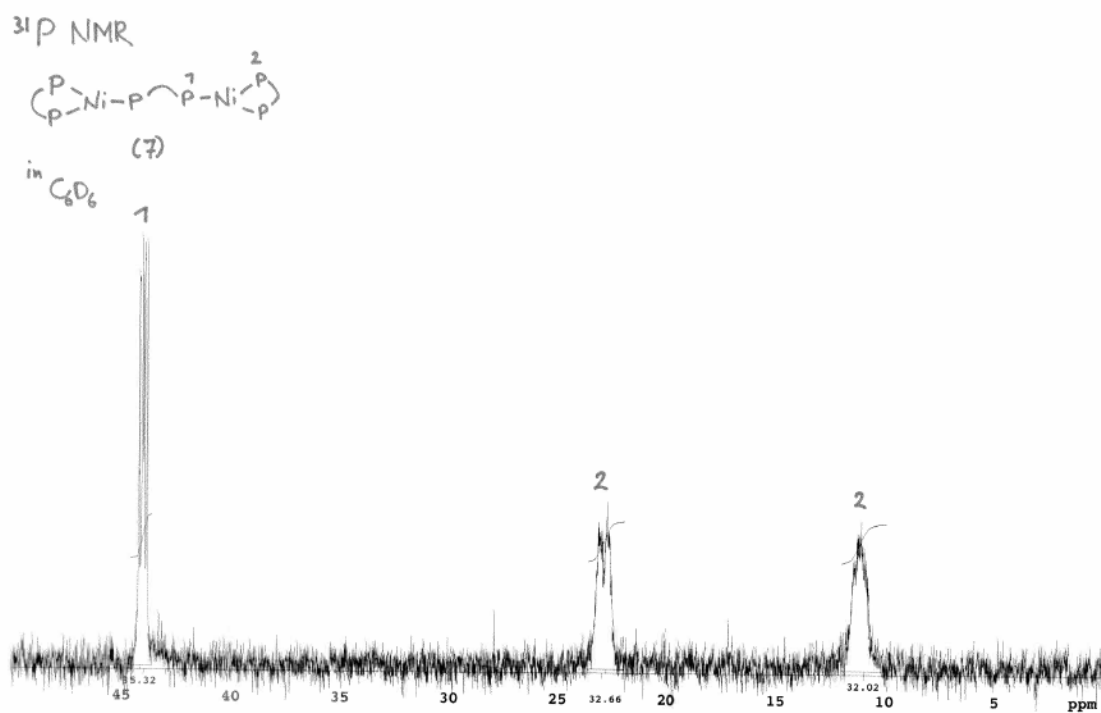
$^1\text{H-NMR}$ - $[\text{Ni}_2(\text{DPK})_3]$ (7) zoom



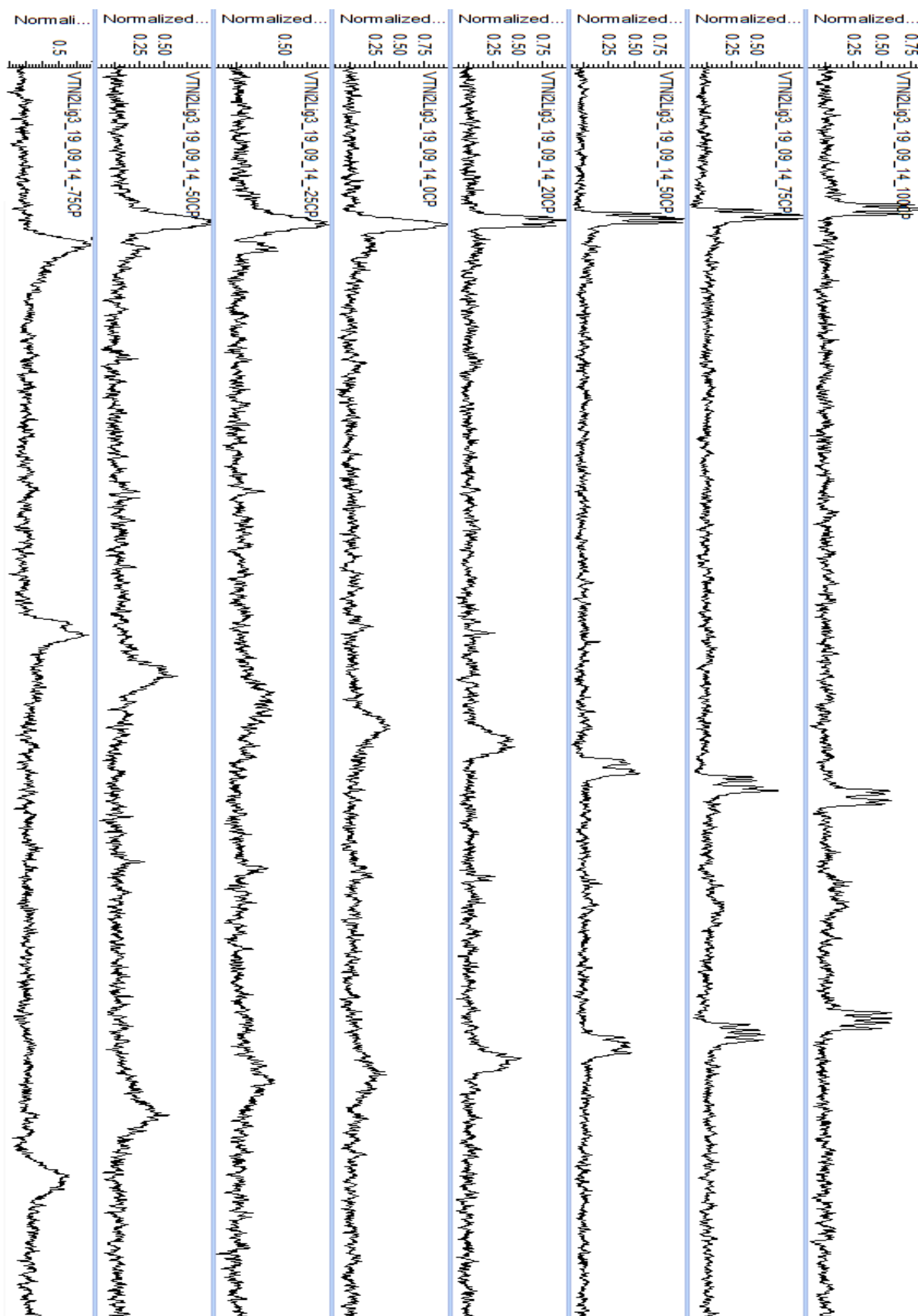
$^{13}\text{C-NMR}$ - $[\text{Ni}_2(\text{DPK})_3]$ (7)



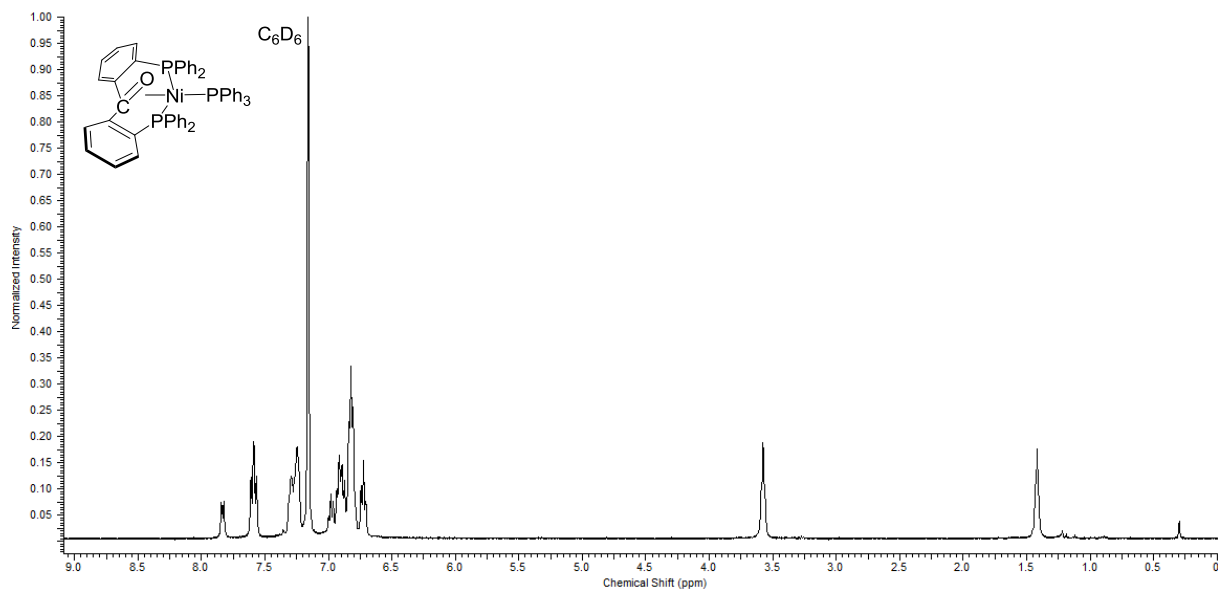
^{31}P -NMR - $[\text{Ni}_2(\text{DPK})_3]$ (7)



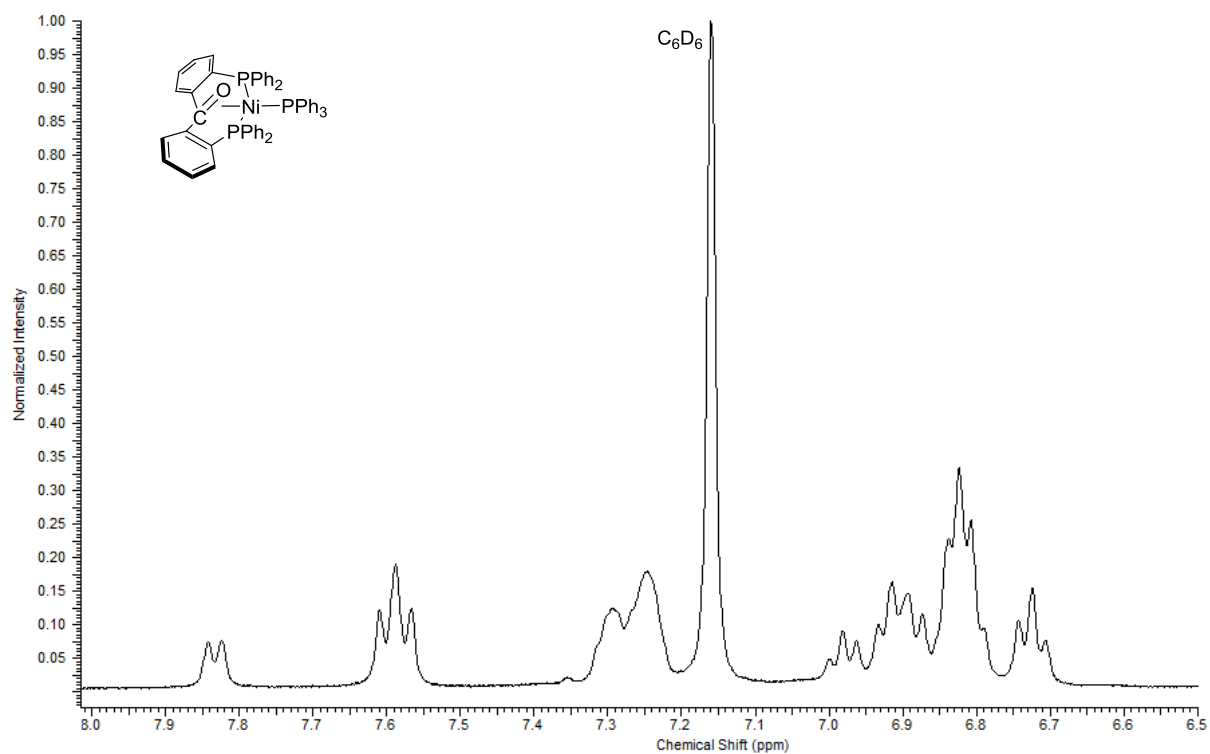
31P-VT-NMR - [Ni₂(DPK)₃] (7)



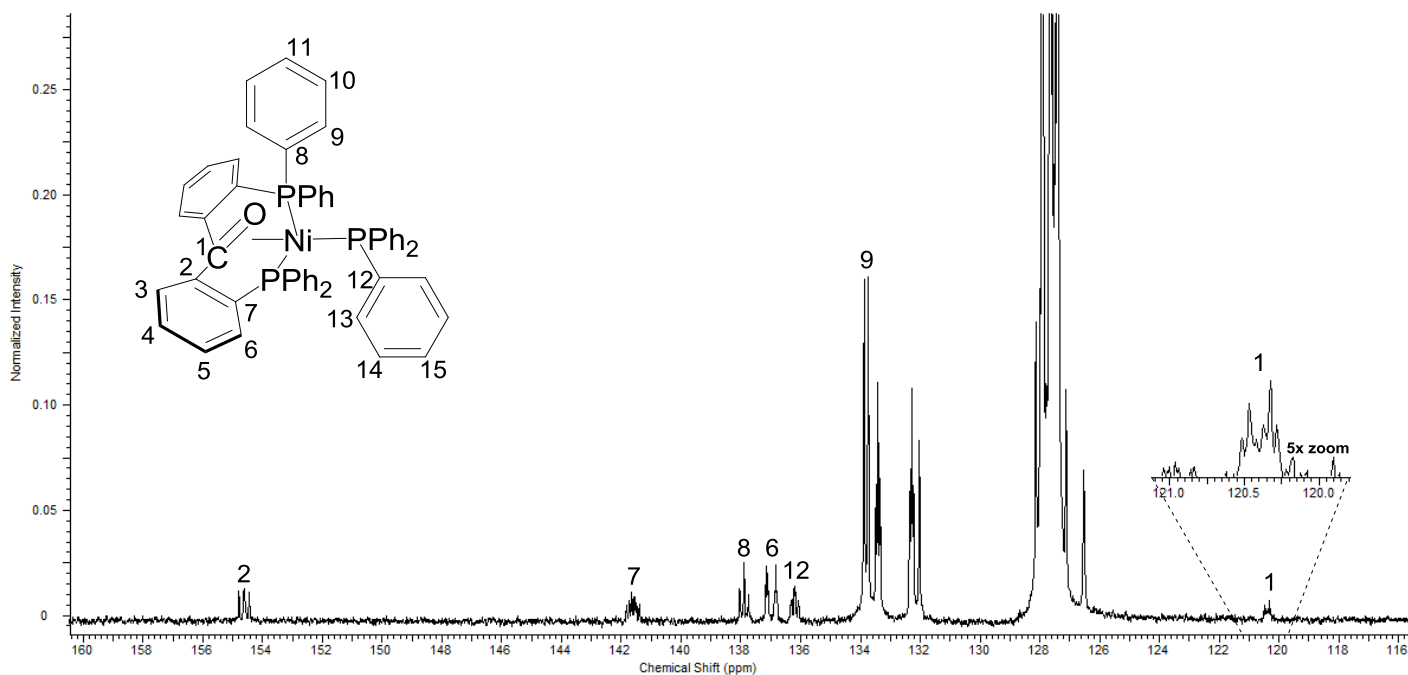
$^1\text{H-NMR}$ - $[\text{Ni}(0)(\text{DPK})(\text{PPh}_3)]$ (**8**)



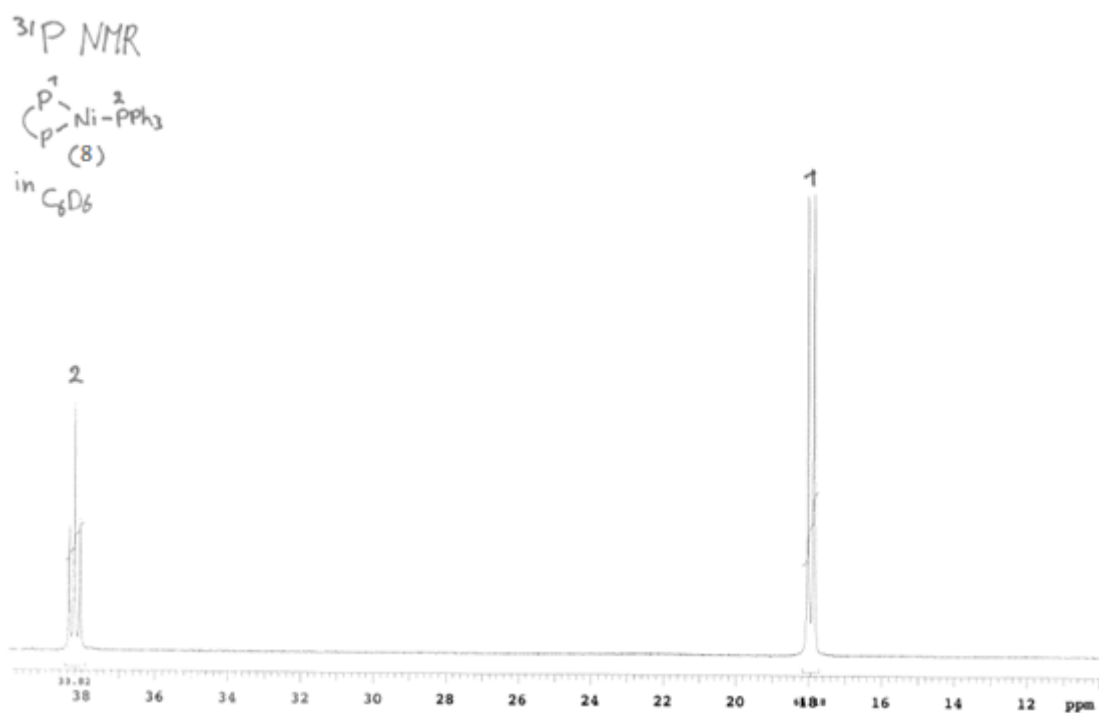
$^1\text{H-NMR}$ - $[\text{Ni}(0)(\text{DPK})(\text{PPh}_3)]$ (**8**) zoom



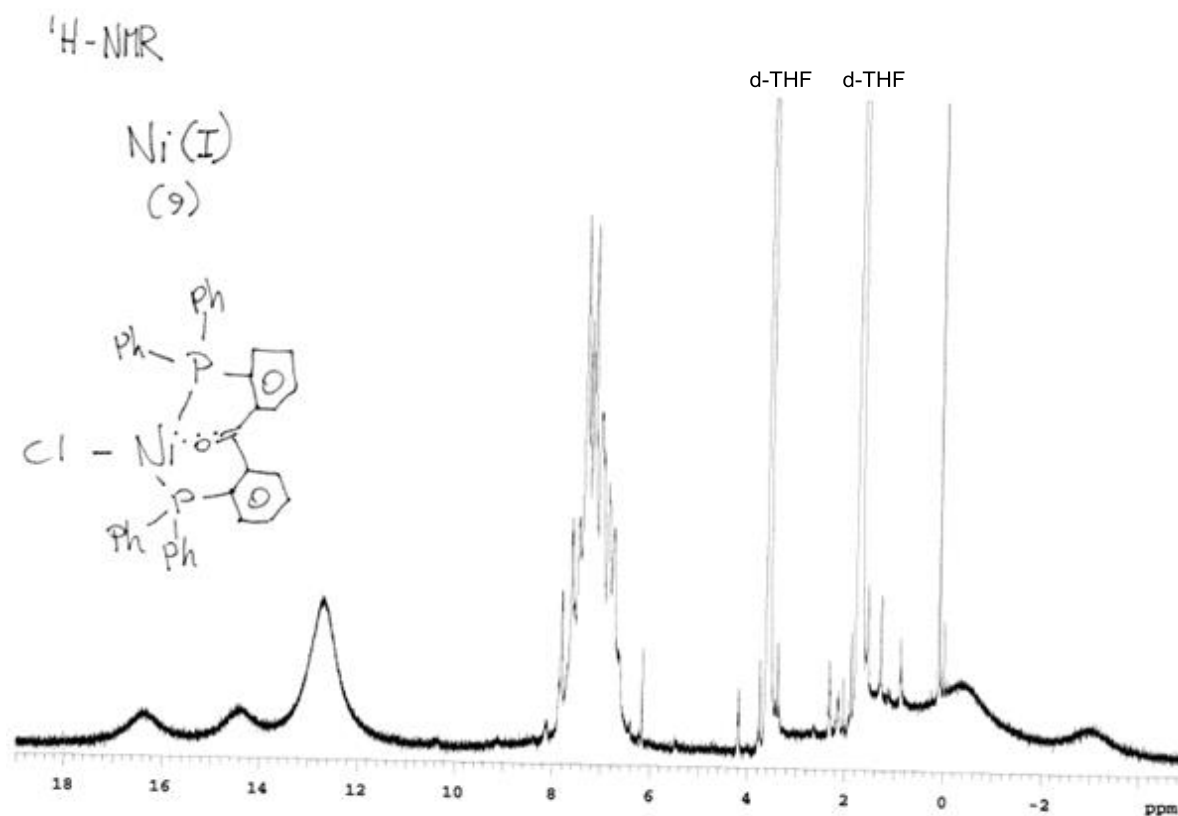
$^{13}\text{C-NMR}$ - $[\text{Ni}(0)(\text{DPK})(\text{PPh}_3)]$ (8**)**



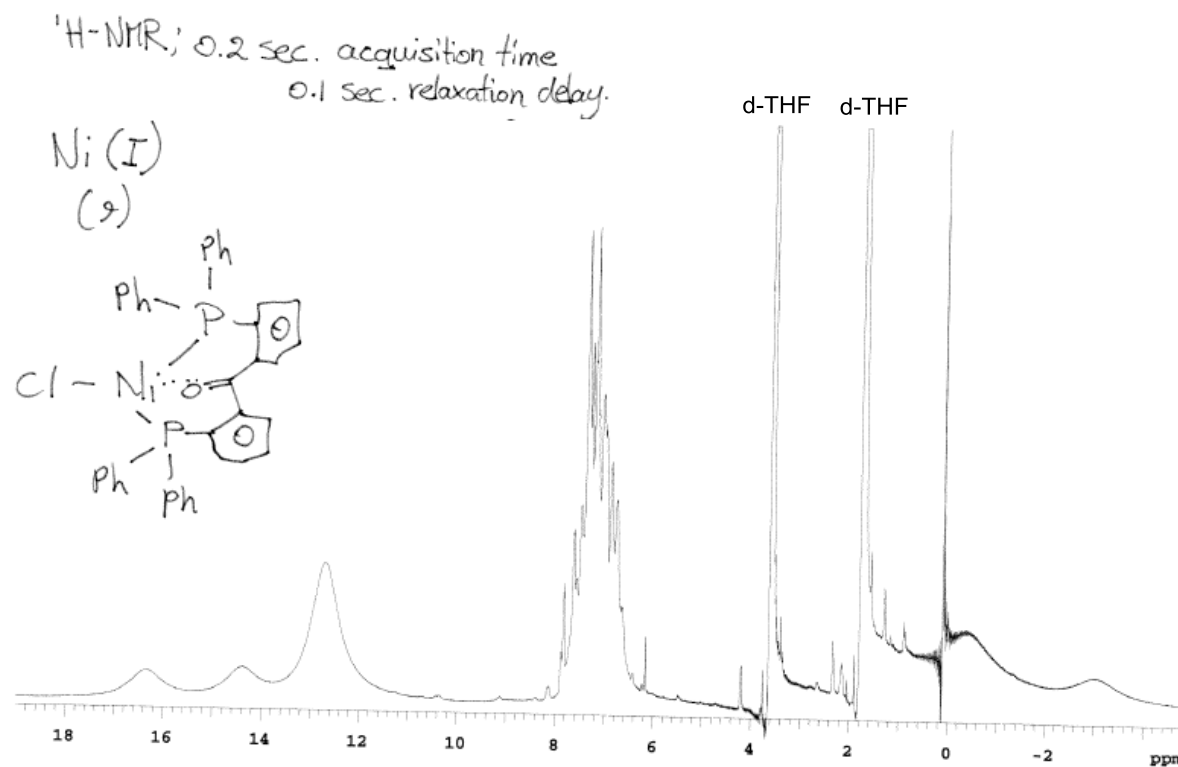
$^{31}\text{P-NMR}$ - $[\text{Ni}(0)(\text{DPK})(\text{PPh}_3)]$ (8**)**



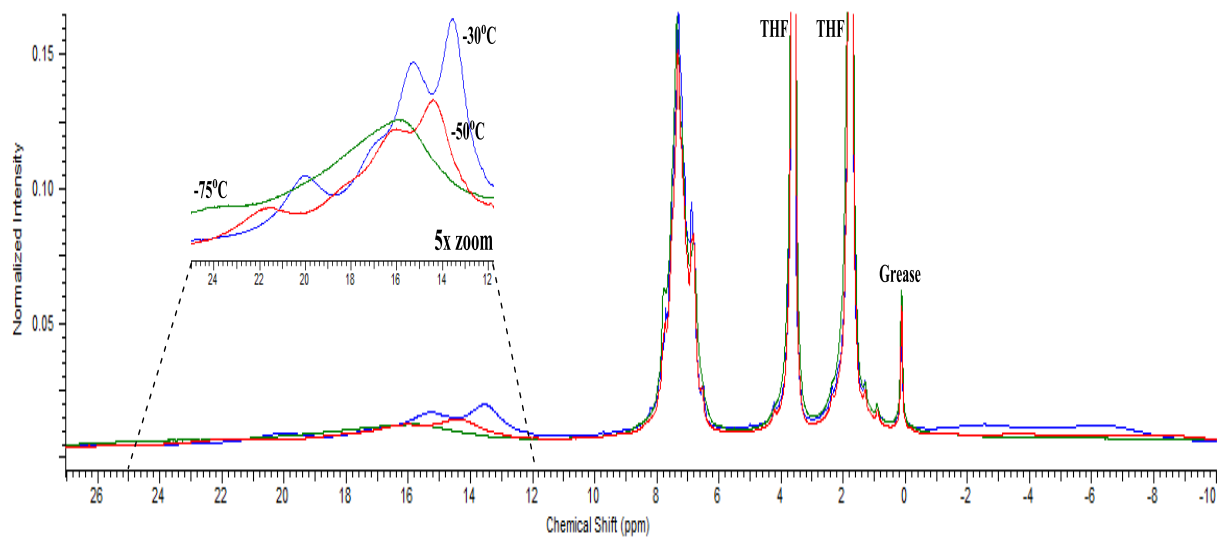
$^1\text{H-NMR}$ - $[\text{Ni}(\text{I})\text{Cl}(\text{DPK})]$ (9)



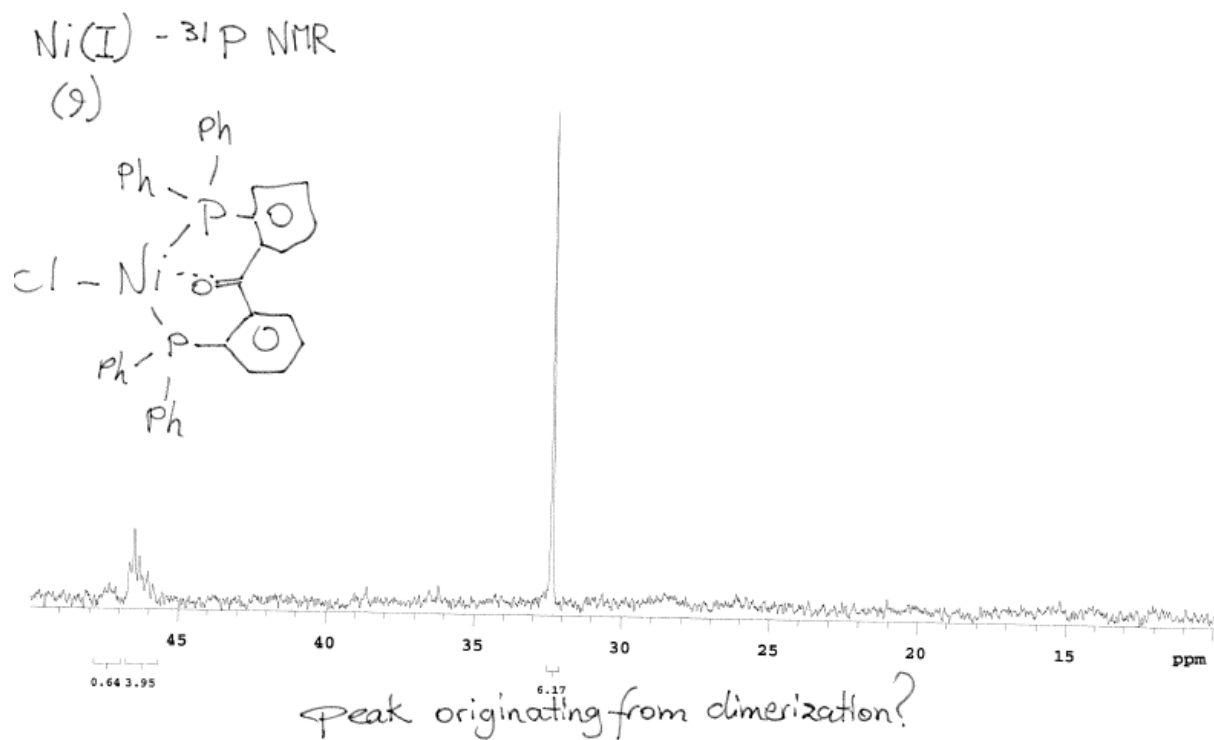
$^1\text{H-NMR}$, Paramagnetic measurement settings - $[\text{Ni}(\text{I})\text{Cl}(\text{DPK})]$ (9)



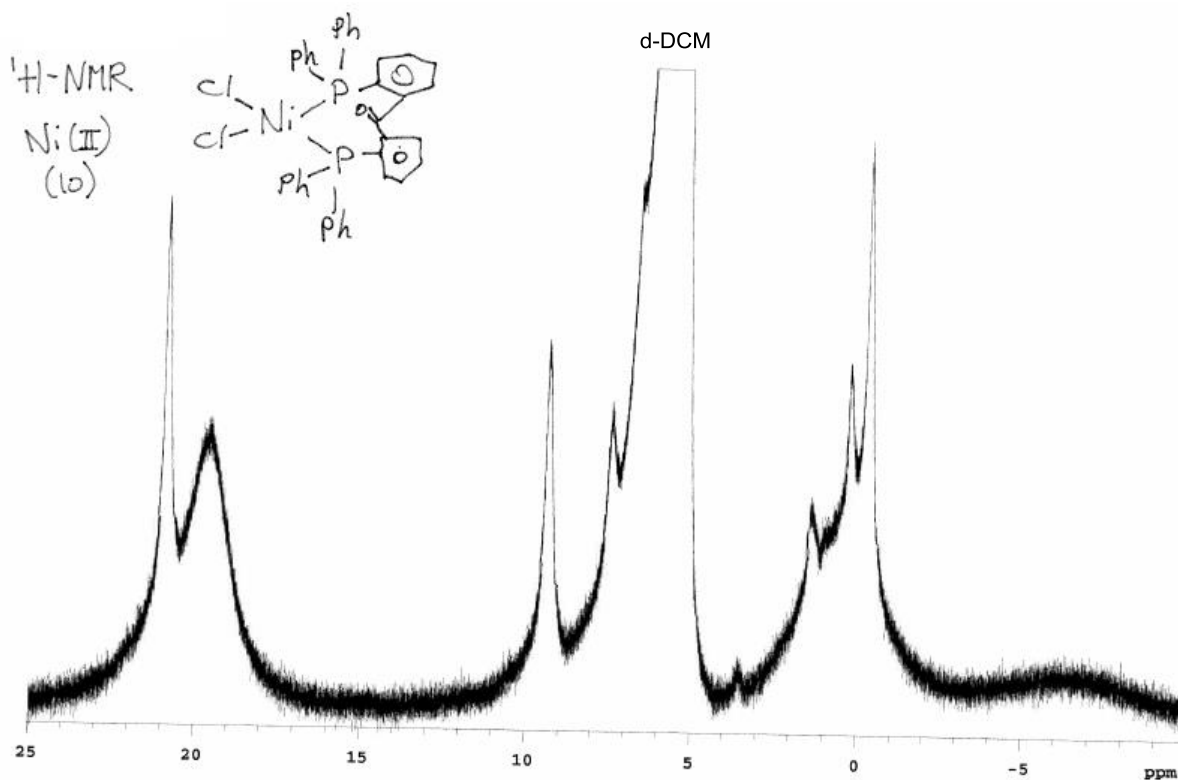
^1H -VT-NMR, Paramagnetic measurement settings - $[\text{Ni}(\text{I})\text{Cl}(\text{DPK})]$ (9)



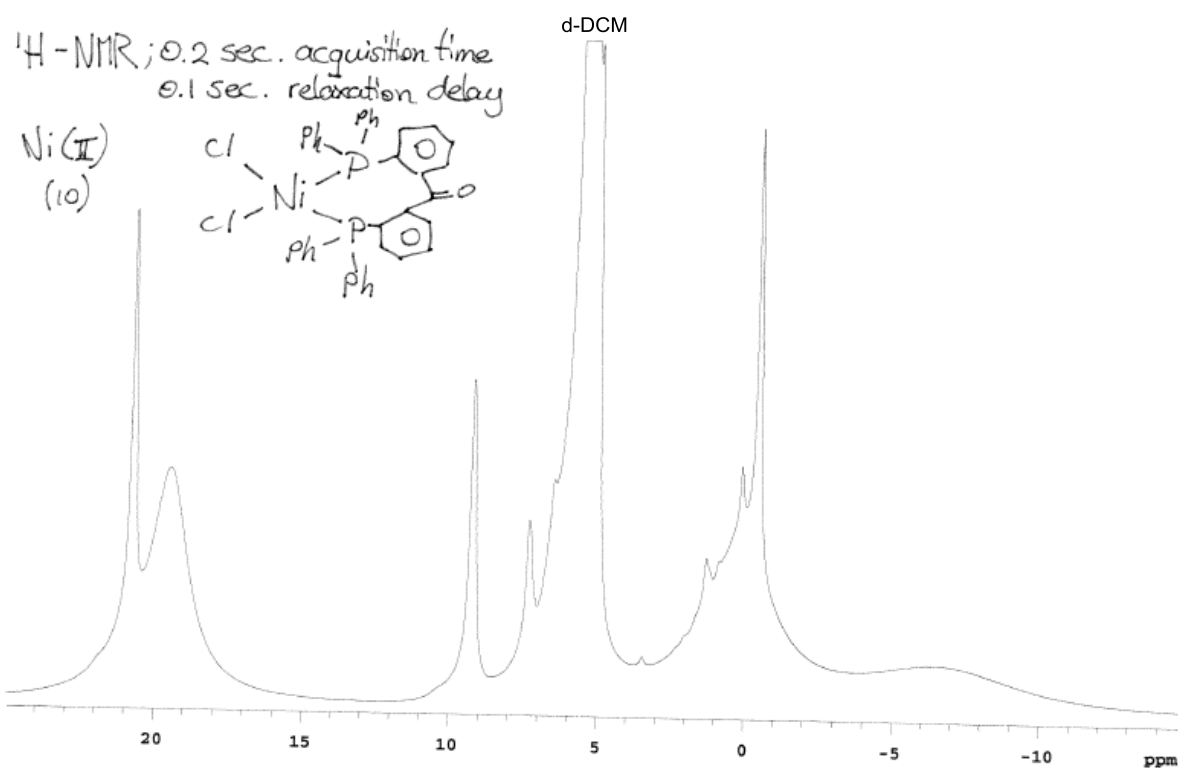
^{31}P -NMR - $[\text{Ni}(\text{I})\text{Cl}(\text{DPK})]$ (9)



$^1\text{H-NMR}$ - $[\text{Ni}(\text{II})\text{Cl}_2(\text{DPK})]$ (10)

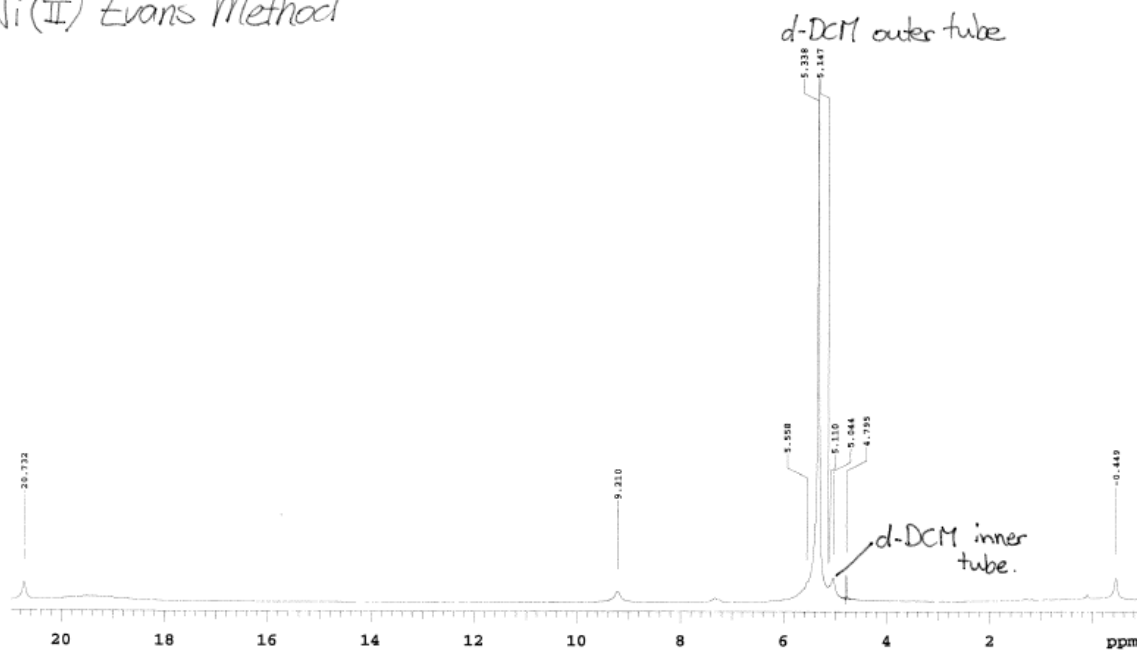


$^1\text{H-NMR}$, Paramagnetic measurement settings - $[\text{Ni}(\text{II})\text{Cl}_2(\text{DPK})]$ (10)

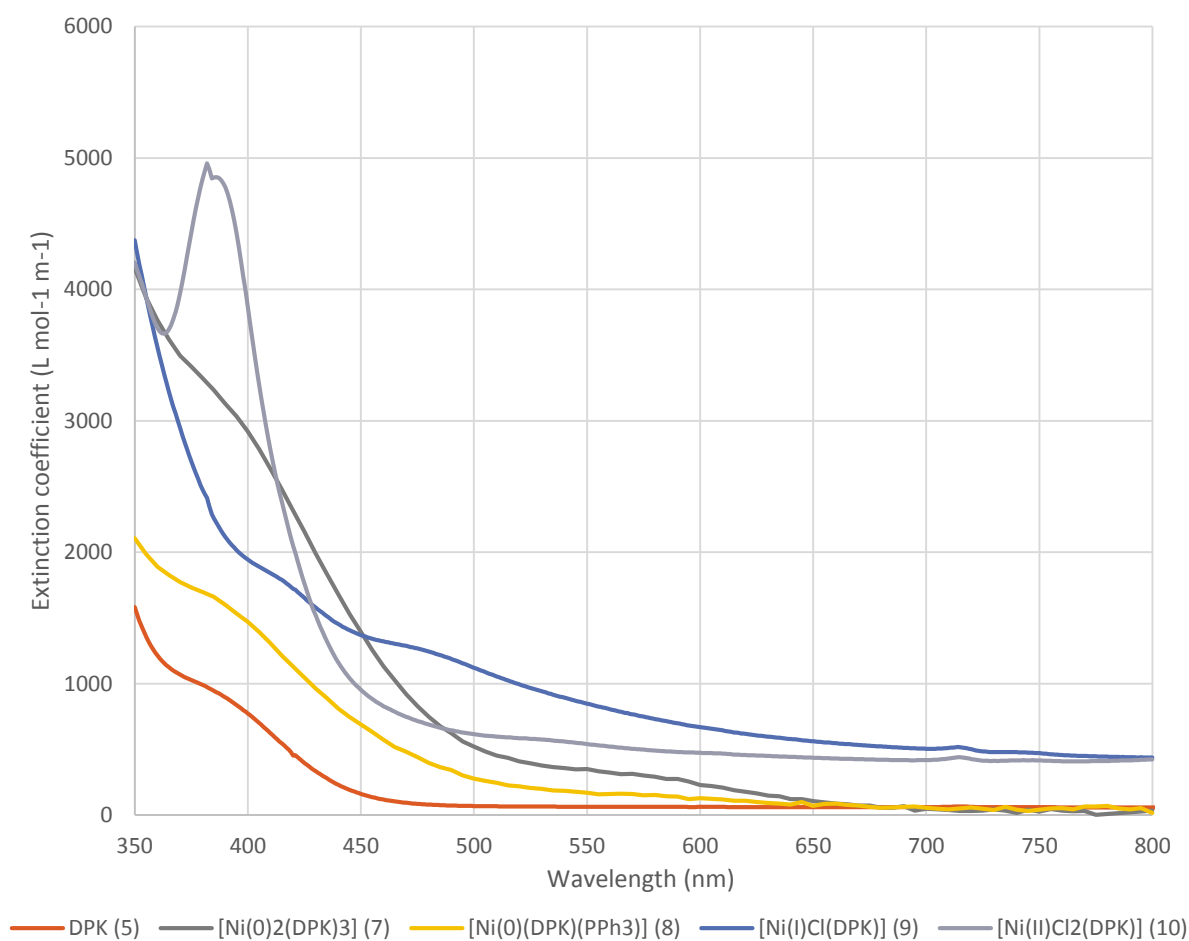


$^1\text{H-NMR}$, Evans method - $[\text{Ni}(\text{II})\text{Cl}_2(\text{DPK})]$ (10)

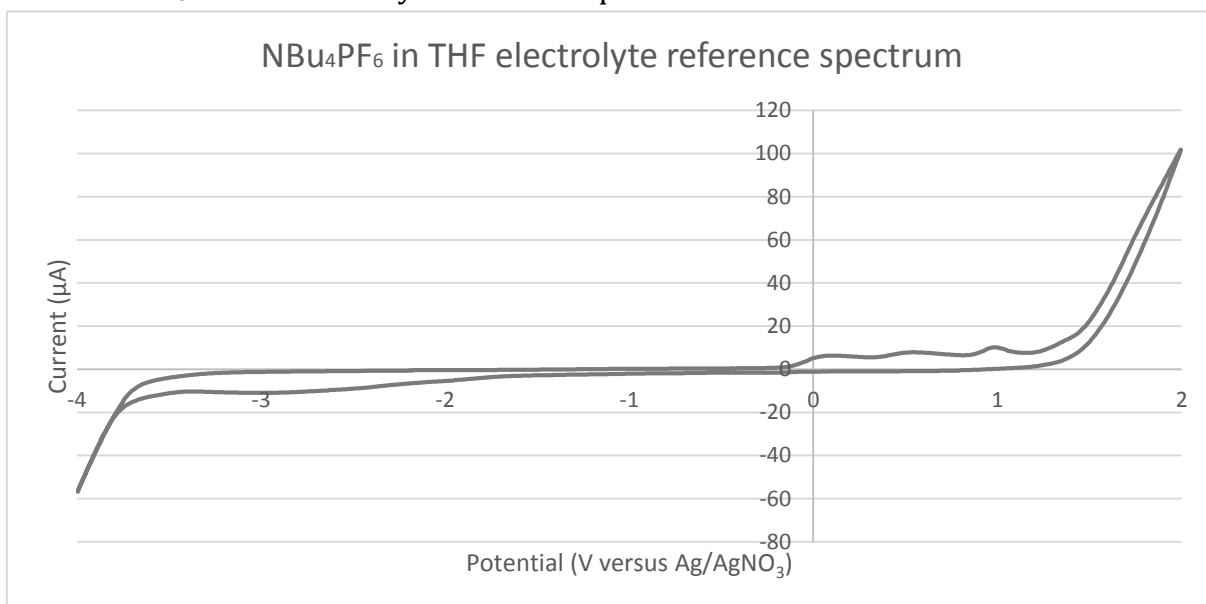
Ni(II) Evans Method



UV-Vis - DPK (5), $[\text{Ni}_2(\text{DPK})_3]$ (7), $[\text{Ni}(\text{O})(\text{DPK})(\text{PPh}_3)]$ (8), $[\text{Ni}(\text{I})\text{Cl}(\text{DPK})]$ (9), $[\text{Ni}(\text{II})\text{Cl}_2(\text{DPK})]$ (10)

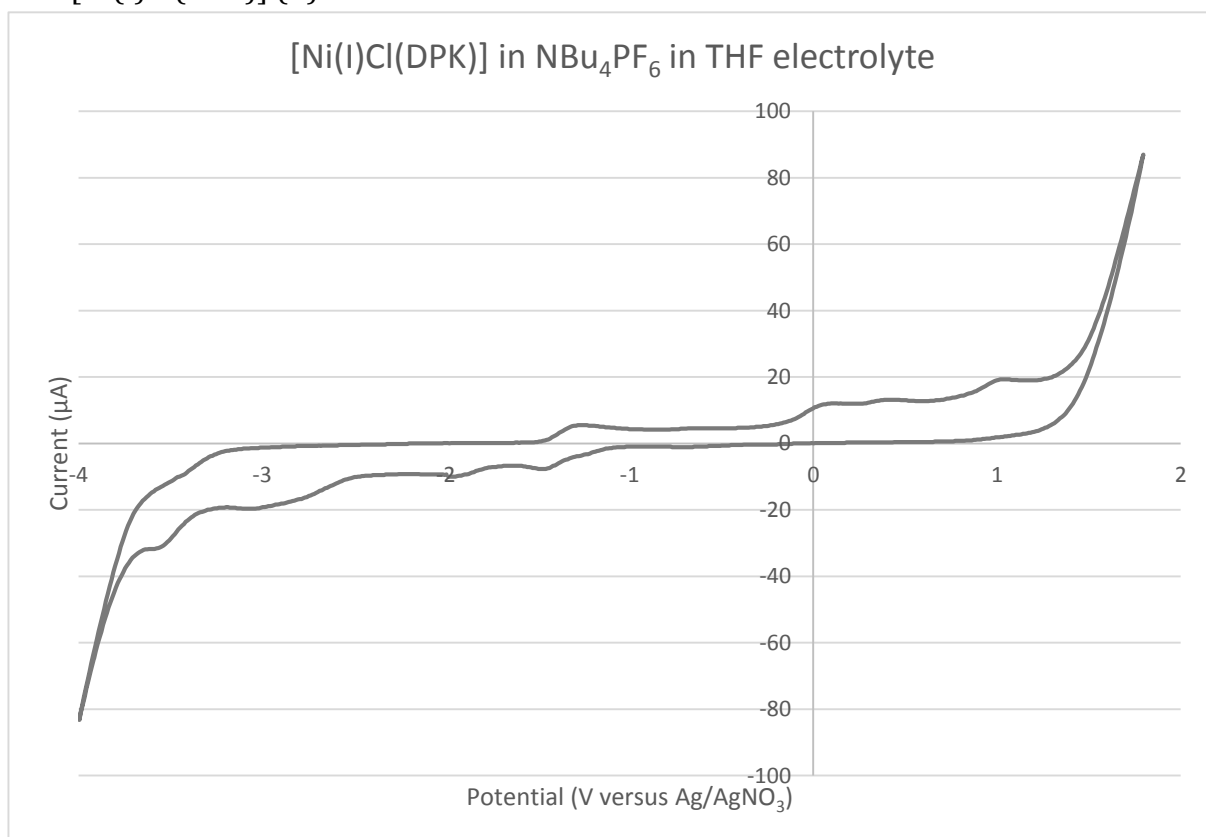


CV - NBu_4PF_6 in THF electrolyte reference spectrum



Vertex 1: -4 V; Vertex 2: 2 V; E_{start} : -1 V; Scanrate: 50 mV/s; 2 cycles.

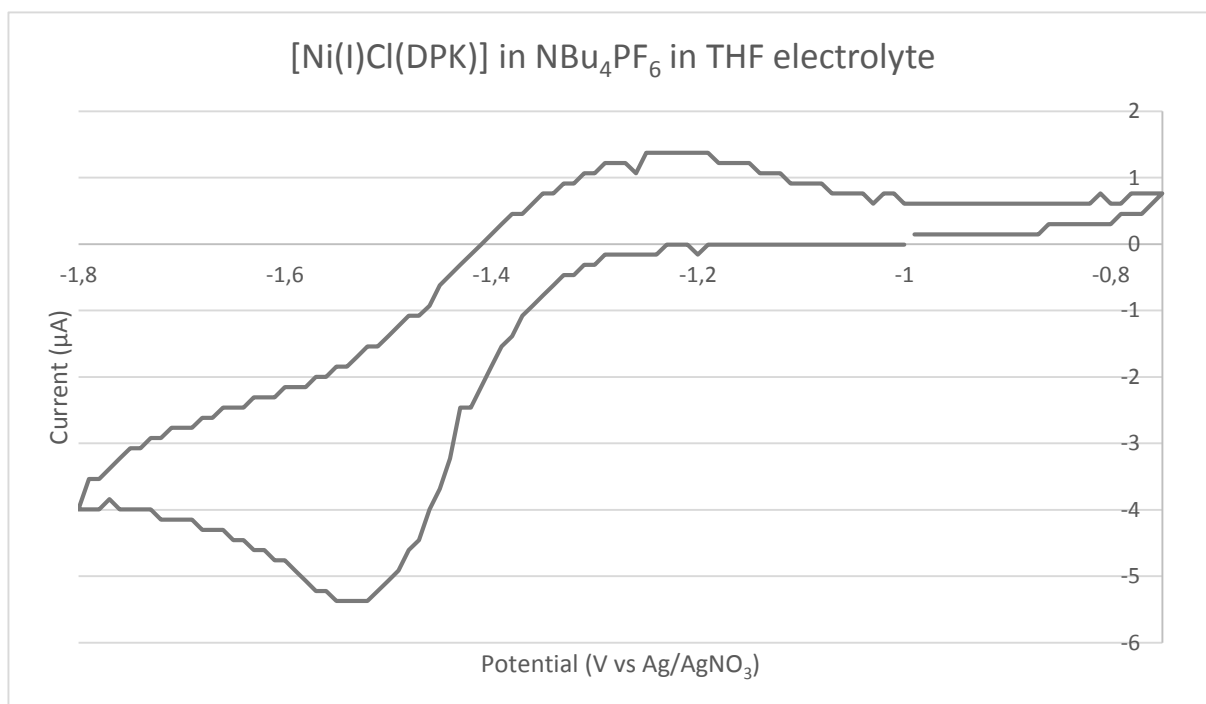
CV - [Ni(I)Cl(DPK)] (9)



Vertex 1: 2 V; Vertex 2: -4 V; E_{start} : -1 V; Scanrate: 200 mV/s; 2 cycles.

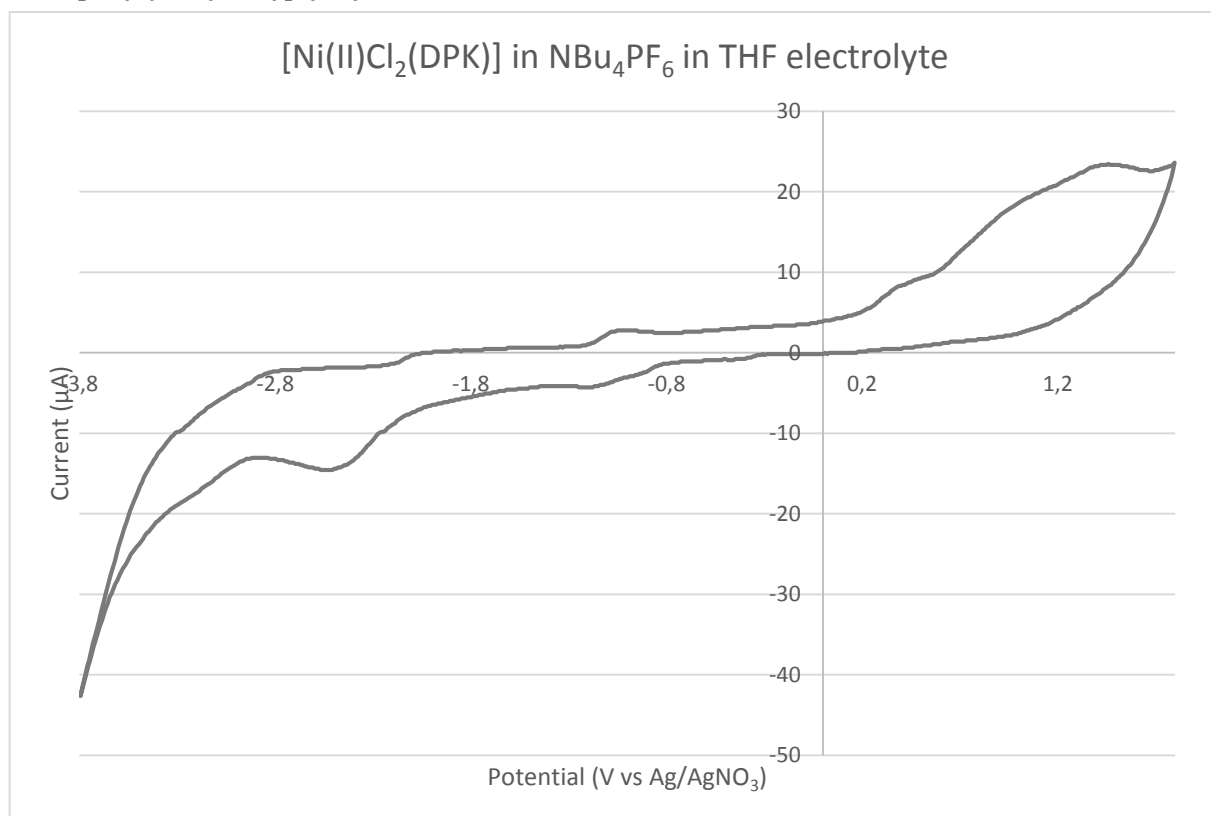


CV - [Ni(I)Cl(DPK)] (9) zoom -1.8V to -0.75V



Vertex 1: -0.75 V; Vertex 2: -1.8 V; E_{start}: -1 V; Scanrate: 100 mV/s; 2 cycles.

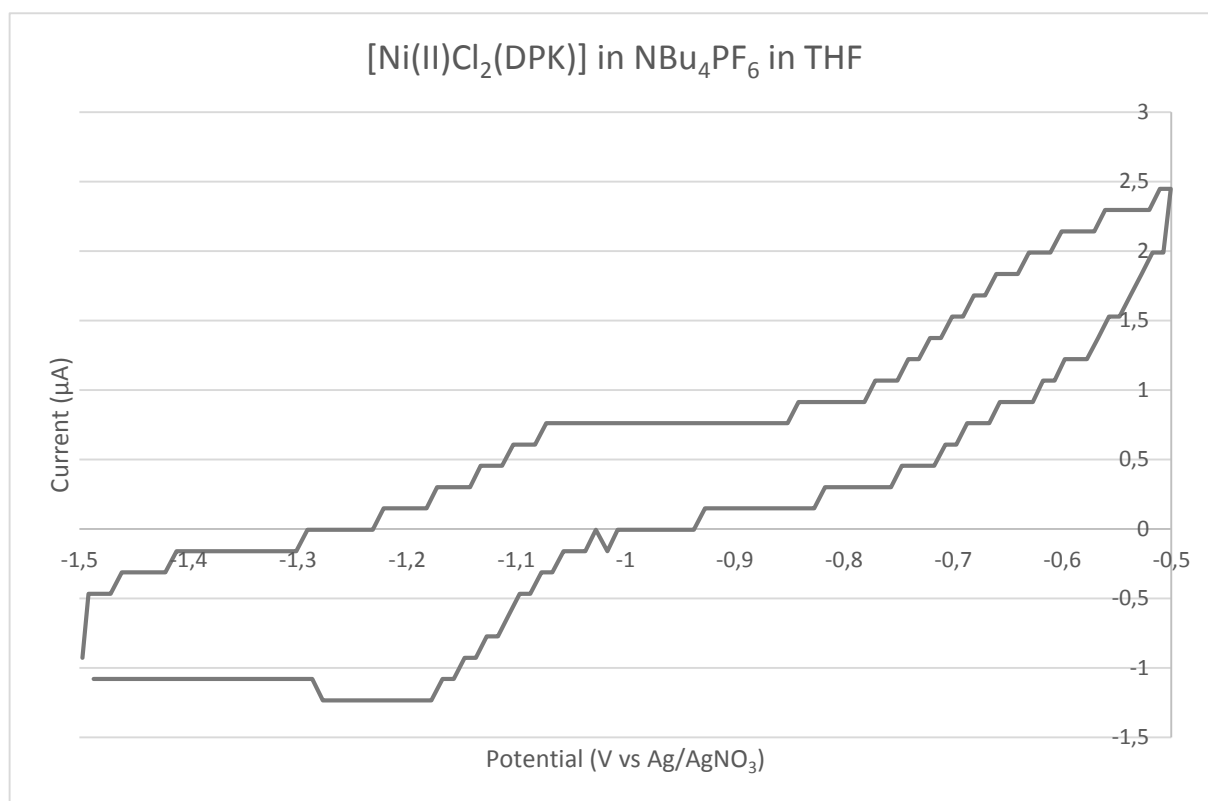
CV - [Ni(II)Cl₂(DPK)] (10)



Vertex 1: 2 V; Vertex 2: -4 V; E_{start}: -1 V; Scanrate: 200 mV/s; 2 cycles.

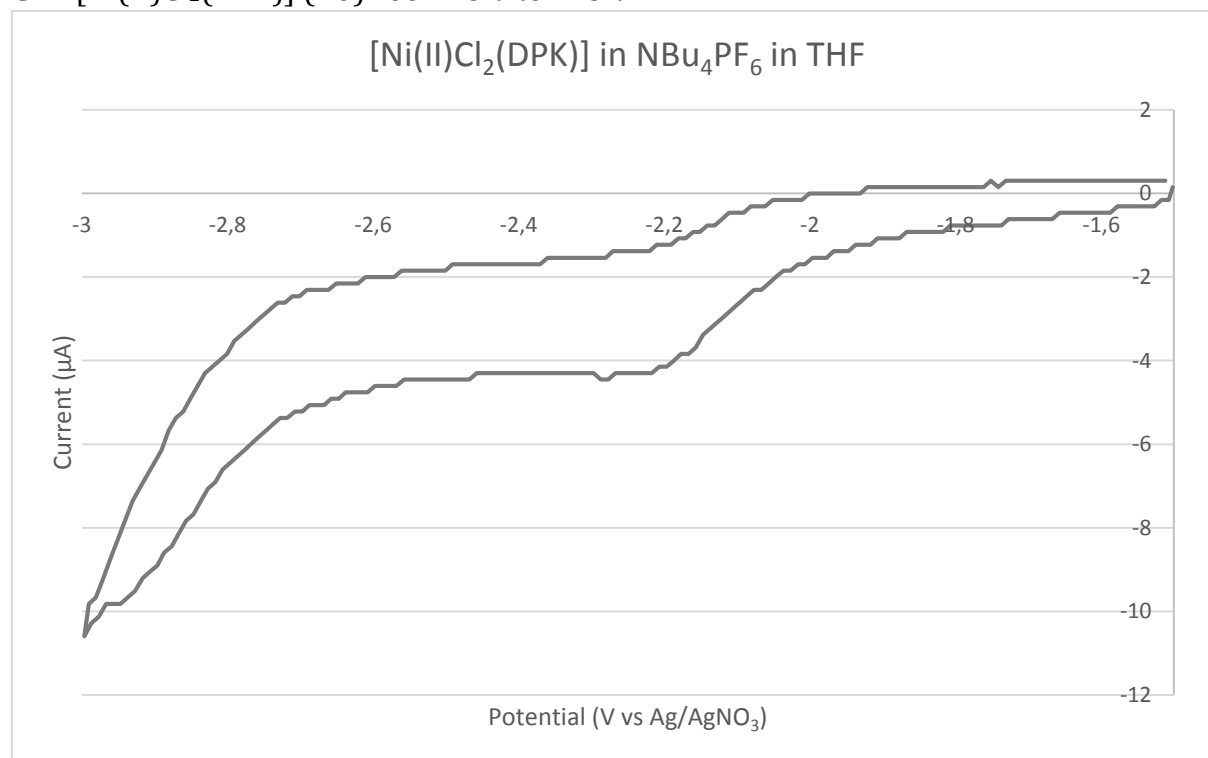


CV - [Ni(II)Cl₂(DPK)] (10) zoom -1.5 V to -0.5 V



Vertex 1: -1.5 V; Vertex 2: -0.5 V; E_{start}: -0.5 V; Scanrate: 100 mV/s; 2 cycles.

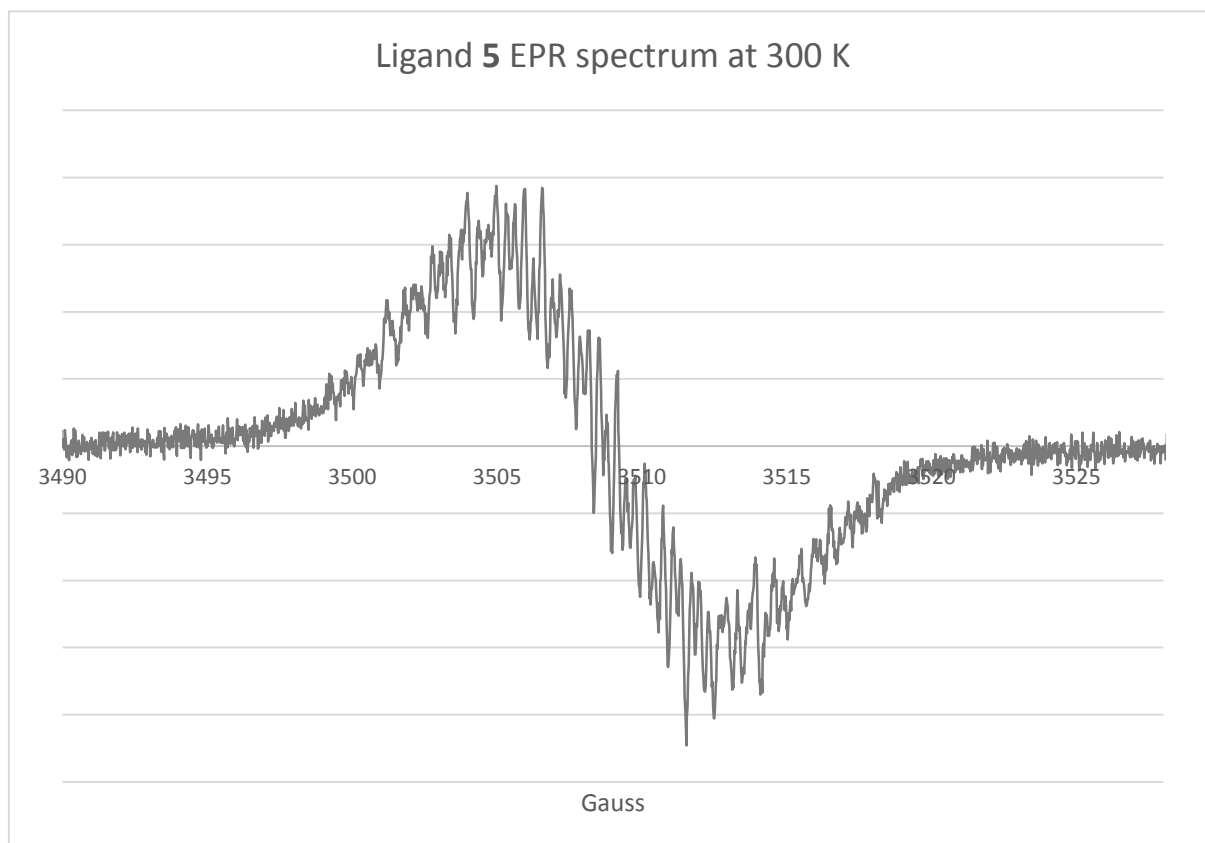
CV - [Ni(II)Cl₂(DPK)] (10) zoom -3 V to -1.5 V



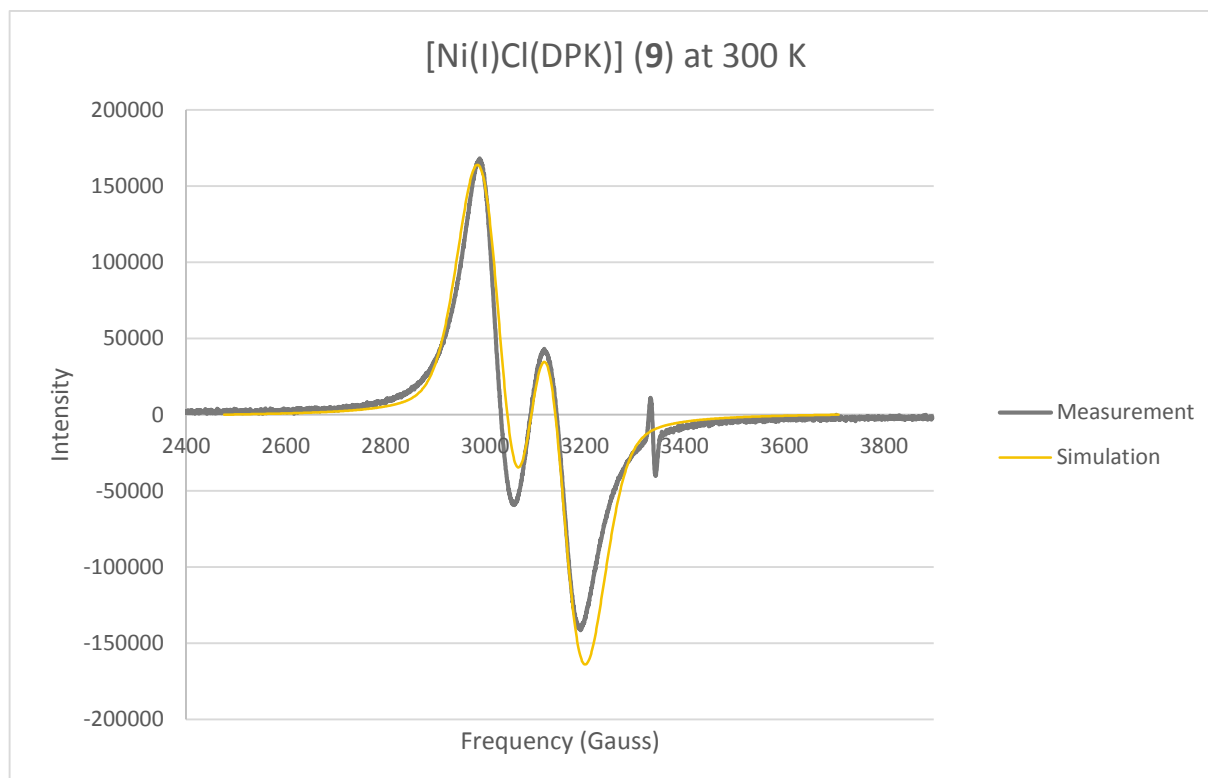
Vertex 1: -3 V; Vertex 2: -1.5 V; E_{start}: -1.5 V; Scanrate: 100 mV/s; 2 cycles.



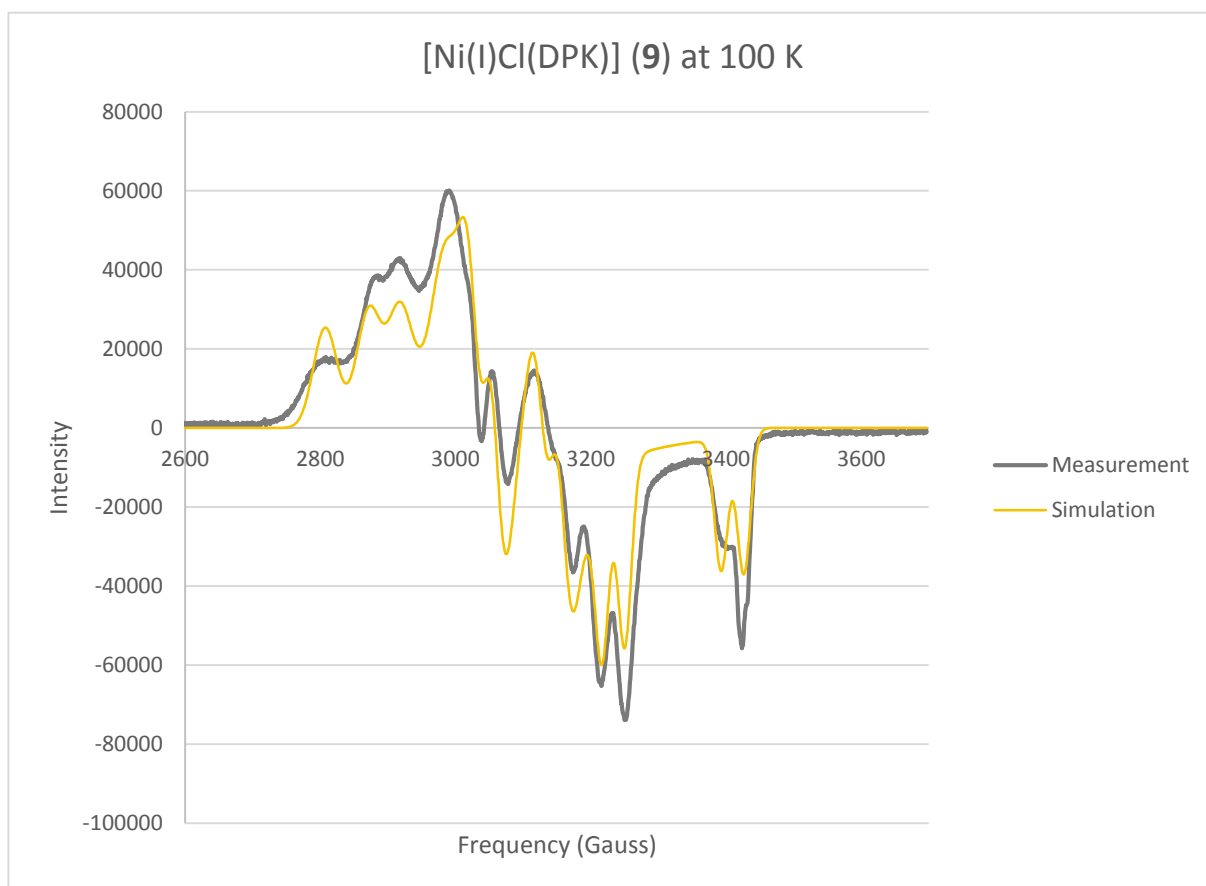
EPR - bis(2-diphenylphosphinophenyl)methanone (DPK, 5)



EPR - [Ni(I)Cl(DPK)] - 300 K (9)



EPR - [Ni(I)Cl(DPK)] - 100 K (9)



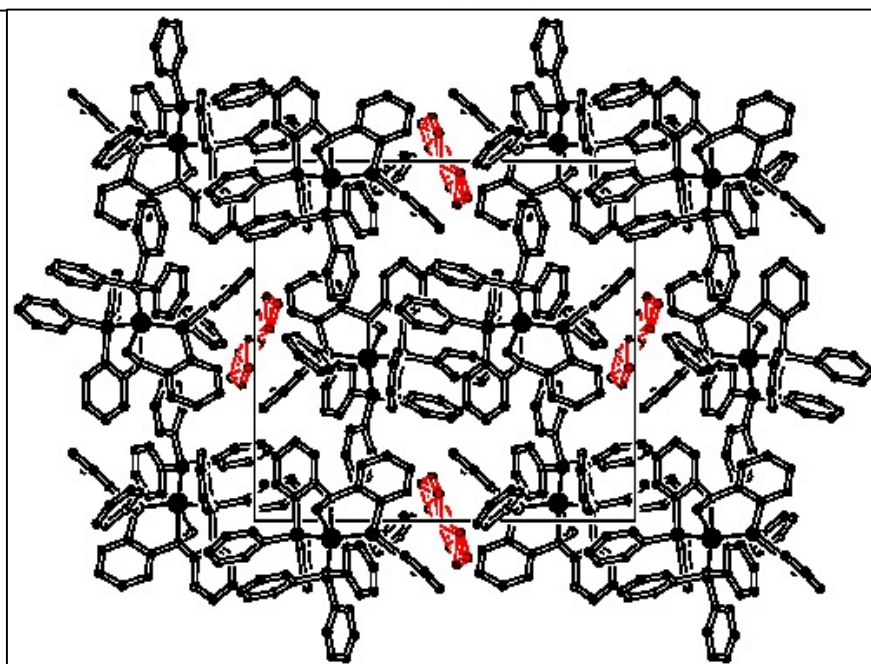
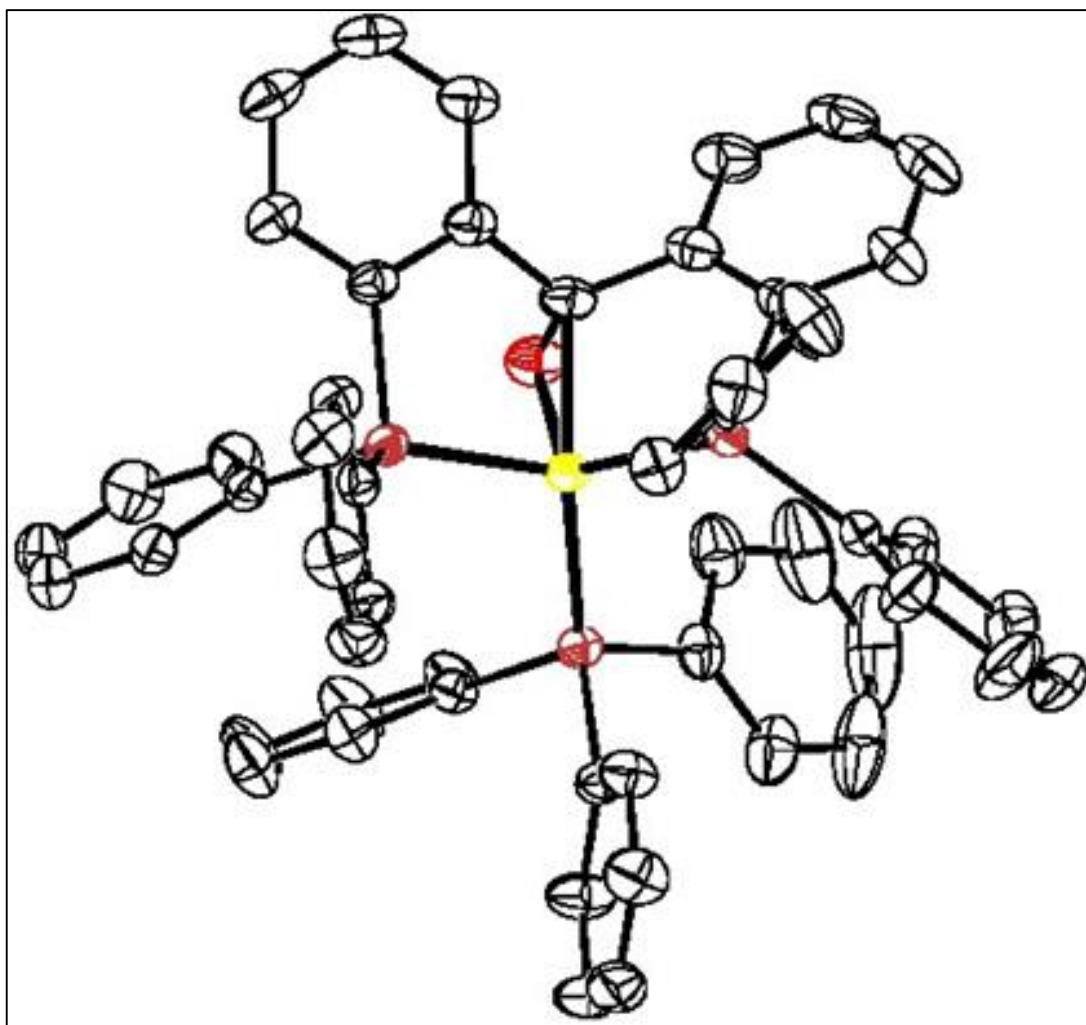
XRD - Crystallographic results for complexes **8**, **9** and **10**

<i>parameter</i>	8	9	10	10
<i>chemical formula</i>	C ₅₅ H ₄₃ NiOP ₃ ·½ C ₄ H ₁₀ O	C ₃₇ H ₂₈ ClNiOP ₂	C ₃₇ H ₂₈ Cl ₂ NiOP ₂	C ₃₇ H ₂₈ Cl ₂ NiOP ₂ ·CH ₂ Cl ₂
<i>molecular weight</i>	908.57	644.69	680.14	765.07
<i>crystal colour</i>	dark red	red	brown	brown
<i>crystal size [mm³]</i>	0.20 x 0.12 x 0.07	0.12 x 0.12 x 0.04	0.29 x 0.29 x 0.06	0.39 x 0.11 x 0.06
<i>T [K]</i>	150(2)	150(2)	150(2)	150(2)
<i>crystal structure</i>	monoclinic	monoclinic	monoclinic	orthorhombic
<i>space group</i>	P21/c (no. 14)	P21/n (no. 14)	P21/c (no. 14)	P2 ₁ 2 ₁ 2 ₁ (no. 19)
<i>a [Å]</i>	13.5071(5)	9.8635(3)	18.7117(7)	9.62126(17)
<i>b [Å]</i>	17.8465(6)	35.4023(14)	11.2342(4)	18.4902(4)
<i>c [Å]</i>	19.8676(6)	17.3720(5)	15.8601(5)	20.0628(5)
<i>β [°]</i>	108.318(2)	93.340(1)	110.302(2)	-
<i>V [Å³]</i>	4546.5(3)	6055.8(4)	3126.83(19)	3569.16(13)
<i>Z</i>	4	8	4	4
<i>D_{calc} [g/cm³]</i>	1.327	1.414	1.445	1.424
<i>(sin θ/λ)_{max} [Å⁻¹]</i>	0.65	0.65	0.65	0.65
<i>μ [mm⁻¹]</i>	0.58	0.86	0.92	0.96
<i>abs. corr.</i>	multi-scan	numerical	multi-scan	numerical
<i>abs. corr. range</i>	0.65-0.75	0.79-1.00	0.68-0.75	0.73-0.95
<i>refl. measured/unique</i>	54739 / 10440	63999 / 13906	47086 / 7186	87198 / 8203
<i>parameters / restraints</i>	586 / 37	757 / 0	388 / 0	415 / 0
<i>R1/wR2 [I>2σ(I)]</i>	0.0385 / 0.0877	0.0356 / 0.0749	0.0222 / 0.0561	0.0292 / 0.0831
<i>R1/wR2 [all refl.]</i>	0.0614 / 0.0965	0.0640 / 0.0832	0.0255 / 0.0576	0.0314 / 0.0846
<i>Flack x parameter^[61]</i>	-	-	-	-0.003(2)
<i>S</i>	1.037	1.028	1.039	1.044
<i>ρ_(min/max) [eÅ⁻³]</i>	-0.28 / 0.64	-0.43 / 0.43	-0.31 / 0.34	-0.72 / 1.01



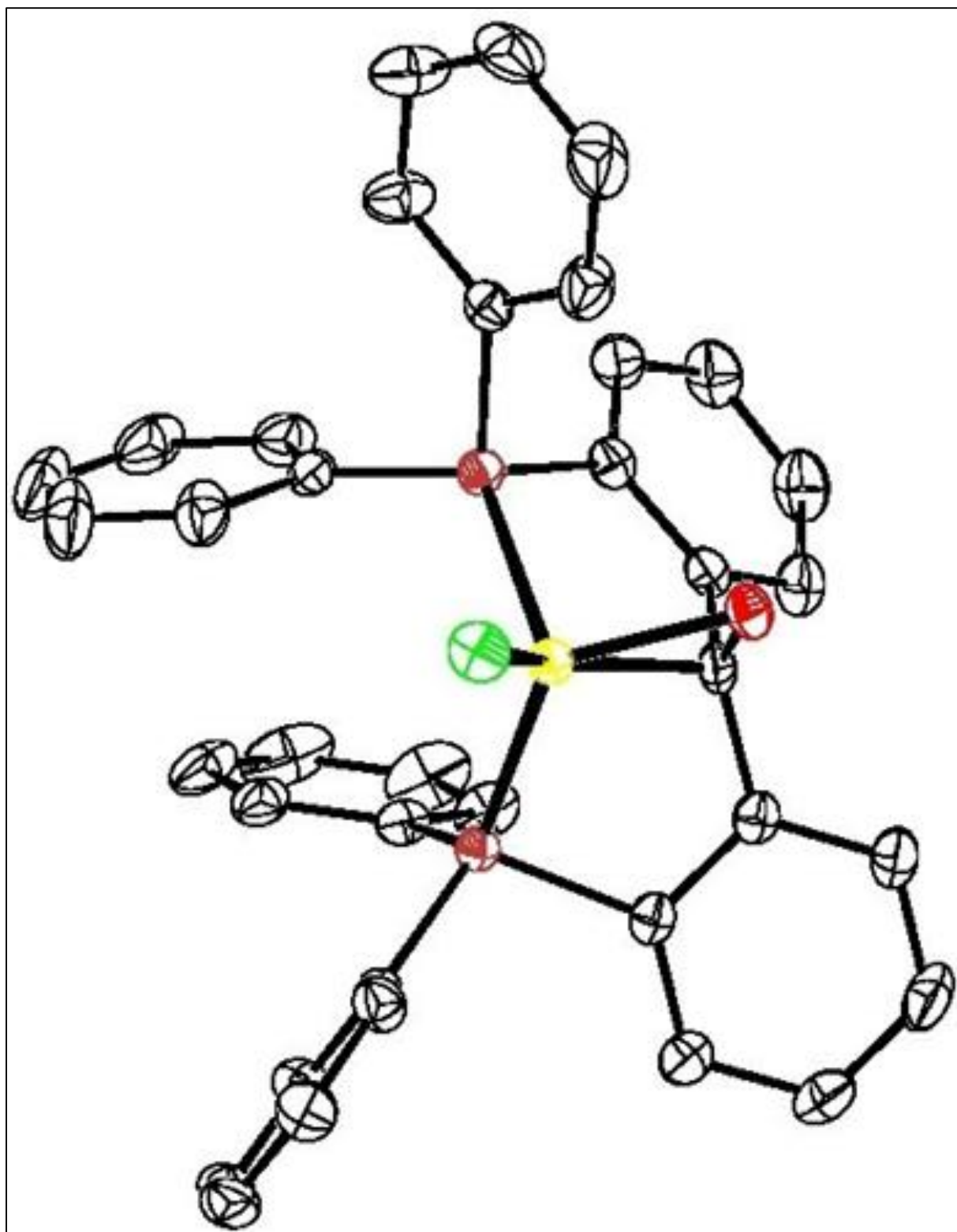
XRD - $[\text{Ni}(\text{O})(\text{DPK})(\text{PPh}_3)]$ (**8**)

The crystal structure is affected by a small contribution of whole-molecule disorder. This has been ignored in the refinement. The co-crystallized diethyl ether molecule is disordered on an inversion center. Restraints have been used for 1,2 and 1,3 distances of the diethyl ether molecule.



XRD - [Ni(I)Cl(DPK)] (9)

The crystal structure was obtained from C₆D₆.



XRD - [Ni(II)Cl₂(DPK)] (10)

Two crystal forms were obtained from the same crystallization batch.

